



저작자표시-비영리-변경금지 2.0 대한민국

이용자는 아래의 조건을 따르는 경우에 한하여 자유롭게

- 이 저작물을 복제, 배포, 전송, 전시, 공연 및 방송할 수 있습니다.

다음과 같은 조건을 따라야 합니다:



저작자표시. 귀하는 원저작자를 표시하여야 합니다.



비영리. 귀하는 이 저작물을 영리 목적으로 이용할 수 없습니다.



변경금지. 귀하는 이 저작물을 개작, 변형 또는 가공할 수 없습니다.

- 귀하는, 이 저작물의 재이용이나 배포의 경우, 이 저작물에 적용된 이용허락조건을 명확하게 나타내어야 합니다.
- 저작권자로부터 별도의 허가를 받으면 이러한 조건들은 적용되지 않습니다.

저작권법에 따른 이용자의 권리는 위의 내용에 의하여 영향을 받지 않습니다.

이것은 [이용허락규약\(Legal Code\)](#)을 이해하기 쉽게 요약한 것입니다.

[Disclaimer](#)

공학석사 학위논문

**Studies on Molecular Design and
Synthesis of Furan-Containing
Diketopyrrolopyrrole Derivatives for
Solution-Processed Organic Solar Cells**

용액공정용 유기태양전지를 위한
퓨란을 포함하는 디케토피롤로피롤 유도체의
분자 설계 및 합성에 관한 연구

2014년 2월

서울대학교 대학원

재료공학부

오 정 아

Studies on Molecular Design and Synthesis of Furan-Containing Diketopyrrolopyrrole Derivatives for Solution-Processed Organic Solar Cells

A THESIS SUBMITTED IN PARTIAL FULFILLMENT OF
THE REQUESTMENTS FOR THE DEGREE OF MASTER
IN ENGINEERING AT THE GRADUATE SCHOOL OF
SEOUL NATIONAL UNIVERSITY

FEBURARY 2014

By

Jeong-A Oh

Supervisor

Prof. Soo Young Park

Abstract

Studies on Molecular Design and Synthesis of Furan-Containing Diketopyrrolopyrrole Derivatives for Solution-Processed Organic Solar Cells

Jeong-A Oh

Department of Materials Science and Engineering

The Graduate School

Seoul National University

In these days, solution-processed bulk heterojunction (BHJ) type organic solar cells have drawn great attention in order to develop alternative energy system for the future. I have been particularly interested in the structure of diketopyrrolopyrrole (DPP) unit, which is a widely used electron-withdrawing building block in the synthesis of organic semiconducting materials owing to its superior optical and electrical properties. Among the recent works, the DPP-based small molecules with well-organized π -conjugated structure of A-D-A or D-A-D type framework have been developed rapidly, exhibiting promising solar cell efficiencies. However, they inevitably encounter a challenging issue about solubility attributed to the strong intermolecular hydrogen bonding capability of DPP cores. Instead of introducing long and branched alkyl side chains, here I adopted alternative strategy that is the

incorporation of furan unit in the conjugated backbone, as a novel design strategy of solution-processable small molecules for the highly efficient organic solar cells.

Several furan-containing DPP-based small molecules were successfully synthesized, characterized and fabricated for the BHJ organic solar cells. In the chapter 2, I designed a novel A-D-A type small molecule as a donor material named **F2**, where A is furan-containing DPP and D is electron-donating dithienothiophene (DTT). I demonstrated that furan moiety can replace thiophene, while maintaining the level of decent photovoltaic properties of thiophene derivatives. It was demonstrated that **F2** showed enhanced solubility and V_{oc} value, with more simple synthetic procedure. Consequently, the device of **F2** and PC₆₁BM exhibits a PCE of 2.1% with the improved V_{oc} of 0.75 V when fabricated with 1 vol% of DIO. In addition, I also discussed about the effects of furan moiety on molecular properties, systematically. In the chapter 3, I designed four different small molecules with A-D-A-D-A type structures depending on the number and position of furan. This study is intended to demonstrate that the furan-containing DPP-based small molecules are also available for the BHJ organic solar cells as acceptor materials, exhibiting promising photophysical properties.

Keywords: Diketopyrrolopyrrole, Organic solar cells, Furan
Student Number: 2012-22539

Contents

Abstract	i
Contents	iii
List of Tables	v
List of Schemes	vii
List of Figures	ix

Chapter 1 Introduction.....1

1.1 Organic solar cells.....	1
1.1.1 Research background.....	1
1.1.2 Active layer materials for bulk heterojunction solar cells	7
1.2 Diketopyrrolopyrrole	9
1.2.1 Introduction of diketopyrrolopyrrole	9
1.2.2 Organic solar cell materials based on diketopyrrolopyrrole	11
1.2.3 Furan-containing diketopyrrolopyrrole-based materials.....	15
1.3 Research objectives.....	18
1.4 References.....	20

Chapter 2 Promising Design Concept of Incorporating Furan Moiety into Diketopyrrolopyrrole-Based Donor Molecule for Solution-Processed Organic Solar Cells with Enhanced Solubility and V_{oc}26

2.1 Introduction.....	26
-----------------------	----

2.2	Experimental section.....	32
2.3	Result and discussion.....	45
2.4	Conclusions.....	77
2.5	References.....	78

Chapter 3 Low Band Gap and Solution-Processable Furan-Containing Diketopyrrolopyrrole-Based Small Molecules as Acceptor Materials in Organic Solar Cells79

3.1	Introduction.....	79
3.2	Experimental section.....	83
3.3	Result and discussion.....	98
3.4	Conclusions.....	129
3.5	References.....	131

Abstract in Korean.....132

List of Presentation134

List of Tables

Table 2.1	Theoretical molecular orbital of T1 , F1 , T2 and F2 by DFT calculations.....	50
Table 2.2	Optical properties of T1 , F1 , T2 and F2	56
Table 2.3	Calculated and experimental data for the molecular energy levels of T1 , F1 , T2 and F2 based on UV-Vis absorption spectra and UPS profiles.	60
Table 2.4	Photovoltaic properties of BHJ organic solar cells fabricated with T1 and PC ₇₁ BM, referring to the paper.	64
Table 2.5	Photovoltaic properties of BHJ organic solar cells fabricated with F2 and PC ₆₁ BM. Specific fabricating conditions were noted at the below of each table. (a) With different blend ratios of F2 :PC ₆₁ BM. (b) With different concentration of chloroform solutions, and spin-rate. (c) Without or with DIO as additive..	67
Table 2.6	Photovoltaic properties of BHJ organic solar cells fabricated with F2 and PC ₇₁ BM. Specific fabricating conditions were noted at the below.....	70
Table 2.7	Photovoltaic properties of BHJ organic solar cells fabricated with F1 and PC ₆₁ BM. Specific fabricating conditions were noted at the below.....	72
Table 3.1	Optical properties of TT , TF , FT and FF	109
Table 3.2	Molecular energy levels obtained from UPS and cyclic	

voltammetric measurements, for **TT**, **TF**, **FT** and **FF**.

.....115

Table 3.3

Photovoltaic properties in (a)-(c). Specific fabricating

conditions were noted at the below of each table. (a)

Screening test of **TT**, **TF**, **FT** and **FF** in toluene solvent.

(b) Vertically alkyl chain modifying for **FT** and **HD-FT**

with high concentration. (c) Horizontally alkyl chain

modifying for **FT-E**, **FT-B**, **FT** and **FT-OD** with

optimized solvent.....120

List of Schemes

Scheme 1.1	Chemical structures of P3HT (poly(3-hexylthiophene)) and PCBM, which are common donor and acceptor materials in the BHJ organic solar cells.....	6
Scheme 1.2	The structure of biphenyl-substituted diketopyrrolopyrrole (DPP).	10
Scheme 1.3	Chemical structures of representative DPP derivatives for the BHJ organic solar cells with respective PCE values. (a): electron donating polymers, (b): electron donating small molecules, (c): electron accepting small molecules. The PCEs were obtained by these materials with P3HT or PCBM as donor or acceptor material.....	14
Scheme 1.4	Chemical structures of DPP-based polymers which contain furan moiety.	17
Scheme 2.1	Chemical structures of T1 , F1 , T2 and F2 with design strategies.	31
Scheme 2.2	Synthesis of F1 and F2	33
Scheme 2.3	Synthesis of T1 and T2	34
Scheme 3.1	Chemical structures of target materials. (a): TT , TF , FT and FF . Alkyl chain modifications of FT were presented by (b) and (c). (b): Vertical modifying for FT , HD-FT and C12-FT . (c): Horizontal modifying for FT-E , FT-B , FT and FT-OD	82
Scheme 3.2	Synthesis of target materials: TT , TF , FT and FF	84

Scheme 3.3	Synthesis of FT derivatives with alkyl chain modifications. (a) : Vertical modifying for FT , HD-FT and C12-FT . (b) : Horizontal modifying for FT-E , FT-B , FT and FT-OD	85
Scheme 3.4	Synthesis, characterization and solar cell applications of FB-B and FTT . Synthesis of FB-B (a) and synthesis of FTT (b) with summarized experimental data and photovoltaic properties.....	122

List of Figures

Figure 1.1	General device architecture of bulk heterojunction (BHJ) organic solar cells and description of common operating mechanism in BHJ active layer.....	4
Figure 1.2	The illustration of the typical current-voltage (J - V) curve with important parameters, Such as: J_{sc} , the short circuit current density; V_{oc} , the open circuit voltage; FF , the fill factor; J_m and V_m , the current and voltage at the maximum power point	5
Figure 2.1	Chemical structures of several A-D-A type small molecules for donor materials, with their energy levels, optical band gap, and photovoltaic properties.	30
Figure 2.2	Energy-minimized structure (B3LYP/6-31G(d, p)) of a methyl-substituted (a) T1 , (b) F1 , (c) T2 and (d) F2 (top/front view) with lineal distance along the molecular π -conjugated backbone and visualization of the HOMO (left) and LUMO (right) molecular orbital. Optimized ground state geometry was obtained from Gaussian view 5.0.....	49
Figure 2.3	Normalized UV-Vis absorption spectra of (a) T1 , (b) F1 , (c) T2 and (d) F2	55
Figure 2.4	Ultraviolet photoelectron spectroscopy (UPS) profiles of the (a) T1 , (b) F1 , (c) T2 , and (d) F2 for the spin-coated (2000 rpm/40 sec) films on the glasses.....	59

Figure 2.5	<i>J-V</i> curves of BHJ organic solar cells fabricated with F2 and PC ₆₁ BM. (a) With different blend ratios of F2 :PC ₆₁ BM. (b) With different concentration of chloroform solutions, and spin-rate. (c) Without or with DIO as additive.65
Figure 2.6	IPCE spectra of solar cells based on F2 and PC ₆₁ BM...66
Figure 2.7	<i>J-V</i> curves of BHJ organic solar cells fabricated with F1 and PC ₆₁ BM.71
Figure 2.8	Morphological images with the amount of DIO and roughness of solar cells based on F2 :PC ₆₁ BM75
Figure 2.9	Morphological images with the amount of DIO and roughness of solar cells based on F2 :PC ₇₁ BM.76
Figure 3.1	Energy-minimized structure (B3LYP/6-31G(d, p)) of a methyl-substituted (a) TT , (b) TF , (c) FT and (d) FF , with top (left) and front (right) view and lineal distance along the molecular π -conjugated backbone obtained from Gaussian view 5.0101
Figure 3.2	UV-Vis absorption spectra of TT , TF , FT and FF . (a) Molar absorption coefficient (molar absorptivity) profiles of compound 3 and 4 (left) and TT , TF , FT and FF (right) in CHCl ₃ (1×10^{-5} M). (b) Normalized UV-Vis absorption spectra of TT , TF , FT and FF in both solution and film state.107
Figure 3.3	Photoluminescence spectra of compound 3 and 4 in (a), and TT , TF and FF in (b), obtained from concentration of 1×10^{-5} M in CHCl ₃ solution.....108

Figure 3.4	Ultraviolet photoelectron spectroscopy (UPS) profiles of the TT , TF , FT and FF , for the spin-coated (1000 rpm/60 sec) films on the glasses111
Figure 3.5	The cyclic voltammograms of TT , TF , FT and FF , in solution (a) and film (b) state. The gray lines were obtained from ferrocene.....114
Figure 3.6	<i>J-V</i> curves of BHJ organic solar cells fabricated with P3HT and DPP small molecules with various backbone and alkyl chin modified derivatives. (a) Screening test of TT , TF , FT and FF in toluene solvent. (b) Vertical modifying for FT and HD-FT with high concentration. (c) Horizontal modifying for FT-E , FT-B , FT and FT-OD . Specific fabricating conditions were noted at the below each curve.....119
Figure 3.7	UV-Vis absorption profiles of FT-B (a, left) and FTT (b, left) in the solution (1×10^{-5} M in CHCl_3) and film by spin-coating (1000 rpm/60 sec) from 10 mg/mL CHCl_3 solution. And absorption spectra of FT-B and FTT in the film state compared with that of FT on the right of (a) and (b).....123
Figure 3.8	Morphological images with roughness obtained by AFM of BHJ organic solar cells. A: (a) TT (toluene), (b) TF (toluene), (c) FT (toluene), (d) FF (toluene). B: (a) FT-B (THF, annealed at 150 °C), (b) FT (toluene), (c) FT-OD (toluene). C: (a) FT (co-solvent of 1:3, 150 °C), (b) FT (co-solvent of 1:1, 150 °C), (c) FT (co-solvent of 3:1,

150 °C). **D:** (a) **FT-B** (toluene, annealed at 150 °C), (b) **FT-B** (THF, annealed at 150 °C), (c) **FT-B** (co-solvent of 1:3, annealed at 150 °C).128

Chapter 1. Introduction

1.1 Organic solar cells

1.1.1 Research background

According to the increasing consumption of fossil fuels, which are limited resources and considered as main causes of environmental pollution, the whole world was confronted with energy crisis and global warming. In this sense, the effort to use clean and sustainable solar energy derived from the most abundant sources of sunlight has become main issue in today's society. Since the first solar cells, converting from sunlight into electric energy, was invented in 1839¹, the efficiency has been reached up to 24.7% for inorganic silicon solar cells². Although organic solar cells exhibited relative lower efficiency, they have drawn great attention because of following advantages; low cost, light weight, flexibility, excellent chemical versatility of materials through various synthetic methods, and easiness of device fabrication.³ In other words, the organic solar cells using organic semiconducting materials would be suitable answer to the alternative energy for the future.

The photovoltaic devices can be generally classified into two types, depending on their forms of active layer containing electron donor and acceptor materials. For the bilayer solar cells, which consist of two planar layers for donor and acceptor, they involve the problem that insufficient number of exciton is separated into holes and electrons. It is because the

diffusion length is too short for the exciton to reach the interface of two layers. This challenging issue would be solved by the bulk heterojunction (BHJ) solar cells, whose active layer is fabricated with donor and acceptor blends. The BHJ network forms similar length scale of internal D-A phase segregation with the exciton diffusion length, which is in the order of approximately 10 nm in organic semiconducting materials, thus facilitating charge separation at the maximized interface area as well.⁴

The mechanism⁵ of the organic solar cell operation is composed of six steps; 1) photon absorption, 2) exciton (hole and electron pair) formation, 3) exciton diffusion, 4) exciton dissociation (charge separation into hole and electron), 5) charge transport, and 6) charge collection. According to such complicated operating processes, the structure of active layer can significantly affect device performance, which means the BHJ network deserves careful consideration.

Figure 1.1 represents general device structure of solution-processed BHJ solar cells. The conventional composition of devices contains four layers on glass substrate; indium tin oxide (ITO) as transparent electrode material at the anode, PEDOT:PSS widely used as hole transport layer (HTL), BHJ active layer fabricated with spin-coating from simple blend solution of donor and acceptor materials, and Al as a lower work-function metal as the cathode.⁶

The typical current-voltage (J - V) curve obtained for the photovoltaic device is illustrated in Figure 1.2, with the parameters which are used to indicate the performance of solar cells. From the parameters of J_{sc} , V_{oc} , and FF , the photovoltaic efficiency, so called power conversion efficiency (PCE) can be

described by the following formula:

$$PCE = FF \times (V_{oc} \cdot J_{sc}) / P_{in}$$

where J_{sc} is the short circuit current density, V_{oc} is the open circuit voltage, FF is the fill factor, and P_{in} is the incident light power density.⁴

In addition, BHJ solar cells have been developed by contribution of advanced organic semiconducting materials, including both π -conjugated polymers and small molecules. The most widely used optimized system is the P3HT:PCBM combination, as polymer donor/small molecular acceptor, exhibiting PCEs of 5%.⁷ (Scheme 1.1) Especially, novel design of donor materials has contributed to enhancing efficiencies, establishing a suitable phase separation of active layer. The PCE of solution-processed BHJ organic solar cells has reached over 10%, when the device was fabricated into tandem solar cells based on two polymer type donor materials and fullerene derivatives.⁸

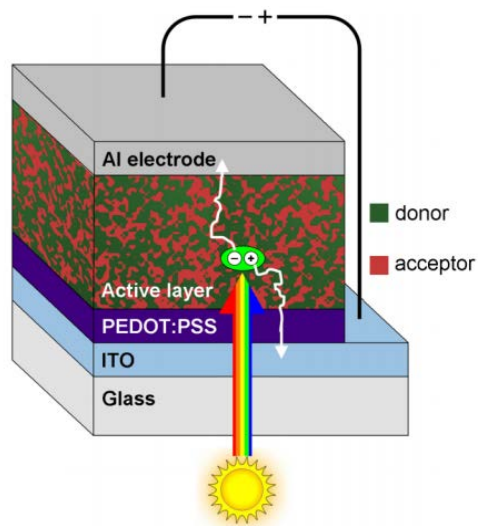


Figure 1.1 General device architecture of bulk heterojunction (BHJ) organic solar cells and description of common operating mechanism in BHJ active layer.⁶

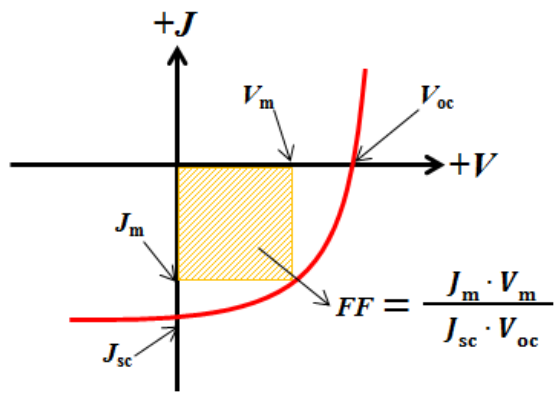
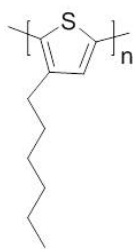
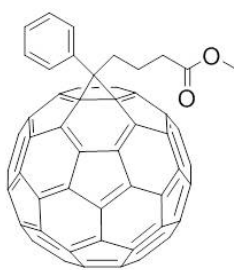


Figure 1.2 The illustration of the typical current-voltage (J - V) curve with important parameters, such as; J_{sc} , the short circuit current density; V_{oc} , the open circuit voltage; FF , the fill factor; J_m and V_m , the current and voltage at the maximum power point.



P3HT



PCBM

Scheme 1.1 Chemical structures of P3HT (poly(3-hexylthiophene)) and PCBM, which are common donor and acceptor materials in the BHJ organic solar cells.

1.1.2 Active layer materials for bulk heterojunction solar cells

In recent years, the BHJ organic solar cells have been greatly developed by using advanced organic semiconducting materials, including both π -conjugated polymers and small molecules. Particularly, as donor materials in the active layer, various small molecules exhibiting well-ordered structures have been discussed, because small molecular type materials present following characteristics; well-defined molecular weight, simpler purifying process, easier control of properties, and higher reproducibility of device fabrication when compared with polymers.⁹ Based on these advantages, solution-processed solar cell efficiencies are currently reaching as high as 8% when devices are comprised of only small molecules.¹⁰

On the other hand, compared to the development of donor materials, relatively few studies for acceptor materials have been reported. The best electron accepting materials are fullerene derivatives, such as phenyl-C61-butyric acid methyl ester (PC₆₁BM) and PC₇₁BM, which have following strengths; high electron affinity, good electron mobility, favorable nano-scale morphology, and electron transport in three dimensions. It is hard to surpass the performance of PCBM; however, the efforts to develop alternative non-fullerene acceptor materials have been increasing steadily, in order to overcome limited light absorption and high cost of PCBM derivatives.¹¹

From a point of view in the structure-property relationships, designing active layer materials deserves to receive much attention to control device functions, which is significant issue for the chemist. When the devices were fabricated

into the thin film, molecular structures can interplay with nano- and meso-scale structures that were originated from self-assembled characteristics. In other words, organic semiconducting materials which show advanced device functions should have favorable supramolecular structures, as well.¹² Thus, the molecular design of active layer materials should be regarded as significant considering bulk heterojunction network in the BHJ organic solar cells.

For the solution-processed BHJ organic solar cells, specific design strategies of π -functional systems have been suggested, which are commonly dealing with two parts; one is rigid and conjugated aromatic core, the other part is flexible and non-conjugated side chain. The core part determines densely π - π stacked structure in the film state, which dictates the overlap and interaction of π -conjugated molecular orbitals. Side chains are as important as cores, since they have great effects on not only solubility for processing but also on the self-assembly into favorable phase separation.

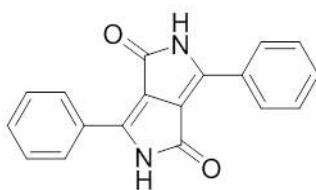
In recent years, a number of organic semiconducting materials have been designed based on the above mentioned strategies, such as alkyl oligothiophene¹⁰, diketopyrrolopyrrole¹³ and perylene diimide¹⁴ derivatives, thus exhibiting advanced device properties. Many review articles have been published recently for the collective or critical review of organic solar cell materials.¹⁵

1.2 Diketopyrrolopyrrole

1.2.1 Introduction of diketopyrrolopyrrole^{16,17}

Since Farnum *et al.* reported the first 2,5-diketopyrrolo[3,4-*c*]pyrrole (DPP) derivative with two phenyl rings¹⁸ (scheme 1.2), and its synthetic pathway was developed by Iqbal and coworkers¹⁹, various DPP derivatives have been widely used as high performing pigments. The DPP unit exhibits exceptional thermal and physical stability due to the exceptional planarity and strong intermolecular hydrogen bonding between lactam rings. For the DPP derivatives, in order to enable wet-processing, this strong hydrogen bonding should be broken off, therefore the chemical modification by introducing solubilizing alkyl chains at the N-position in lactam rings was exploited.

Recently many research groups^{16,17,20} have been interested in the structure of DPP unit, as electron-withdrawing building block in organic semiconducting materials, such as organic light emitting diodes (OLEDs), organic thin-film transistors (OTFTs) and organic photovoltaics (OPVs), owing to its superior optical and electrical properties. In addition, the DPP derivatives have well-ordered and densely packed π - π stacking properties, thus providing favorable supramolecular structures in device applications.



Scheme 1.2 The structure of biphenyl-substituted diketopyrrolopyrrole (DPP).

1.2.2 Organic solar cell materials based on diketopyrrolopyrrole^{16,17}

Since the diketopyrrolopyrrole (DPP) derivatives have superb intrinsic optical and electrical properties, many research groups have been interested in DPP unit exploring solution-processed organic solar cells. The BHJ organic solar cells, which are advantageous over bilayer devices, have been also fabricated with DPP-based polymers²¹ and small molecules^{9,13,22}. (Scheme 1.3)

Because the DPP moiety shows high electron affinity, lowering the frontier energy levels, it is available to design low band gap materials by introducing various electron-donating (D) building blocks. Especially, the DPP-based polymers exhibiting well-ordered π -conjugation along the backbone, show efficient intramolecular charge transfer (ICT), thus leading to outstanding development, as donor materials, especially. However, it is hard to find notable progress as acceptor materials using DPP-based polymers.

On the other hand, for the DPP-based small molecules as both donor and acceptor, there has been remarkable improvement of device performances, in the recent years. Like other small molecular materials, they are also exhibiting following characteristics; 1) independency on molecular weight, 2) high reproducibility to device fabrication, 3) greater tendency of self-assembly, 4) relative easiness of synthesis and purification, and 5) free of additional processing against end-group contamination.⁹ In accordance with these advantages, the DPP-based small molecules exhibit greater potentials for using in solution-processed BHJ organic solar cells.

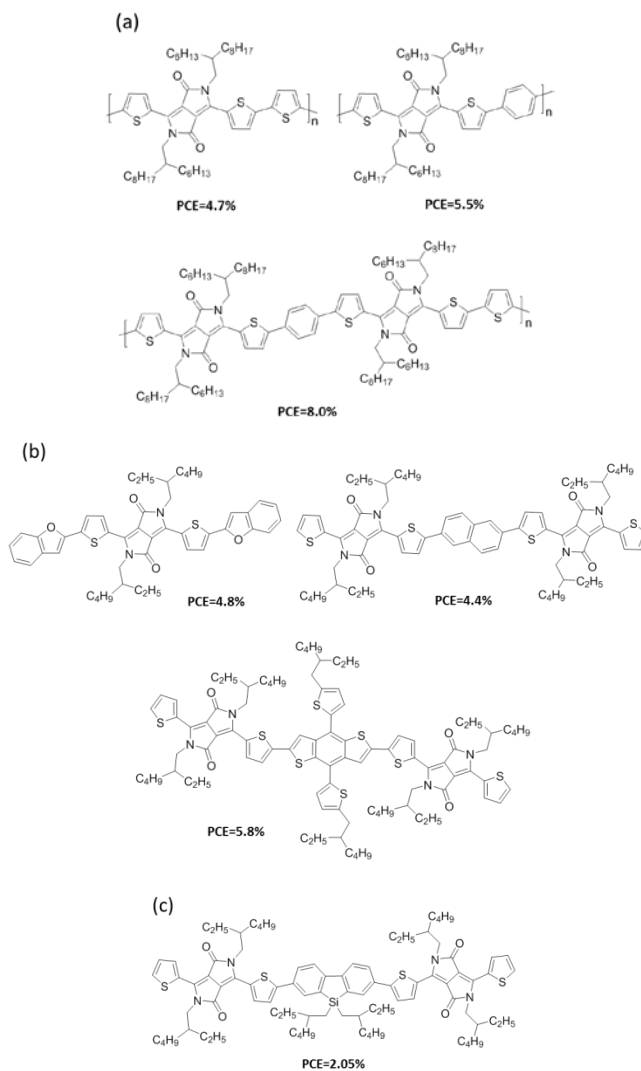
One of the promising studies might be the effort to design novel electron-accepting small molecules which can show comparable properties with PCBM derivatives. This is because fewer acceptor materials have been reported so far, in contrast to the studies about donors. The DPP was considered as an excellent electron-withdrawing block, thus allowing energy levels to be lowered sufficiently. The DPP-based acceptor materials designed with well-organized push-pull structures would have superior photophysical properties, thereby absorbing light deep into the longer wavelength region.

As already described before, regarding to the structure-property relationships, the efficiencies of BHJ organic solar cells based on diketopyrrolopyrrole (DPP) can be affected by design of materials. Common DPP-based materials are designed considering two parts mainly, like other organic semiconducting materials; one part is rigid and conjugated aromatic core based on DPP unit, the other is flexible and non-conjugated alkyl side chain.

For both polymers and small molecules, (Scheme 1.3) most of the high performing DPP-based materials are consisted of effective π -conjugation system, thus facilitating intramolecular charge transfer (ICT) along the backbone, with well-organized push-pull structure. Like D-A type low band gap polymers, extended π -conjugation can be available in DPP-based small molecules with D-A-D or A-D-A type, synthesized by adequate coupling reactions, such as Suzuki, Stille, Sonogashira, and so on. Since the DPP unit acts as an electron-accepting (A) block, it can be paired with various electron-donating (D) blocks which are varying from oligothiophene^{23,24} to fused acene²⁵⁻²⁷ derivatives. The resulting π -conjugation system of DPP-based small

molecules could determine materials' fundamental characteristics, such as physical, optical, electrical properties, etc. Molecular orbital and band gap were also affected. In addition, π -conjugated aromatic cores induced intermolecular π - π stacking in supramolecular structures, thus bringing about well-ordered domains and effective charge transport in the thin film.

In recent years, on the other hand, the studies which are about the effects of side chains and their synthetic modification with further fine-tuning have begun to emerge. With regard to the structure-property relationships, side chains significantly influenced molecular self-assembly, thereby controlling nano- and meso-scale structures in the thin film. Generally, side chains inevitably reduce intermolecular π - π stacking and ordered packing property, therefore several research groups tried to control phase separation, by changing the length (short/long) and shape (linear/branched) of alkyl side chains, systematically.^{28,29} Moreover, there was other strategies of introducing non-hydrocarbonyl side chains, like ethylene glycol into DPP-based polymer, in order to induce intended supramolecular structures, hence improving efficiencies.³⁰



Scheme 1.3 Chemical structures of representative DPP derivatives for the BHJ organic solar cells with respective PCE values. **(a)**: electron donating polymers²¹, **(b)**: electron donating small molecules^{9,13(a),22}, **(c)**: electron accepting small molecules^{13(b)}. The PCEs were obtained by these materials with P3HT or PCBM as donor or acceptor material.

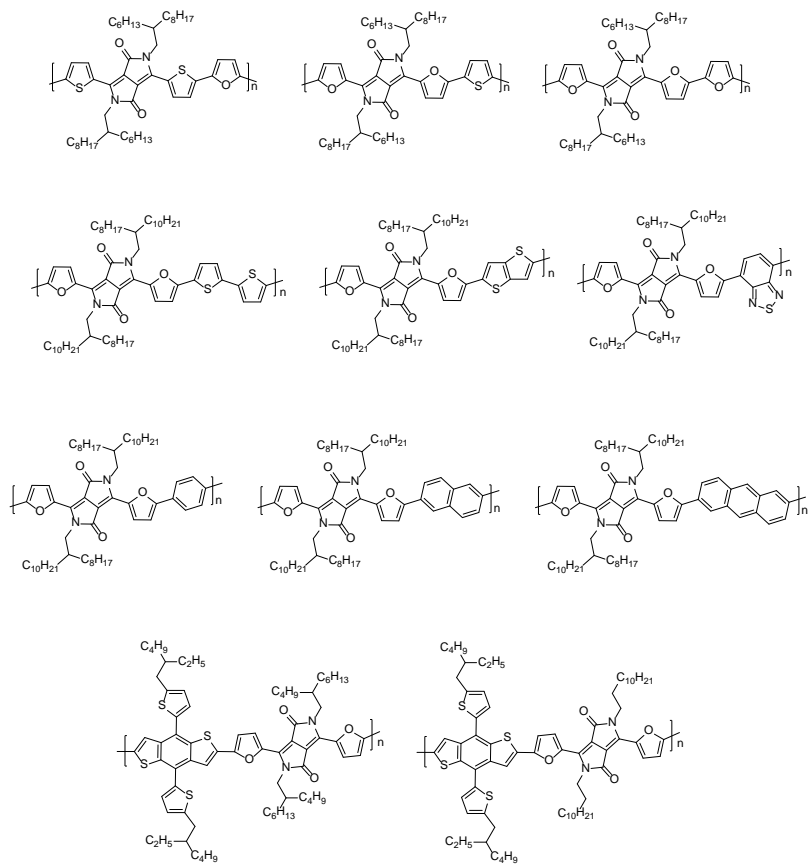
1.2.3 Furan-containing diketopyrrolopyrrole-based materials

The chalcogens are the name designating several atoms in group 16 of periodic table, and the chalcogenophenes substituted with one chalcogen in the ring frame, are belonging to the five-membered heteroaromatic ring compounds, including furan³¹, thiophene^{32,33}, selenophene^{33,34} and tellurophene^{33,34}. In the field of organic semiconducting materials science, a large number of thiophene-containing molecules have been investigated for a long time. Because of not only suitable optoelectronic properties, but also the intra- or intermolecular sulfur-sulfur interactions which are related to the molecular self-assembly, these materials can cause favorable supramolecular structures for advanced device properties.^{31(c)} In contrast, other chalcogenophenes have rarely been discussed for the organic semiconductors, in spite of their promising potentials.

Among them, furan and furan-based materials are available from bio renewable resources attributed to their biodegradable properties, thus considered as “green” materials.³² While furan has lower aromaticity and electron-donating properties, it is more planar and thus easier for dense packing than thiophene^{31(e),35} According to the previous works dealing with furan moieties in the fused aceneblocks³⁶, promising ability of furan was demonstrated as organic semiconducting materials.

A couple of years ago, by Fréchet and coworkers, the first study on furan-containing diketopyrrolopyrrole (DPP) polymers was reported, which exhibited effective solar cell efficiencies compared with thiophene-containing

ones. They also demonstrated that furan-containing DPP polymers had similar optical and electrical properties and even significantly improved solubility for wet-processing.^{37,38} Since then, various polymers (Scheme 1.4)³⁹ have been investigated, expressing enhanced charge transport in transistors as well as high power conversion efficiencies in solar cells.



Scheme 1.4 Chemical structures of DPP-based polymers which contain furan moiety.³⁹

1.3 Research Objectives

The research about the relationships between structure, property and processing has drawn great attention in an area of material science and engineering, recently. I was particularly interested in the interplay of molecular structures and device properties, which is a significant issue for designing materials at a first level. It is important to understand their correlations, since molecular structures can determine self-assembled properties and even supramolecular structures, which are the decisive factors in device functions.

In these days, among the high performing materials, diketopyrrolopyrrole (DPP) unit have been widely used, and its derivatives have proven to be outstanding of organic semiconductors. Since the DPP-based molecules have superior physical, optical and electrical properties, the BHJ organic solar cells have been fabricated, with showing advanced progress.

Especially, I was dealing with incorporating furan moiety along the conjugated backbone of DPP-based small molecules. In general, at the DPP core which shows high electron affinity as electron-accepting (A) block, a variety of thiophene-based electron-donating (D) building blocks have been adopted, owing to their suitable characteristics for advanced functions.²⁴ In this study, I noticed a challenging issue about solubility problem attributed to strong intermolecular hydrogen bonding of the DPP core in common thiophene-containing DPP derivatives. The most general approach to this

problem is introducing long and branched alkyl side chains which inevitably reduce intermolecular π - π stacking and packing property in the film state.

According to related papers, on the other hand, it was found that substitution of furan in DPP-based copolymers shows great solubility and promising potential for replacing thiophene, with comparable device properties.^{37,39(a)} In this regard, I adopted a promising strategy that is incorporation of furan unit in the conjugated backbone, expecting novel design of solution-processable electron donating and accepting materials.

Here, furan moiety was introduced into the π -conjugated backbone with the DPP unit, thereby exploring both donor and acceptor small molecules for solution-processed BHJ solar cells. For the chapter 2, a novel donor molecule which was simply substituted with furan was synthesized, to improve solubility and even align energy levels for the enhanced V_{oc} through more simple procedure. In the chapter 3, I designed low band gap and solution-processable electron-accepting materials which were containing furan moieties in different amounts and at different positions, systematically. From this work, the effects of furan moieties and applications as acceptors in the BHJ organic solar cells were discussed.

1.4 References

1. Becquerel, A. E. *C. R. Hebd. Seances Acad. Sci.* **1839**, *9*, 561.
2. Taguchi, M.; Yano, A.; Tohoda, S.; Matsuyama, K.; Nakamura, Y.; Nishiwaki, T.; Fujita, K. and Maruyama, E. *Photovoltaics* **2014**, *4*, 96.
3. Lin, Y.; Li, Y. and Zhan, X. *Chem. Soc. Rev.* **2012**, *41*, 4245.
4. Fréchet, J. M. J. and Thompson, B. C. *Angew. Chem. Int. Ed.* **2008**, *47*, 58.
5. Delgado, J. L.; Bouit, P. -A.; Filippone, S.; Herranz, M A. and Martín, N. *Chem. Commun.* **2010**, *46*, 4853.
6. Verploegen, E.; Mondal, R.; Bettinger, C. J.; Sok, S.; Toney, M. F. and Bao, Z. *Adv. Funct. Mater.* **2010**, *20*, 3519.
7. Ma, W.; Yang, C.; Gong, X.; Lee, K. and Heeger, A. J. *Adv. Funct. Mater.* **2005**, *15*, 1617.
8. You, J.; Dou, L.; Yoshimura, K.; Kato, T.; Ohya, K.; Moriarty, T.; Emery, K.; Chen, C. -C.; Gao, J.; Li, G. and Yang, Y. *Nature Communications* **2013**, *4*, 1446.
9. Walker, B.; Tamayo, A. B.; Dang, X.-D.; Zalar, P.; Seo, J. H.; Garcia, A.; Tantiwivat, M. and Nguyen, T.-Q. *Adv. Funct. Mater.* **2009**, *19*, 3063.
10. Zhou, J.; Zuo, Y.; Wan, X.; Long, G.; Zhang, Q.; Ni, W.; Liu, Y.; Li, Z.; He, G.; Li, C.; Kan, B.; Li, M. and Chen, Y. *J. Am. Chem. Soc.* **2013**, *135*, 8484.
11. Liu, T. and Troisi, A. *Adv. Mater.* **2013**, *25*, 1038.

12. Beaujuge, P. M. and Fréchet, J. M. J. *J. Am. Chem. Soc.* **2011**, *133*, 20009.
13. (a) Lin, Y.; Ma, L.; Li, Y.; Liu, Y.; Zhu, D. and Zhan, X. *Adv. Energy Mater.* **2013**, *3*, 1166. (b) Lin, Y.; Li, Y. and Zhan, X. *Adv. Energy Mater.* **2013**, *3*, 724.
14. Jiang, B.; Zhang, X.; Zhan, C.; Lu, Z.; Huang, J.; Ding, X.; He, S. and Yao, J. *Polym. Chem.* **2013**, *4*, 4631.
15. (a) Brabec, C. J.; Gowrisanker, S.; Halls, J. J. M.; Laird, D.; Jia, S. and Williams, S. P. *Adv. Mater.* **2010**, *22*, 3839. (b) Helgesen, M.; Søndergaarda, R. and Krebs, F. C. *J. Mater. Chem.* **2010**, *20*, 36. (c) Facchetti, A. *Chem. Mater.* **2011**, *23*, 733. (d) Walker, B.; Kim, C. and Nguyen, T. -Q. *Chem. Mater.* **2011**, *23*, 470. (e) Hains, A. W.; Liang, Z.; Woodhouse, M. A. and Gregg, B. A. *Chem. Rev.* **2010**, *110*, 6689. (f) Liu, F.; Gu, Y.; Shen, X.; Ferdous, S.; Wang, H. -W. and Russell, T. P. *Prog. Polym. Sci.* **2013**, *38*, 1990.
16. Qu, S. and Tian, H. *Chem. Commun.* **2012**, *48*, 3039.
17. Li, Y.; Sonar, P.; Murphya, L. and Hong, W. *Energy Environ. Sci.* **2013**, *6*, 1684.
18. Farnum, D. G.; Mehta, G.; Moore, G. G. I. and Siegel, F. P. *Tetrahedron Lett.* **1974**, *29*, 2549.
19. Iqbal, A. and Cassar, L. *U.S. Pat.* 4,415,685, 1983.
20. Yoon, W. S.; Park, S. K.; Cho, I.; Oh, J.-A.; Kim, J. H. and Park, S. Y. *Adv. Funct. Mater.* **2013**, *23*, 3519.
21. (a) Bijleveld, J. C.; Gevaerts, V. S.; Di Nuzzo, D.; Turbiez, M.;

- Mathijssen, S. G. J.; de Leeuw, D. M.; Wienk, M. M. and Janssen, R. A. *J. Adv. Mater.* **2010**, *22*, E242. (b) Bijleveld, J. C.; Zoombelt, A. P.; Mathijssen, S. G.; Wienk, M. M.; Turbiez, M.; de Leeuw, D. M. and Janssen, R. A. *J. Am. Chem. Soc.* **2009**, *131*, 16616. (c) Hendriks, K. H.; Heintges, G. H. L.; Gevaerts, V. S.; Wienk, M. M. and Janssen, R. A. *J. Angew. Chem. Int. Ed.* **2013**, *52*, 8341.
22. Choi, Y. S. and Jo, W. H. *Organic Electronics* **2013**, *14*, 1621.
23. Li, Y.; Sonar, P.; Singh, S. P.; Soh, M. S.; Meurs, M. v. and Tan, J. *J. Am. Chem. Soc.* **2011**, *133*, 2198.
24. (a) Tamayo, A. B.; Dang, X.-D.; Walker, B.; Seo, J.; Kent, T. and Nguyen, T.-Q. *Appl. Phys. Lett.* **2009**, *94*, 103301. (b) Huang, J.; Jia, H.; Li, L.; Lu, Z.; Zhang, W.; He, W.; Jiang, B.; Tang, A.; Tan, Z.; Zhan, C.; Li, Y. and Yao, J. *Phys. Chem. Chem. Phys.* **2012**, *14*, 14238. (c) Chen, M.; Fu, W.; Shi, M.; Hu, X.; Pan, J.; Ling, J.; Lia, H. and Chen, H. *J. Mater. Chem. A* **2013**, *1*, 105. (d) Lee, J. W.; Choi, Y. S. and Jo, W. H. *Organic Electronics* **2012**, *13*, 3060.
25. (a) Li, Y.; Singh, S. P. and Sonar, P. *Adv. Mater.* **2010**, *22*, 4862. (b) Chen, Z.; Lee, M. J.; Shahid Ashraf, R.; Gu, Y.; Albert-Seifried, S.; Meedom Nielsen, M.; Schroeder, B.; Anthopoulos, T. D.; Heeney, M.; McCulloch, I. and Sirringhaus, H. *Adv. Mater.* **2012**, *24*, 647.
26. (a) Shahid, M.; Ashraf, R. S.; Huang, Z.; Kronemeijer, A. J.; McCarthy-Ward, T.; McCulloch, I.; Durrant, J. R.; Sirringhaus, H. and Heeney, M. *J. Mater. Chem.* **2012**, *22*, 12817. (b) Sonar, P.; Singh, S. P.; Li, Y.; Soh, M. S. and Dodabalapur, A. *Adv. Mater.* **2010**, *22*, 5409.

27. (a) Loser, S.; Bruns, C.; Miyauchi, H.; Ortiz, R. P.; Facchetti, A.; Stupp, S. I. and Marks, T. J. *J. Am. Chem. Soc.* **2011**, *133*, 8142. (b) Lee, O. P.; Yiu, A. T.; Beaujuge, P. M.; Woo, C. H.; Holcombe, T. W.; Millstone, J. E.; Douglas, J. D.; Chen, M. S. and Fréchet, J. M. J. *Adv. Mater.* **2011**, *23*, 5359. (c) Park, J. K.; Kim, C.; Walker, B.; Nguyen, T.-Q. and Seo, J. H. *RSC. Advances* **2012**, *2*, 2232. (d) Liu, J.; Walker, B.; Tamayo, A.; Zhang, Y. and Nguyen, T.-Q. *Adv. Funct. Mater.* **2013**, *23*, 47. (e) Huang, J.; Zhan, C.; Zhang, X.; Zhao, Y.; Lu, Z.; Jia, H.; Jiang, B.; Ye, J.; Zhang, S.; Tang, A.; Liu, Y.; Pei, Q. and Yao, J. *ACS Appl. Mater. Interfaces* **2013**, *5*, 2033. (f) Walker, B.; Liu, J.; Kim, C.; Welch, G. C.; Park, J. K.; Lin, J.; Zalar, P.; Proctor, C. M.; Seo, J. H.; Bazana, G. C. and Nguyen, T.-Q. *Energy Environ. Sci.* **2013**, *6*, 952.
28. Li, Z.; Zhang, Y.; Tsang, S.-W.; Du, X.; Zhou, J.; Tao, Y. and Ding, J. *J. Phys. Chem. C* **2011**, *115*, 18002.
29. (a) Tamayo, A.; Kent, T.; Tantitiwat, M.; Dante, M. A.; Rogers, J. and Nguyen, T.-Q. *Energy Environ. Sci.* **2009**, *2*, 1180. (b) Wang, E.; Hou, L.; Wang, Z.; Ma, Z.; Hellström, S.; Zhuang, W.; Zhang, F.; Inganäs, O. and Andersson, M. R. *Macromolecules* **2011**, *44*, 2067. (c) Lei, T.; Dou, J.-H. and Pei, J. *Adv. Mater.* **2012**, *24*, 6457.
30. (a) Mei, J.; Graham, K. R.; Stalder, R.; Tiwari, S. P.; Cheun, H.; Shim, J.; Yoshio, M.; Nuckolls, C.; Kippelen, B.; Castellano, R. K. and Reynolds, J. R. *Chem. Mater.* **2011**, *23*, 2285. (b) Kanimozhi, C.; Yaacobi-Gross, N.; Chou, K. W.; Amassian, A.; Anthopoulos, T. D. and Patil, S. *J. Am. Chem. Soc.* **2012**, *134*, 16532.

31. (a) Gandini, A. and Belgacem, M. N. *Prog. Polym. Sci.* **1997**, *22*, 1203.
(b) Miyata, Y.; Nishinaga, T. and Komatsu, K. *J. Org. Chem.* **2005**, *70*, 1147. (c) Hayashi, N.; Saito, Y.; Higuchi, H. and Suzuki, K. *J. Phys. Chem. A* **2009**, *113*, 5342. (d) Lundgren, R. J. and Stradiotto, M. *Angew. Chem. Int. Ed.* **2010**, *49*, 5037. (e) Gidron, O.; Dadvand, A.; Sheynin, Y.; Bendikov, M. and Perepichka, D. F. *Chem. Commun.* **2011**, *47*, 1976. (f) Henssler, J. T. and Matzger, A. J. *J. Org. Chem.* **2012**, *77*, 9298.
32. Lipshutz, B. H. *Chem. Rev.* **1986**, *86*, 795.
33. Gronowitz, S. *Phosphorus Sulphur and Silicon*, **1998**, *59*, 136.
34. Gribble, G. W. and Gilchrist, T. L. Progress in Heterocyclic Chemistry In Pelkey, E. T., Editor *Five-membered ring systems: Thiophenes & Se, Te analogs* vol.10, **1998**, 87-108.
35. Bunz, Uwe H. F. *Angew. Chem. Int. Ed.* **2010**, *49*, 5037.
36. (a) Takimiya, K.; Konda, Y.; Ebata, H.; Niihara, N. and Otsubo, T. *J. Org. Chem.* **2005**, *70*, 10569. (b) Takimiya, K.; Kunugi, Y.; Konda, Y.; Niihara, N. and Otsubo, T. *J. Am. Chem. Soc.* **2004**, *126*, 5084. (c) Nakano, M.; Mori, H.; Shinamura, S. and Takimiya, K. *Chem. Mater.* **2012**, *24*, 190. (4) Nakano, M.; Niimi, K.; Miyazaki, E.; Osaka, I. and Takimiya, K. *J. Org. Chem.* **2012**, *77*, 8099.
37. Woo, C. H.; Beaujuge, P. M.; Holcombe, T. W.; Lee, O. P. and Fréchet, J. M. J. *J. Am. Chem. Soc.* **2010**, *132*, 15547.
38. Yiu, A. T.; Beaujuge, P. M.; Lee, O. P.; Woo, C. H.; Toney, M. F.; and Fréchet, J. M. J. *J. Am. Chem. Soc.* **2012**, *134*, 2180.
39. (a) Biljlevled, B. P.; Karsten, S. G. J.; Wienk, M. M.; de Leeuw D. M.

and Janssen, R. A. J. *J. Mater. Chem.* **2011**, *21*, 1600. (b) Li, Y.; Sonar, P.; Singh, S. P.; Zeng, W. and Soh, M. S. *J. Chem. Mater.* **2011**, *21*, 10829. (c) Li, Y.; Sonar, P.; Singh, S. P.; Ooi, Z. E.; Lek, E. S. and Loh, M. Q. *Phys. Chem. Chem. Phys.* **2012**, *14*, 7162. (d) Sonar, P.; Foong, T. R. B.; Singh, S. P.; Li, Y. and Dodabalapur, A. *Chem. Commun.* **2012**, *48*, 8383. (e) Sonar, P.; Singh, S. P.; Williams, E. L.; Li, Y.; Soh, M. S.; and Dodabalapur, A. *J. Mater. Chem.* **2012**, *22*, 4425. (f) Dou, L.; Chang, W.-H.; Gao, J.; Chen, C.-C.; You, J. and Yang, Y. *Adv. Mater.* **2013**, *25*, 825. (g) Chen, C.-C.; Dou, L.; Gao, J.; Chang, W.-H.; Lia, G. and Yang, Y. *Energy Environ. Sci.* **2013**, *6*, 2714.

Chapter 2. Promising Design Concept of Incorporating Furan Moiety into Diketopyrrolopyrrole-Based Donor Molecule for Solution-Processed Organic Solar Cells with Enhanced Solubility and V_{oc}

2.1 Introduction

In order to obtain an ideal donor material in the BHJ organic solar cells, several requirements should be achieved for the high performing devices: (1) sufficient light absorption throughout broad region, (2) high short circuit current (J_{sc}) derived from efficient charge carrier transport, and (3) high open circuit voltage (V_{oc}) and suitable molecular orbitals for exciton dissociation.¹ A low band gap material might be one of strategy to gain broad and strong light absorption. Generally, it can be synthesized with electron-donating (D) and electron-accepting (A) units in alternative combination. According to the D and A units in the structure, the molecular orbitals are also determined, thus considering the V_{oc} and exciton dissociation at the same time. The difference between LUMO energy levels of donor and acceptor materials should be larger than 0.3 eV for the exciton dissociation; hence there is a limitation of

LUMO level of donor material. Meanwhile, since the V_{oc} can be determined from the difference between HOMO level of donor and LUMO level of acceptor, a high-lying HOMO level derived from obtaining low band gap material leads to sacrifice the value of V_{oc} . Furthermore, high J_{sc} can be also established by the structures of constructing units of D-A type molecules. Because the charge carrier mobility is favored in effectively packed crystalline structures, incorporating planar molecular structures of D and A units can enhance the value of J_{sc} .

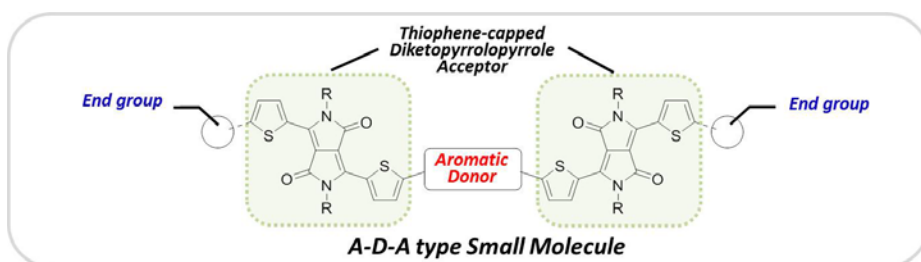
In this chapter, with the purpose of above requirements, I studied several A-D-A type small molecules for donor materials in the organic solar cells, where A is thiophene-containing diketopyrrolopyrrole (DPP) and D is electron-donating unit based on thiophene derivatives, such as thiophene², bithiophene¹, thienothiophene¹, and dithienothiophene (DTT)³, as shown in the Figure 2.1. Among the materials, I noticed some parameters for the high performance organic solar cells. (1) Compared to compound **A**² which hasn't any electron donating unit, others showed lower V_{oc} s due to raising HOMO energy levels. However, there are little difference among compound **B**², **C**¹ and **D**¹, except for **T1** (**DTTDPP**)³. (2) Relative high J_{sc} s can be obtained in the compound **D** and **T1** incorporated with fused aromatic thiophene rings as electron-donating units, owing to their planar molecular structures favoring efficient packing. (3) Unlike other compounds, only **T1** has additional end groups of two hexyl thiophene, thus resulting extended π -conjugation length for the low optical band gap, high-lying HOMO energy levels and low V_{oc} , as well as complicated synthetic procedure.

Herein, I've especially interested in **T1**, an A-D-A type small molecule donor material, which was reported by Seo, *et al.*, in last year. As shown in the Figure 2.1, **T1** consists of two electron-accepting DPP units with thiophene linkages, and an electron-donating DTT block which shows great rigidity and planarity, thus favoring highly ordered π -stacked structures in the film state.⁴ When it was fabricated with PC₇₁BM acceptor in the BHJ organic solar cells, **T1** exhibited disappointing device properties, like PCEs of 0.33-0.48% without additive, which is pretty lower than other A-D-A type small molecules, such as **B**, **C** and **D**. Through further optimization of film morphology by using additive, efficiency was enhanced up to 2.19% with 1 vol% of 1-chloronaphthalene (CN) condition.

The main reason for those low properties could be explained by low values of V_{oc} , which were only ~ 0.57 V. In general, open circuit voltage, V_{oc} is determined by the energy differences between the LUMO of the acceptor and the HOMO of the donor material, and allowing devices to attain driving force to charge separation.⁵ For the **T1**, since low V_{oc} was attributed to relative high-lying HOMO level (-5.0 eV), energy level alignment is required to improve device performances. According to this point of view, it would be the simplest designing method to remove two hexyl thiophene units from at the both ends of **T1** molecule, thus generating **T2** described in Scheme 2.1. The **T2** can be prepared by quite easier and shorter synthetic process, moreover its HOMO level would be lowered sufficiently. However, in the reported paper, there wasn't any comment or discussion about **T2**, even though it was synthesized during the synthetic process. At this time, I paid attention to a challenging

issue about solubility problem in common thiophene-containing DPP small molecules. The most general approach to this problem is introducing long and branched alkyl side chains. Because of low solubility of **T2** without two hexyl solubilizing alkyl chains, it seems not to be fabricated for wet-processing devices.

Based on above reasonable insights related with solubility issue, I adopted a promising strategy that is incorporation of furan unit in the conjugated backbone, expecting novel design of solution-processable donor material.⁶ In this study, I synthesized and characterized **F2** (Scheme 2.1), a new small molecule with replacing thiophene with furan moiety. Its design concept was followed by two motives: 1) to achieve high photovoltage, V_{oc} , through low-lying HOMO level, and 2) to impart sufficient solubility for wet-processing, without aid of long and branched alkyl chains which might be causing unintended film morphology. In addition, I also prepared a control molecule, **F1**, containing furan unit as well as two hexyl thiophene groups. The BHJ organic solar cells were fabricated with **F2** as a donor material and PC₆₁BM as an acceptor material, thus yielding PCEs of 2.1% with 1 vol% of DIO, and enhancing V_{oc} up to 0.75 V.



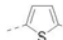
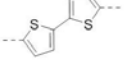
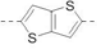
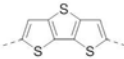
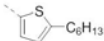
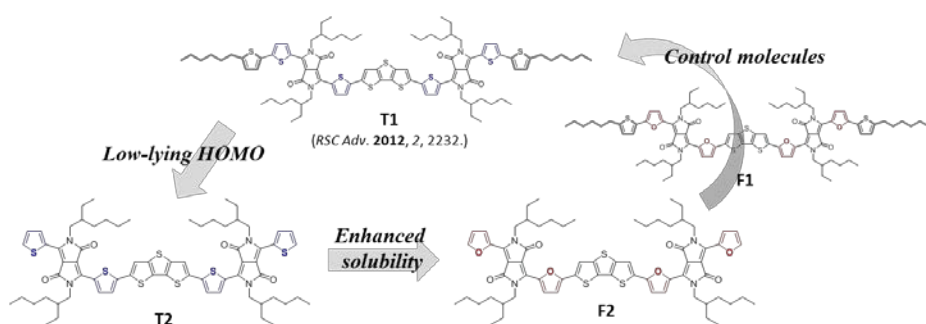
	Aromatic Donor	End group	
A	None	H	HOMO=-5.19 eV, LUMO=-3.68 eV, $E_g^{opt}=1.51$ eV PCE=2.31%, $V_{oc}=0.84$ V, $J_{sc}=7.40$ mA/cm ² , FF=37%
B		H	HOMO=-5.17 eV, LUMO=-3.66 eV, $E_g^{opt}=1.51$ eV PCE=1.49%, $V_{oc}=0.80$ V, $J_{sc}=4.30$ mA/cm ² , FF=43%
C		H	HOMO=-5.14 eV, LUMO=-3.49 eV, $E_g^{opt}=1.65$ eV PCE=3.0%, $V_{oc}=0.78$ V, $J_{sc}=6.8$ mA/cm ² , FF=57%
D		H	HOMO=-5.11 eV, LUMO=-3.51 eV, $E_g^{opt}=1.60$ eV PCE=4.0%, $V_{oc}=0.81$ V, $J_{sc}=9.3$ mA/cm ² , FF=53%
T1 (DTTDP)			HOMO=-5.0 eV, LUMO=-3.5 eV, $E_g^{opt}=1.5$ eV PCE=2.19%, $V_{oc}=0.57$ V, $J_{sc}=7.67$ mA/cm ² , FF=50%

Figure 2.1 Chemical structures of several A-D-A type small molecules for donor materials, with their energy levels, optical band gap, and photovoltaic properties.

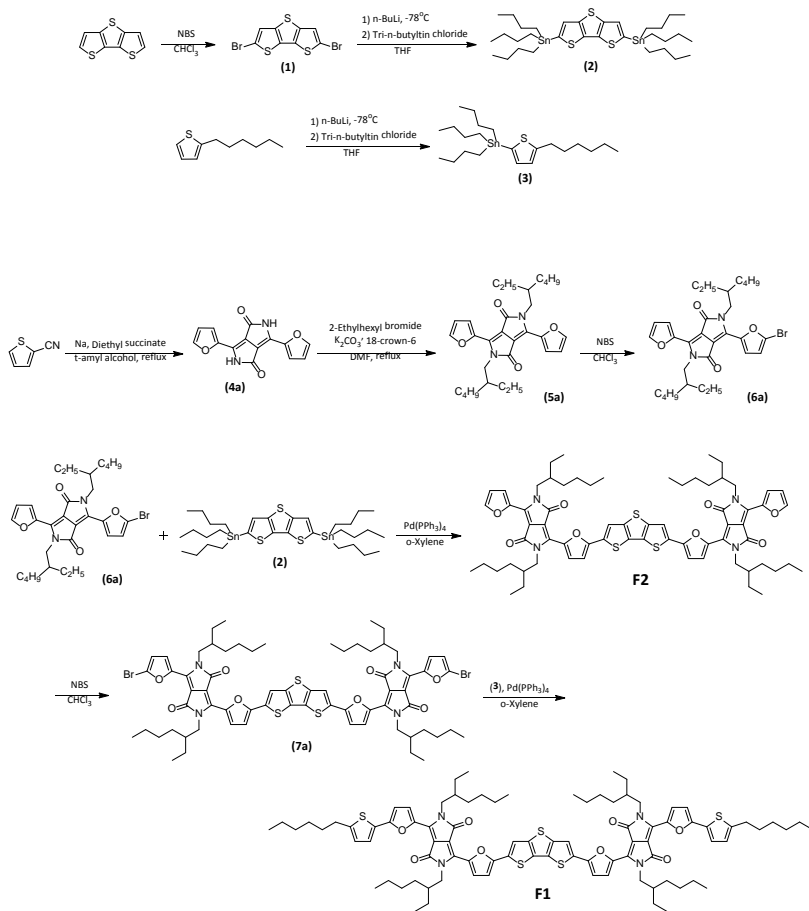


Scheme 2.1 Chemical structures of **T1**, **F1**, **T2** and **F2** with design strategies.

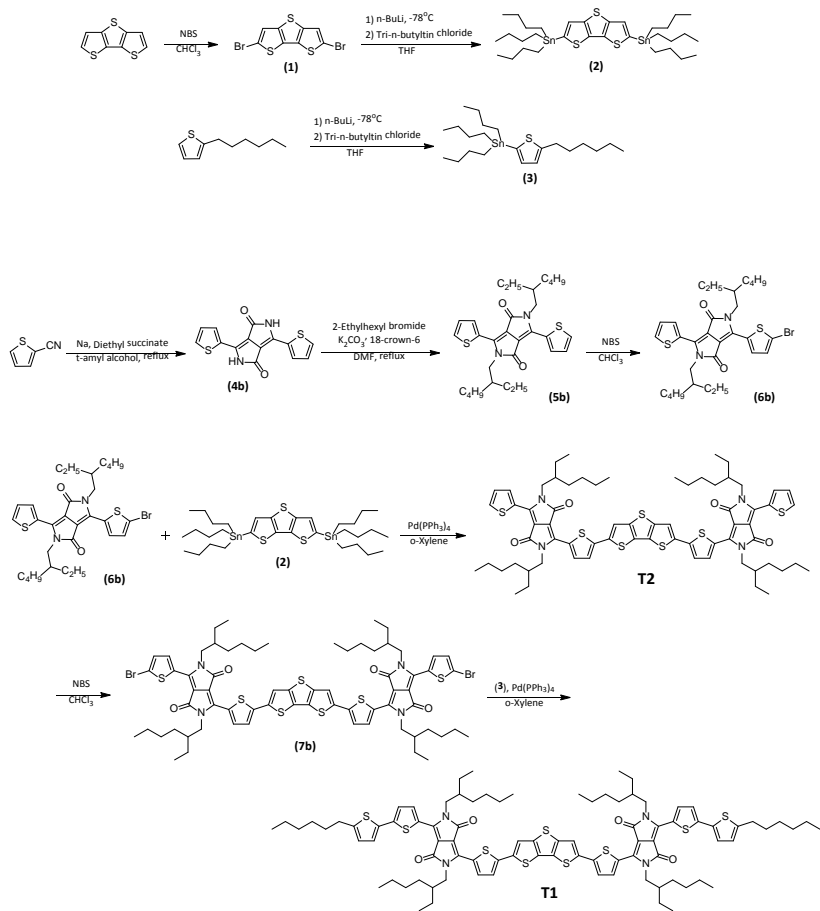
2.2 Experimental section

2.2.1 Synthesis

Scheme 2.2 illustrated a synthetic procedure of a target material, **F2**, a control material, **F1**. And reference materials, both **T1** and **T2**, were also prepared by using synthetic scheme of Scheme 2.3. All reagents were commercially available from Sigma-Aldrich, TCI chemicals, and Alfa-Aesar. The solvents which were used in each reaction were purchased from above companies or Junsei chemicals without further purification, except tetrahydrofuran (THF), freshly distilled one before use. Other chemicals required during workup or purifying processes in each procedure were affordable from Samchun Chemicals and Daejung Chemicals & Metals. The reference materials and target material were synthesized according to the literature, with some modification in case of need.



Scheme 2.2 Synthesis of **F1** and **F2**.



Scheme 2.3 Synthesis of **T1** and **T2**.

Synthesis of 2,6-dibromodithieno[3,2-*b*:2',3'-*d*]thiophene (1): To a 100 mL three-neck round bottom flask, dithieno[3,2-*b*:2',3'-*d*]thiophene (465 mg, 2.37 mmol) was dissolved in chloroform (25 mL) and acetic acid (25 mL), stirred it for 30 min at 0 °C. In the dark, N-bromosuccinimide (NBS, 940 mg, 5.26 mmol) was added in step-wise. After 1 hr, it was stirred for 1 hr more, at room temperature. To neutralize this solution, 20% NaOH solution (50 mL) was added at 0 °C, then solution was washed with water, and extracted using methylene chloride. After it was dried over magnesium sulfate, the crude product was purified by using silica gel column chromatography with methylene chloride eluent. Solvent was removed under reduced pressure, and then white solid product of 731 mg was affordable by methanol filtration. (Yield = 87%) ¹H NMR (300 MHz, CDCl₃): δ (ppm) 7.28 (s, 2H).

Synthesis of 2,6-bis(tri-*n*-butylstannyl)dithieno[3,2-*b*:2',3'-*d*]thiophene (2): Before added compound **1** (320 mg, 0.904 mmol) to a 100 mL three-neck round bottom flask, prepared flask dried condition, by heating harshly using a torch for more than 3 times. Then let it in argon atmosphere for 30 min. Fresh distilled THF (12 mL) was added, then cooling at -78 °C. After 30 min, 1.6 M solution of *n*-BuLi in *n*-Hex (1.24 mL, 2.00 mmol) was added by dropwise. The solution was stirred for 1hr, then put tri-*n*-butyltin chloride (0.54 mL, 2.00 mmol), slowly. After 10 min, the solution was stirred for 3 hrs at room temperature. The solution was washed with water, extracted by using *n*-Hex, and then dried over MgSO₄. After evaporation, the crude product was dissolved in 50 mL of triethylamine (TEA), and stirred together for 2 hrs. It

was further purified by column chromatography of TEA-pretreated silica gel using n-Hex, quickly, thus affording pale yellow liquid product. ¹H NMR (300 MHz, CDCl₃): δ (ppm) 7.25 (s, 2H), 1.59 (m, 12H), 1.34 (m, 12H), 1.15 (m, 12H), 0.90 (m, 18H).

Synthesis of 2-(tri-*n*-butylstannyl)-5-hexylthiophene (3): A 100 mL three-neck round bottom flask was heated harshly using a torch, for more than 3 times. Then, added 2-hexylthiophene (1.0 g, 5.94 mmol) and fresh distilled THF (30 mL) together, in argon condition. At -78 °C, after the solution was stirred for 20 min, 1.6M n-BuLi in n-Hex (4.09 mL, 6.54 mmol) was added dropwise. After 30 min at -78 °C, the solution was stirred for further 30 min at the room temperature. The reaction temperature was cooled down -78 °C again, then leading additional stirring for 20 min. Tributyltin chloride (1.93 mL, 7.13 mmol) was added by dropping and the solution was stirred for 30min. At room temperature, it was stirred for overnight. After the reaction was completed, the solution was poured into water and extracted with diethyl ether. The organic phase was dried over magnesium sulfate, then affording light yellow liquid form of product. ¹H NMR (300 MHz, CDCl₃): δ (ppm) 6.98 (d, 1H), 6.90 (d, 1H), 2.85 (t, 2H), 1.74-0.68 (m, 38H).

Synthesis of 3,6-di(furan-2-yl)pyrrolo[3,4-*c*]pyrrole-1,4(2H,5H)-dione (4a): Under nitrogen atmosphere, small sodium metal pieces (2.47 g, 107 mmol) were added in tert-amyl alcohol (60 mL) to a 250 mL two-neck round bottom flask connected with reflux system, and then the solution was stirred

overnight at 120 °C. After all of sodium metals were dissolved, furan-2-carbonitrile (5.00 g, 53.7 mmol) was added. Diethyl succinate (3.74 g, 21.5 mmol) was then injected by dropping, and the solution was stirred for 3 hrs. After cooled to room temperature, the mixture was poured in 200 mL of MeOH and 10 mL of HCl solution at 0 °C. After stirred for 1.5 hrs at room temperature, the precipitated product was filtered and washed several times using MeOH, thereby collecting dark purple solid. This procedure was repeated with 2.5 g (26.9 mmol) scale of furan-2-carbonitrile, therefore total affording 9.1 g of product. (Yield = 42-44%)

Synthesis of 3,6-di(thiophene-2-yl)pyrrolo[3,4-*c*]pyrrole-1,4(2H,5H)-dione (4b): This compound was prepared by the same procedure as that described for compound **4a** with 2-thiophenecarbonitrile (10.0 g, 91.62 mmol), affording 17.8 g. (Yield = 65%)

Synthesis of 2,5-di-(2-ethylhexyl)-3,6-di(furan-2-yl)pyrrolo[3,4-*c*]pyrrole-1,4(2H,5H)-dione (5a): Put compound **4a** (7.00 g, 26.1 mmol), K₂CO₃ (11.9 g, 86.1 mmol), 18-crown-6 ether (0.76 g, 2.87 mmol) and 200 mL of DMF into 500 mL two-neck round bottom flask, and then connected a condenser and 100 mL dropping funnel. While the solution was stirred until temperature rose to 120 °C, prepared 2-ethylhexylbromide (16.6 g, 86.1 mmol) dissolved in 30 mL of DMF. By using dropping funnel, put the mixture into the solution of flask, and then further stirred it for 2 days. After cooled to room temperature, organic layer was extracted using diethyl ether and brine. After

the crude product dried over magnesium sulfate was purified by column chromatography using CHCl_3 , re-precipitation was followed by using excess amount of cold MeOH. Finally, resulting 4.86 g of red-orange solid was isolated. (Yield = 38%) $^1\text{H NMR}$ (300 MHz, CDCl_3): δ (ppm) 8.33 (d, 2H), 7.61 (d, 2H), 6.69 (dd, 2H), 4.04 (d, 4H), 1.80-1.68 (m, 2H), 1.39-1.26 (m, 16H), 0.95-0.85 (m, 12H).

Synthesis of 2,5-di-(2-ethylhexyl)-3,6-di(thiophene-2-yl)pyrrolo[3,4-c]pyrrole-1,4(2H,5H)-dione (5b): This compound was prepared by the same reaction condition as that described for compound **5a** with compound **4b** (10.0 g, 33.3 mmol), except that it took just overnight for the reaction at 120 °C. After same procedures, the extracted and dried crude product was precipitated with cold MeOH to afford dark red solid product. Without column chromatography, 3.56 g of product was isolated. (Yield = 20%) $^1\text{H NMR}$ (300 MHz, CDCl_3): δ (ppm) 8.89 (dd, 2H), 7.63 (dd, 2H), 7.28 (d, 2H), 4.05 (dd, 4H), 1.8-1.9 (m, 2H), 1.2-1.4 (m, 16H), 0.8-1.0 (m, 12H).

Synthesis of 3-(5-bromofuran-2-yl)-2,5-di-(2-ethylhexyl)-6-(furan-2-yl)pyrrolo[3,4-c]pyrrole-1,4(2H,5H)-dione (6a): The compound **5a** (1.00 g, 2.03 mmol) was dissolved in CHCl_3 (30 mL) by using 100 mL two-neck round bottom flask, then cooled at 0 °C. In the dark, N-bromosuccinimide (NBS, 0.36 g, 2.03 mmol) was added in portions slowly, and stirred for 5 hrs at room temperature. The resulting solution was poured into water and diluted using methylene chloride, and then for only organic phase extracted. After

dried over MgSO₄, the crude was purified by column chromatography with silica gel packed. By using mixed eluent (CHCl₃:n-Hex=1:1), pure product was separated, thus isolated 400mg through precipitation in cold MeOH. (Yield = 34%) ¹H NMR (300 MHz, CDCl₃): δ (ppm) 8.34 (d, 1H), 8.29 (d, 1H), 7.62 (d, 1H), 6.69 (dd, 1H), 6.34 (d, 1H), 4.02 (t, 4H), 1.75 (m, 2H), 1.39-1.26 (m, 16H), 0.95-0.84 (m, 12H).

Synthesis of 3-(5-bromothiophene-2-yl)-2,5-di-(2-ethylhexyl)-6-(thiophene-2-yl)pyrrolo[3,4-c]pyrrole-1,4(2H,5H)-dione (6b): This compound was prepared by the same procedure as described for compound **6a**, with using a compound **5b** (790 mg, 1.51 mmol), thus affording 495 mg of dark red powder. (Yield = 54%) ¹H NMR (300 MHz, CDCl₃): δ (ppm) 8.90 (dd, 1H), 8.63 (d, 1H) 7.64 (dd, 1H), 7.29–7.22 (m, 2H), 4.03–3.92 (m, 4H), 1.84 (m, 2H), 1.38–1.23 (m, 16H), 0.91–0.85 (m, 12H).

Synthesis of F2: The compound **5a** (300 mg, 0.525 mmol) was dissolved in anhydrous o-xylene (7 mL). Added the argon-purged solution into the 10 mL microwave tube with compound **2** (203 mg, 0.262 mmol) and Pd(PPh₃)₄ (15 mg, 0.013 mmol), and sealed the cap as fast as possible. The tube was subjected to the following reaction procedures in a microwave reactor; pre-stirring for 2 min, 120 °C for 1min, 140 °C for 1min, 160 °C for 1 min, and 175 °C for 1 h. After reaction and cooling, the resulting product was precipitated in cold MeOH. The filtered residual solid was further purified by column chromatography on a silica gel. The first eluent is the mixture of

CHCl₃:n-Hex = 4:1, which separated side products out, and the second eluent is adding 1 vol% triethylamine (TEA) into the first eluent. After evaporated under vacuum and recrystallized in ethyl acetate, the 220 mg of purple solid was isolated. (Yield = 35-50%) ¹H NMR (300 MHz, CDCl₃): δ (ppm) 8.46 (d, 2H), 8.35 (d, 2H), 7.61 (d, 2H), 7.56 (s, 2H), 6.87 (d, 2H), 6.69 (dd, 2H), 4.15-4.03 (m, 8H), 1.93 (m, 2H), 1.76 (m, 2H), 1.42-1.26 (m, 32H), 0.95-0.87 (m, 24H). MS (m/z): [M]⁺ calculated for C₆₈H₈₀N₄O₈S₃, 1177.52; found 1177.52.

Synthesis of T2: This compound was prepared by the same procedure as described for compound **F2**, with using a compound **6b** (0.25 g, 0.414 mmol) and a microwave reactor, thus affording 140 mg of purple colored powder. (Yield = 55%) ¹H NMR (300 MHz, CDCl₃): δ (ppm) 8.95 (d, 2H), 8.90 (d, 2H), 7.62 (d, 2H), 7.50 (s, 2H), 7.36 (d, 2H), 7.32 (d, 2H), 4.04 (m, 8H), 1.93 (m, 4H), 1.37-1.25 (m, 32H), 0.96-0.86 (m, 24H).

Synthesis of compound 7a: To a 250mL two-neck round bottom flask, the **F2** (350 mg, 0.297 mmol) was dissolved in 100 mL of CHCl₃. At 0 °C, in the dark, N-bromosuccinimide (NBS, 110 mg, 0.624 mmol) was added in portions. The solution was stirred for overnight at room temperature, and then organic phase was extracted with chloroform. After dried over MgSO₄, the crude product was purified by column chromatography on a silica gel using mixed eluent (CHCl₃:n-Hex = 4:1, adding triethylamine 1 vol%). The dark blue precipitates were affordable by using cold MeOH, thus isolating 356 mg

of product. (Yield = 90%) ^1H NMR (300 MHz, CDCl_3): δ (ppm) 8.53 (d, 2H), 8.29 (dd, 2H), 7.53 (s, 2H), 6.85 (d, 2H), 6.60 (d, 2H), 4.12-3.98 (m, 8H), 1.91-1.73 (m, 4H), 1.43-1.30 (m, 32H), 0.93-0.88 (m, 24H).

Synthesis of compound 7b: This compound was prepared by the same procedure as described for compound **7a**, with using a compound **T2** (100 mg, 0.081 mmol), thus 50 mg of product. (Yield = 44%) ^1H NMR (300 MHz, CDCl_3): δ (ppm) 8.96 (d, 2H), 8.65 (dd, 2H), 7.47 (s, 2H), 7.43 (d, 2H), 7.23 (d, 2H), 4.03-3.95 (m, 8H), 1.92-1.86 (m, 4H), 1.43-1.25 (m, 32H), 0.96-0.88 (m, 24H).

Synthesis of F1: Compound **7a** (80 mg, 0.060 mmol) was dissolved in 8 mL of anhydrous o-xylene, and argon purged for 10 min. To a 10 mL microwave tube, added compound **3** (67 mg, 0.146 mmol) and $\text{Pd}(\text{PPh}_3)_4$ (16 mg, 0.014 mmol), with this solution together, cautiously. Using a microwave reactor, the same reaction conditions as described for compound **F2** were followed. After resulting solution was precipitated in cold MeOH, the residual solid was further purified by column chromatography using CHCl_3 adding 1 vol% of triethylamine as an eluent. Removed solvent, and then 64 mg of the dark blue powder form was isolated from precipitation in cold MeOH. (Yield = 71%) ^1H NMR (300 MHz, CDCl_3): δ (ppm) 8.50-8.41 (m, 4H), 7.45 (s, 2H), 7.17 (d, 2H), 6.81 (d, 2H), 6.73 (d, 2H), 6.68 (d, 2H), 4.11-4.06 (m, 8H), 2.88-2.79 (m, 4H), 1.92 (bs, 4H), 1.69 (bs, 4H), 1.39-1.26 (m, 44H), 0.92-0.85 (m, 30H).

Synthesis of T1: This compound was prepared by the same procedure as described for compound **F1**, with using a compound **7b** (40 mg, 0.087 mmol) and a microwave reactor, thus affording 28 mg of dark blue colored powder. (Yield = 49%) ¹H NMR (300 MHz, CDCl₃): δ (ppm) 9.04-8.90 (m, 4H), 7.39 (s, 2H), 7.17 (d, 2H), 7.13 (d, 2H), 7.09 (d, 2H), 6.73 (d, 2H), 4.20-3.98 (m, 8H), 2.80-2.75 (m, 4H), 1.99-1.91 (m, 4H), 1.68-1.65 (m, 4H), 1.50-1.20 (m, 44H), 0.99-0.85 (m, 30H).

2.2.2 Characterization methods and instrumental measurements

Chemical structures were identified by ^1H NMR spectra obtained from a Bruker Avance DPX 300 NMR spectrometer with deuterated chloroform (CDCl_3) solvent. Density functional theory (DFT) calculation was accomplished with Gaussian09 quantum-chemical package at B3LYP/6-31G (d, p) level, and optimized by global minimum, in the gas phase. The program of Gauss View 5.0 was explored, providing information about optimized ground state geometry and electron density at HOMO and LUMO states. The solubility of materials was measured by using a 0.50 μm PTFE syringe filter which was purchased from Toyo Roshi Kaisha. Photophysical properties were performed by UV-Vis spectrophotometer (SHIMADZU UV-1650PC), in both solution and film state. The materials' energy levels were characterized by measuring their work function obtained from ultraviolet photoelectron spectrometer (Hitachi High Tech, AC-2), thereby determining HOMO levels. The LUMO level was calculated by the difference of optical band gap energy and HOMO level. The study on thin film morphology was carried out through atomic force microscopy (AFM), whose operating measurement is a Multimode with a NanoScope V controller, Bruker.

2.2.3 Device fabrication and measurements of solar cells

The materials comprising solar cell device were purchased and fabricated according to following terms. The ITO glass substrates exhibiting a sheet resistance of less than $10 \Omega/\text{square}$ were cleaned with three steps in ultrasonication bath; each step was taking 10min, by using trichloroethylene, acetone, and isopropyl alcohol respectively. After these washed glasses were dried by blowing nitrogen stream, exposed to UV light (360 nm) for 20 min. On the substrate, PEDOT:PSS (Clevios P VP AI 4083) was spin-coated at 5000 rpm for 30 sec, achieving 30 nm of thickness, and baked at $150 \text{ }^\circ\text{C}$ for 20 min. The day before device fabrication, the synthetic materials and PC_{61}BM (Nano-C), or PC_{71}BM (Nano-C) dissolved in anhydrous chloroform were prepared without or with 1,8-diiodooctane (DIO) followed by stirring for overnight. These prepared solutions were spin-coated on the PEDOT:PSS layer, thus providing approximately 70nm of thickness for active layer. (KLA Tencor, Nanospec AFT/200) The aluminum at the cathode was deposited on the top by thermal evaporation, thus accomplishing 100 nm thick electrodes. The effective active area of each cell was 0.04 cm^2 .

The photovoltaic properties were characterized by the current density-voltage (J - V) curves, which were accomplished with a Keithley 4200 source measurement unit. The solar simulation conditions provided by an Oriel Sol 3A were under AM 1.5G ($100 \text{ mW}/\text{cm}^2$). The J - V characteristics were measured by using a metal mask of 0.04 cm^2 .

2.3 Result and discussion

2.3.1 Synthesis and characterization

In the BHJ organic solar cells, small molecules have been widely used for both donor and acceptor materials, based on following advantages; independency on molecular weight, high reproducibility to device fabrication, greater tendency of self-assembly, relative easiness of synthesis and purification, and free of processing against end-group contamination.⁷ In order to design high performing organic semiconducting small molecules, the optimum combination of the electron-donating (D) and electron-accepting (A) unit is essential, thereby facilitating efficient ICT and remaining planar geometry.

I was interested in diketopyrrolopyrrole (DPP) and dithienothiophene (DTT) units, as electron-accepting (A) and electron-donating (D) building blocks, respectively. In recent year, Seo, *et al.* have already represented a novel A-D-A type small molecule, which were comprised with an DTT and two DPP units, named **T1**.³ This low band gap (~1.5 eV) material exhibited power conversion efficiency of 2.19%, with PC₇₁BM acceptor and 1 vol% CN in the active layer condition. In spite of superior building blocks, such as DTT and DPP, however, its efficiency was quiet lower than my expectations. I found the main reason in the low V_{oc} value, which was less than 0.57 V, resulting from high-lying HOMO level of **T1** (-5.0 eV).

In this respect, I considered **T2** which has lower HOMO levels than **T1** as donor materials, to enhance V_{oc} . However, fundamental characteristics as well

as photovoltaic properties of **T2** have been reported, even though it was synthesized during the process. To my knowledge, low solubility of **T2** without two hexyl solubilizing alkyl chains might be a challenging issue, which is the problem discovered in common thiophene-containing DPP derivatives.

Hence I synthesized **F2**, which has furan moieties instead of thiophene, in order to improve solubility, maintaining same amounts of side chains at the DPP core. This is a promising design strategy to improve solubility as well as V_{oc} , with much easier synthetic process, and without aid of additional solubilizing alkyl chains which might cause unintended film morphology.

Herein, **F2** was successfully synthesized by using Stille coupling and conventional reactions with some modifications. In addition, as a control molecule, **F1** was also prepared. I referred to the paper³ for preparing **T1** and **T2** as comparative materials. Final materials were purified with several repetitive column chromatographies on a silica gel, and kept in argon-purged vial with dried and pure condition. All of synthetic molecular structures were identified by ^1H NMR spectroscopy.

2.3.2 Density functional theory (DFT) calculation

By using density functional theory (DFT) calculations, the optimized geometry and electron density of frontier energy levels in gas phase were obtained as shown in Figure 2.2, and calculated energy levels were arranged in Table 2.1. To identify the effects of hexyl thiophene and furan moiety in those materials briefly, theoretical calculation was carried out for energy-minimized structure of methyl-substituted **T1**, **F1**, **T2** and **F2**.

As you can see in the front view, dithienothiophene (DTT) and diketopyrrolopyrrole (DPP) units could maintain their planarity along the both thiophene and furan linkages. However, a slight tilt in the geometry of **T1** was found because of hexyl thiophene at the ends, estimating around 19.6 ° of torsion angle. Interestingly, I couldn't observe such tilt in the optimized geometry of **F1**, despite it is substituted with hexyl thiophene. On the other hand, **T2** and **F2**, without hexyl thiophene, showed excellent structural planarity, which favors efficient intermolecular π - π overlaps and charge carrier transport.

Due to the smaller atomic radius of oxygen, furan moieties affected more compact geometry of **F2**, thus resulting in shorter lineal distance than that of **T2**. You can see the similar effect in **F1** compared to the **T1**, as well.

The theoretical molecular orbital of target materials agreed well with my expectation. Since thiophene which has been widely used for electron-donating unit could raise molecular HOMO level, **T2** had pretty lower energy state in gas phase. However, the substitution of thiophene with furan also

affects molecular orbital significantly in DFT calculation. Though furan-containing molecules commonly exhibit high-lying HOMO over thiophene-containing ones, the result of calculation in the Table 2.1 might overstate this effect. The HOMO level of **F1** and **F2** would be aligned slight highly over that of **T1** and **T2**, but the difference might be quiet smaller than the difference between **T1** and **T2**. From the Table 2.1, the low-lying HOMO level of both **T2** and **F2** which are without hexyl thiophene was successfully estimated by the theoretical calculation.

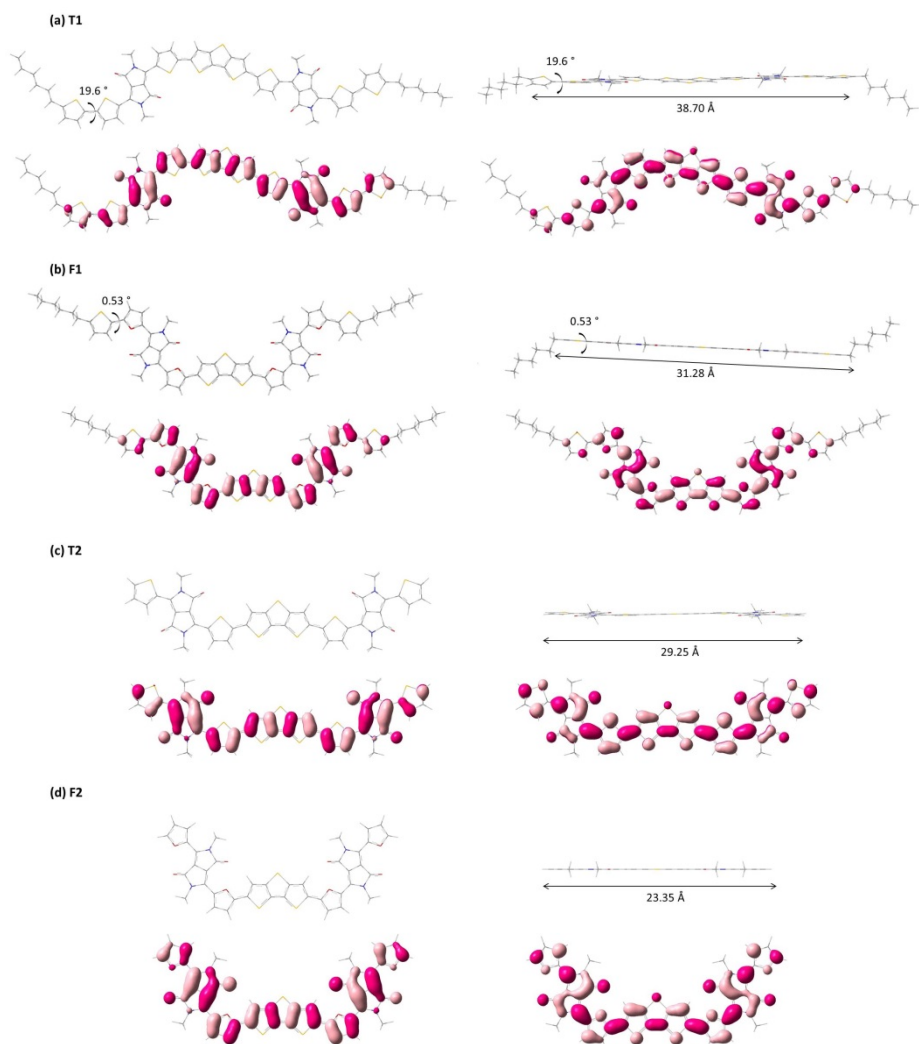


Figure 2.2 Energy-minimized structure (B3LYP/6-31G(d, p)) of a methyl-substituted **(a) T1**, **(b) F1**, **(c) T2** and **(d) F2** (top/front view) with lineal distance along the molecular π -conjugated backbone and visualization of the HOMO (left) and LUMO (right) molecular orbital. Optimized ground state geometry was obtained from Gaussian view 5.0.

Table 2.1 Theoretical molecular orbital of **T1**, **F1**, **T2** and **F2** by DFT calculations.

	HOMO (eV)	LUMO (eV)	E_g (eV) ^{b)}
T1 ^{a)}	-4.64	-2.80	1.84
F1 ^{a)}	-4.52	-2.58	1.94
T2 ^{a)}	-4.79	-2.83	1.96
F2 ^{a)}	-4.66	-2.61	2.05

^{a)} DFT calculation was carried out on molecular structures of **T1**, **F1**, **T2** and **F2** modified with methyl group at N-position in lactam unit, instead of 2-ethylhexyl group. ^{b)} Calculated from the differences between theoretical HOMO and LUMO levels.

2.3.3 Solubility assay

In the BHJ organic solar cells, the active layer has to maintain optimum thickness to satisfy two contradictory requisitions simultaneously: one is absorbing sufficient photon energy with a thick layer, and the other is facilitating charge transport with a short distance between two electrodes. The easiest method to control film thickness is changing concentration of blend solution, which emphasizes solubility issue. Here, solubility of the materials was measured by using a 0.50 μm PTFE syringe filter which was purchased from Toyo Roshi Kaisha. I prepared 7 mg, 10 mg, 20 mg, 25 mg, and 30 mg of **F1** and **F2** in the 8 mL of vials, and then added 1 mL of chloroform solvent, respectively. After mild heating, solution was ejected using a syringe with this filter. Next, injecting solution into the vial, the syringe filter was then examined whether there were remained undissolved molecules, or not. At the same procedure, I prepared 5 mg, 7 mg, 10 mg, 12 mg, and 15 mg of **T1** and **T2** in the 8 mL of vials, as well.

For the **F2**, 25 mg was completely soluble in the 1 mL of chloroform, without much effort to dissolve. However, **T2** was quite insoluble at 7 mg/mL concentration. To dissolve 7 mg of **T2**, more solvent should be added. With much effort, such as heating and using an ultra-sonication, 5 mg of **T2** was barely dissolved in 1 mL of chloroform, but it is hard to maintain solution state in the room temperature. For the **T1**, 7 mg was soluble in the 1 mL of chloroform with much effort. On the other hand, 12 mg of **F1** was dissolved in 1 mL of chloroform, easily.

From the experimental process, I concluded that furan-containing **F2** has great solubility of over 25 mg/mL rather than **T2** (5 mg/mL), **T1** (7 mg/mL) and even **F1** (12 mg/mL), which indicates **F2** would be suitable for solution processed organic solar cells. It was interesting that solubility of **F1** substituted with hexyl thiophene at the both ends was quite lower than that of **F2**.

2.3.4 Photophysical properties

In order to compare photophysical properties of **T2** and **F2** with a reference and control material, **T1** and **F1**, the optical characteristics were investigated by using UV-Vis absorption spectroscopy, at the same condition in the reported paper³. The specific condition was noted at the below of the table. The UV-Vis absorption spectra of target materials was recorded in both solution and film state, which results in the Figure 2.3 and Table 2.2.

In the solution state, all of absorption spectra displayed similar profiles. However, molar absorption coefficient (ϵ_{\max}) significantly increased when furan moiety was introduced. Such large molar absorptivity of **F1** and **F2** would facilitate charge carrier transport and contribute improving current in solar cells.

In the film state, both spectra exhibited aggregation band, indicating efficient intermolecular interaction, which is different from the **T1** and **F1** absorption. It means that aggregation could be effectively obtained in **T2** and **F2** because of absence of hexyl side chains at the both ends.

On the other hand, since **T2** and **F2** without two hexyl thiophene units were shortened in conjugation length, their absorption spectra were blue-shifted from that of **T1** and **F1**, in both solution and film state, thus resulting in larger optical band gap (1.62 and 1.70 eV, respectively) than **T1** (1.51 eV) and **F1** (1.60 eV).

The reason that **F1** and **F2** have larger E_g^{opt} than **T1** and **T2** might be mainly due to lower aromaticity of furan. Such low aromatic stability of furan moiety

affects inefficient delocalization of π -electrons along the backbone, thereby reducing effective π -conjugation length.⁸ Nevertheless, both materials still have appropriate band gap energies and sufficient light absorption in long wavelength region, which indicates they show suitable photophysical properties as donor materials in the solar cells. In addition, for the **T1**, the experimental result was quite accordance with reported one.

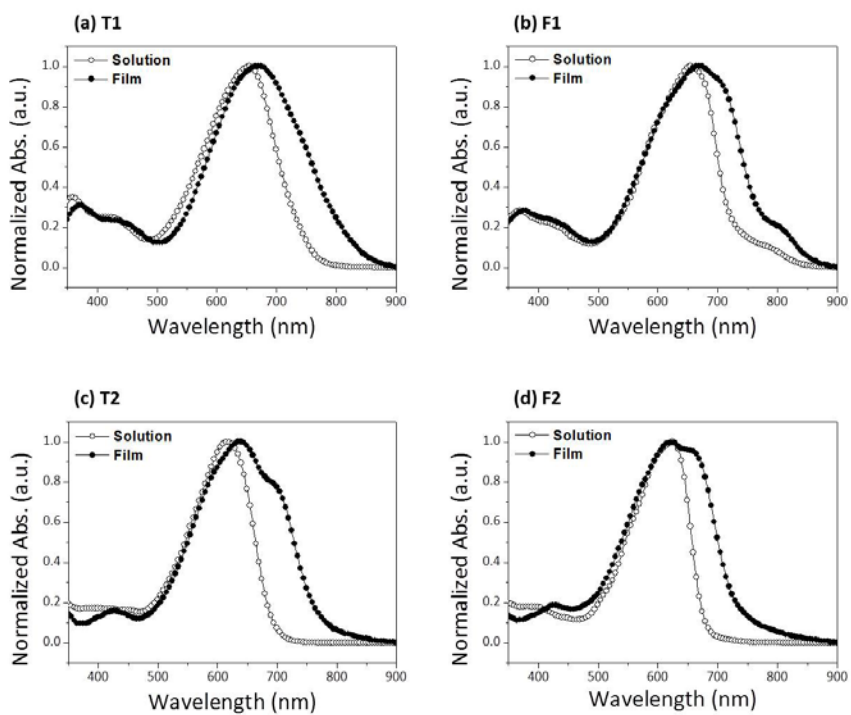


Figure 2.3 Normalized UV-Vis absorption spectra of (a) T1, (b) F1, (c) T2 and (d) F2.

Table 2.2 Optical properties of **T1**, **F1**, **T2** and **F2**.

	$\lambda_{\text{abs.sol}}$ (nm) ^{c)}	ϵ_{max} (M ⁻¹ cm ⁻¹) ^{c)}	$\lambda_{\text{abs.film}}$ (nm) ^{d)}	$\lambda_{\text{onset.film}}$ (nm)	$E_{\text{g}}^{\text{opt}}$ (eV) ^{e)}
T1 ^{a)}	670		670	827	1.5
T1 ^{b)}	653	75,000	669	820	1.51
F1	654	100,500	667	776	1.60
T2	615	87,400	630	765	1.62
F2	624	112,500	621	731	1.70

^{a)} Optical properties of **T1** were referred to in the paper³. ^{b)} Experimental optical properties of **T1**. ^{c)} Measured in solution state which was 1×10^{-5} M concentration in CHCl₃. ^{d)} Measured in film state which was fabricated with spin-coating (2000 rpm/40 sec) from 10 mg/mL CHCl₃ solution on the cleaned glass. ^{e)} Optical band gap was calculated from the $\lambda_{\text{onset.film}}$, according to the equation of: $E_{\text{g}}^{\text{opt}}$ (eV) = $[1240 / \lambda_{\text{onset.film}}(\text{nm})]$.

2.3.5 Photoelectrical properties

In the BHJ organic solar cells, the donor materials should have adequate energy level considering molecular orbital of acceptor material. First, the LUMO level should be aligned more than 0.3 eV higher than that of acceptor, because the difference between the LUMO levels of donor and acceptor determines the driving force of photo-induced electron transfer.⁹ In addition the photovoltage, V_{oc} , is determined by the difference between HOMO level of donor and LUMO of acceptor material, so low-lying HOMO level of donor would be advantageous to charge separation.⁵

Herein, energy levels of the **T1**, **F1**, **T2** and **F2** were characterized in the solid. The HOMO level was obtained by UPS measurement, and the LUMO level was calculated based on the HOMO and optical band gap. UPS profiles at the cutoff in the Figure 2.4 indicated work function, thereby deriving HOMO levels of **T1**, **F1**, **T2** and **F2**. From the equation of $E_{LUMO} = - [E_{HOMO} + E_g^{opt}]$, their energy levels were summarized in the Table 2.3, which correlates well with my initial research objectives.

Since both **T2** and **F2** showed lower HOMO level (-5.34 and -5.31 eV, respectively) than **T1** (-5.0 eV)³, I could expect enhanced V_{oc} values in the solar cells. In addition, the difference of the LUMO levels between donor and acceptor is large enough to transfer electron (> 0.3 eV), for **T2** and **F2**.

However, as shown in the Table 2.3, the experimental result of **T1** was quite different from the value in the reported paper³. I obtained -5.15 eV of the HOMO level for the **T1** and -5.17 eV for the **F1**, respectively. The main

reason of the difference between the values is unclear, until now.

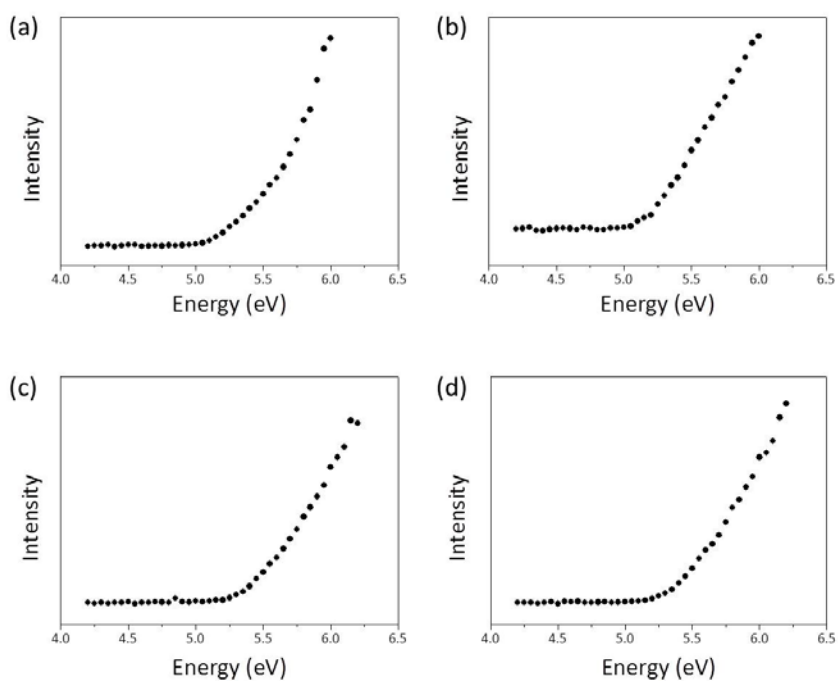


Figure 2.4 Ultraviolet photoelectron spectroscopy (UPS) profiles of the (a) **T1**, (b) **F1**, (c) **T2**, and (d) **F2**, for the spin-coated (2000 rpm/40 sec) films on the glasses.

Table 2.3 Calculated and experimental data for the molecular energy levels of **T1**, **F1**, **T2** and **F2**, based on UV-Vis absorption spectra and UPS profiles.

	E_g^{opt} (eV) ^{c)}	HOMO (eV) ^{d)}	LUMO (eV) ^{e)}
T1 ^{a)}	1.5	-5.0	-3.5
T1 ^{b)}	1.51	-5.15	-3.64
F1	1.60	-5.17	-3.57
T2	1.62	-5.34	-3.72
F2	1.70	-5.31	-3.61

^{a)} Referred to in the paper³. ^{b)} Obtained from experimental result. ^{c)} Optical band gap was calculated from the $\lambda_{\text{onset.film}}$ in the UV-Vis absorption spectra of film, according to the equation of: E_g^{opt} (eV) = $[1240/ \lambda_{\text{onset.film}}(\text{nm})]$. ^{d)} Obtained from work functions by UPS. ^{e)} Calculated from the equation of: $E_{\text{LUMO}} = -[E_{\text{HOMO}} + E_g^{\text{opt}}]$.

2.3.6 Photovoltaic properties

The photovoltaic properties of target molecules, **T1**, **F1**, and **F2**, for donor materials were characterized by fabricating BHJ organic solar cell devices with PC₆₁BM or PC₇₁BM as an acceptor. Only the **T2** which showed extremely poor solubility for solution-processing couldn't be fabricated in the BHJ organic solar cells. I referred to the device structure in the reported paper³ for the reference compound of **T1**, thus confirming its photovoltaic properties. The photovoltaic properties of **T1** are summarized in the Table 2.4, referring to the paper.³ However I couldn't achieve reproducible data due to existence of a variety of experimental variations in processing. The solar cells based on the **F1** and **F2**, furan-containing novel compounds, were also established with different optimized conditions, respectively.

The device structure was comprised of [ITO/PEDOT:PSS/**F2**:PC₆₁BM/Al], and J-V characteristics of each solar cells were displayed under AM 1.5G (100 mW/cm²) condition. As shown in the Figure 2.5(a), I could found optimized blend ratio of 1:2 in chloroform solvent, offering improved J_{sc} as well as V_{oc} . There is summary of photovoltaic properties of **F2**:PC₆₁BM according to the blend ratios, in the Table 2.5(a). In order to absorb sufficient light, an optimized thickness of active layer for **F2**:PC₆₁BM was investigated through different concentrations of solution with different spin-rate. You can see the results in the Figure 2.5(b) and Table 2.5(b). As already mentioned before, furan-containing **F2** showed great solubility over thiophene-containing materials, thus establishing thicker active layer rather than **T1**:PC₇₁BM, which

favors light absorption and charge carrier transport. Consequently, I could obtain comparative photovoltaic properties for **F2**:PC₆₁BM with additive, as summarized in the Figure 2.5(c) and Table 2.5(c). With 1 vol% of DIO, the BHJ organic solar cells exhibited power conversion efficiency of as high as 2.1%, which might be mainly resulted from the enhanced V_{oc} owing to low-lying HOMO energy level of **F2**. In addition, the value of J_{sc} was further improved when DIO was added. I could obtain enhanced IPCE (Incident photon-to-current efficiency), as shown in the Figure 2.6. Comparing with the reported paper using **T1**:PC₇₁BM, the V_{oc} increased as high as around 0.2 eV, thus exhibiting 0.75 V. The results indicated that my first research objectives could be successfully accomplished which is enhanced V_{oc} and solubility by more simple synthetic procedure. On the other hand, I also tried to fabricate the BHJ organic solar cells using PC₇₁BM as an acceptor with **F2**, however it wasn't preferable. (Table 2.6)

The BHJ organic solar cells using another furan-containing molecule, **F1**, as a donor material was comprised of device structure as same method. It displayed J - V characteristics shown in the Figure 2.7, under AM 1.5G (100 mW/cm²) condition. The result summarized in the Table 2.7. Owing to enhanced solubility of **F1**, I could obtain thicker active layer with higher concentration of solutions. However, solar cell efficiency was pretty low (0.43%) due to the low V_{oc} (0.52 V), as I'd expected. In addition, it seems that two hexyl chains at both ends of **F1** might influence phase separation of active layer in different way with **F2**.

In order to investigate phase separation in active layer at the surface, I carried

out morphological study using AFM in the following part.

Table 2.4 Photovoltaic properties of BHJ organic solar cells fabricated with **T1** and PC₇₁BM, referring to the paper.³

Blend ratio	Additive	<i>PCE</i> (%)	<i>V</i> _{OC} (V)	<i>J</i> _{SC} (mA/cm ²)	<i>FF</i> (%)
1:0.5	None	0.42	0.55	1.51	51
1:1	None	0.48	0.57	1.67	50
1:2	None	0.41	0.56	1.45	50
1:4	None	0.33	0.49	1.34	51
1:1	DIO	0.65	0.57	3.33	34
1:1	CN	2.19	0.57	7.67	50

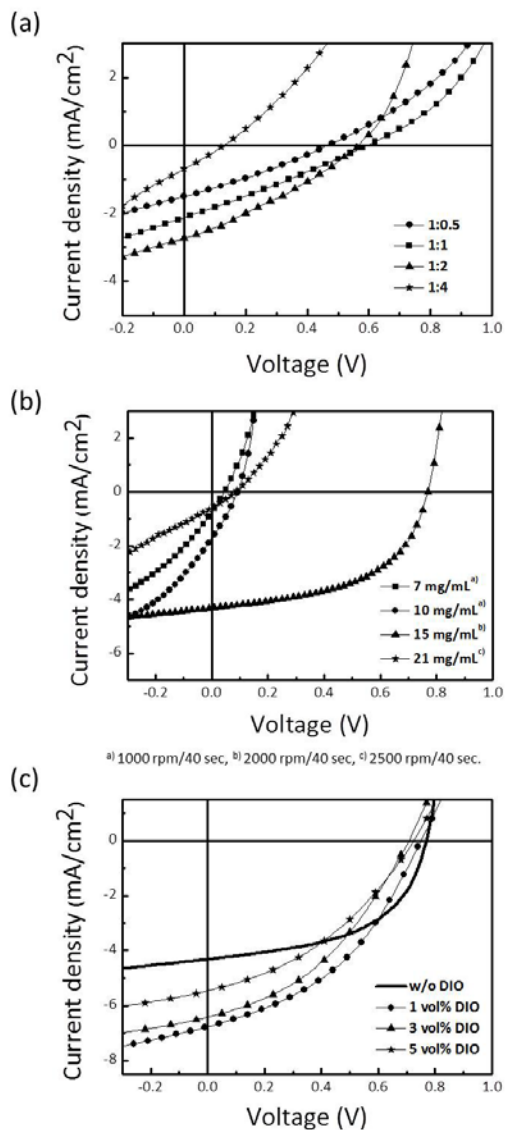


Figure 2.5 *J-V* curves of BHJ organic solar cells fabricated with **F2** and PC₆₁BM. (a) With different blend ratios of **F2**:PC₆₁BM. (b) With different concentration of chloroform solutions, and spin-rate. (c) Without or with DIO as additive.

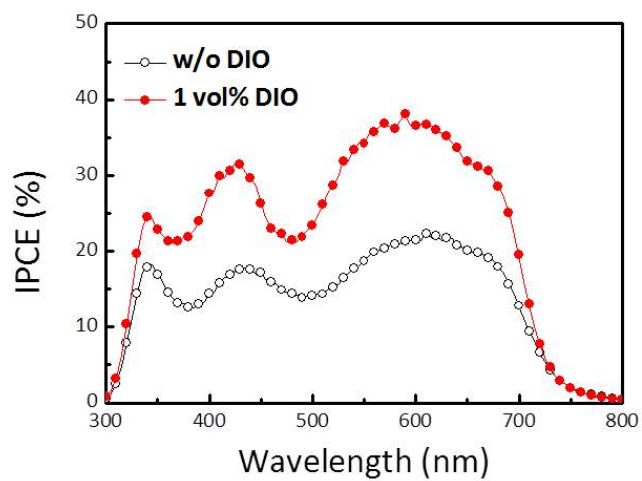


Figure 2.6 IPCE spectra of solar cells based on **F2** and PC₆₁BM.

Table 2.5 Photovoltaic properties of BHJ organic solar cells fabricated with **F2** and PC₆₁BM. Specific fabricating conditions were noted at the below of each table.

(a) With different blend ratios of **F2:PC₆₁BM**.*

Blend ratio	<i>PCE</i> (%)	<i>V</i> _{OC} (V)	<i>J</i> _{SC} (mA/cm ²)	<i>FF</i> (%)
1:0.5	0.20	0.46	1.50	29
1:1	0.35	0.60	2.13	27
1:2	0.47	0.56	2.73	30
1:4	0.23	0.12	0.69	28

*Active layer was fabricated by spin-coating (2000 rpm/40 sec) from 7 mg/mL chloroform solution.

(b) With different concentration of chloroform solutions, and spin-rate.*

Concentration	Spin-rate	<i>PCE</i> (%)	V_{OC} (V)	J_{SC} (mA/cm ²)	<i>FF</i> (%)
7 mg/mL	1000rpm	0.63	0.60	3.36	31
	1000 rpm	0.99	0.68	4.42	33
10 mg/mL	1500 rpm	0.81	0.68	3.77	32
	2000 rpm	0.53	0.64	2.93	28
	2500 rpm	0.51	0.64	2.90	28
15 mg/mL	1000 rpm	1.3	0.74	3.99	45
	1500 rpm	1.4	0.76	3.91	48
	2000 rpm	1.7	0.77	4.32	52
	2500 rpm	1.6	0.76	4.43	47
21 mg/mL	2500 rpm	0.36	0.66	1.99	27

*Active layer was fabricated by spin-coating for 40 sec from chloroform solution with 1:2 of blend ratio.

(c) Without or with DIO as additive.*

Additive	<i>PCE</i> (%)	V_{OC} (V)	J_{SC} (mA/cm ²)	<i>FF</i> (%)
None	1.7	0.77	4.32	52
1 vol% DIO	2.1	0.75	6.77	41
3 vol% DIO	1.8	0.71	6.42	39
5 vol% DIO	1.5	0.72	5.47	38

*Active layer was fabricated by spin-coating (2000~2500 rpm/40 sec) from 15 mg/mL chloroform solution with 1:2 of blend ratio.

Table 2.6 Photovoltaic properties of BHJ organic solar cells fabricated with **F2** and PC₇₁BM. Specific fabricating conditions were noted at the below.*

Additive	<i>PCE</i> (%)	V_{OC} (V)	J_{SC} (mA/cm ²)	<i>FF</i> (%)
None	0.18	0.45	1.39	28
1 vol% DIO	1.04	0.71	3.60	41
3 vol% DIO	0.50	0.72	2.14	32

*Active layer was fabricated by spin-coating (2000 rpm/40 sec) from 15 mg/mL chloroform solution with 1:2 of blend ratio.

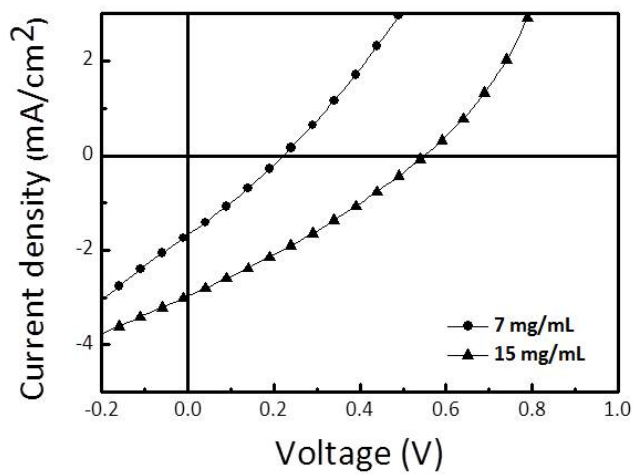


Figure 2.7 *J-V* curves of BHJ organic solar cells fabricated with **F1** and PC₆₁BM.

Table 2.7 Photovoltaic properties of BHJ organic solar cells fabricated with **F1** and PC₆₁BM. Specific fabricating conditions were noted at the below.*

Concentration	<i>PCE</i> (%)	V_{OC} (V)	J_{SC} (mA/cm ²)	<i>FF</i> (%)
7 mg/mL	0.10	0.22	1.68	28
15 mg/mL	0.43	0.52	2.85	29

*Active layer was fabricated by spin-coating (2000 rpm/40 sec) from 15 mg/mL chloroform solution with 1:1 of blend ratio.

2.3.7 Morphology investigations

For the high performing BHJ organic solar cells, the morphology control of active layer has been considered as significant issue, in these days. Since exciton diffusion and charge carrier transport are determined by phase separation, I should understand molecular ordering and supramolecular structures to obtain favorable nano morphologies.

Herein, the surface morphology of the pristine films fabricated from **F2** with PC₆₁BM was investigated by using tapping mode AFM measurement. Through the images in the Figure 2.8, I confirmed that DIO could influence surface morphology of active layer with enlarging degree of percolation between **F2** and PC₆₁BM. In spite of increasing roughness with DIO condition, the phase separation was more favorable for enhanced charge carrier transport and solar cell efficiencies. As increases with content of DIO, from 1 vol% to 5 vol%, the roughness decreased steadily. However, the photovoltaic properties also decreased, which might be due to residual DIO as being trap site. I tried to anneal the films under various temperature conditions to get rid of residual DIO, but resulting dramatic decrease in efficiency.

Interestingly, the surface morphology of the films fabricated with **F2** and PC₇₁BM was quite different, as shown in the Figure 2.9. Without DIO condition, uneven and round-shaped features were observed with varying diameters approximately 250 nm. Since the exciton diffusion length is estimated to be range of around 10nm, such large aggregated domains could limit exciton dissociation, hence offering decreased current. After I adding

additive, DIO, the miscibility of **F2** and PC₇₁BM increased with diminishing such large aggregated domains and lowering roughness sufficiently. Like with **F2:PC₆₁BM**, as the amount of DIO increased, the photovoltaic properties decreased due to the residual DIO which might become trap sites.

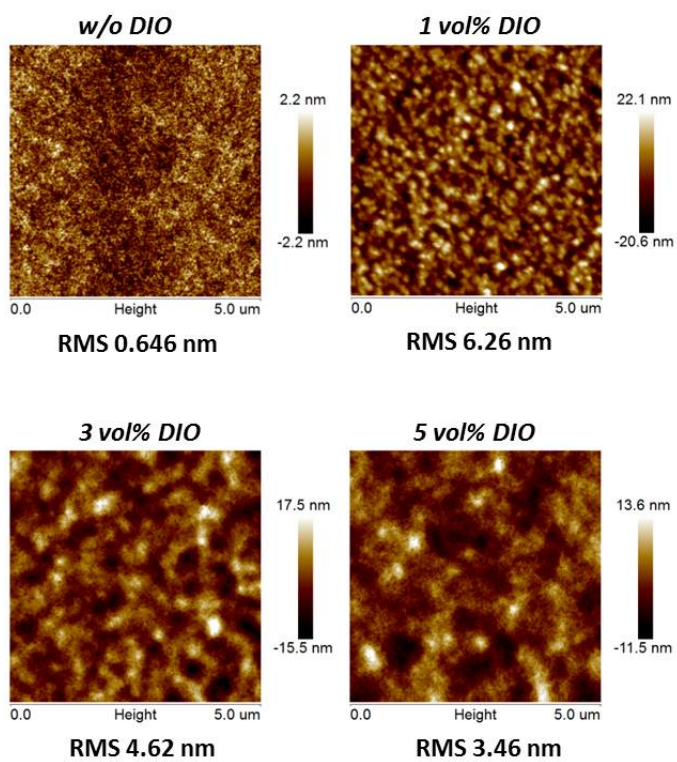


Figure 2.8 Morphological images with the amount of DIO and roughness of solar cells based on F2:PC₆₁BM.

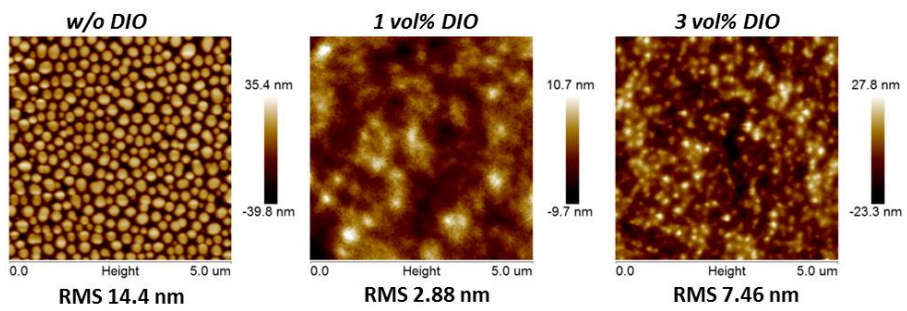


Figure 2.9 Morphological images with the amount of DIO and roughness of solar cells based on **F2:PC₇₁BM**

2.4 Conclusions

Diketopyrrolopyrrole (DPP)-based small molecules are drawing great attention towards high performance organic semiconductor; however, solubility problem due to strong intermolecular hydrogen bonding of the DPP core has been a challenging issue. The most general approach to this problem is to introduce long and branched alkyl side chains which inevitably reduce intermolecular π - π stacking and packing property in the film state. Instead, I adopted a promising design strategy that is incorporation of furan unit in the conjugated backbone, expecting a novel design of solution-processable electron donating materials, for the BHJ organic solar cells.

I noticed **T1**, an A-D-A type small molecule, where A is thiophene-containing DPP and D is electron-donating DTT unit. It has been already reported in recent year, exhibiting low V_{oc} of 0.57 V and efficiency of 2.2% with PC₇₁BM in additive condition.³ To improve photovoltage and device properties, **T2** which has low-lying HOMO level was suggested, but solubility was not enough to fabricate BHJ devices. Therefore, I designed **F2** substituted with furan into the backbone, thus enhancing solubility as well as V_{oc} through simple synthetic process over **T1** and with same amounts of side chains with **T2**. Organic solar cells comprising of **F2** with PC₆₁BM acceptor were fabricated to show PCEs as high as 2.1%, and enhancing V_{oc} up to 0.75 V. This work demonstrated furan moiety has promising potential for replacing thiophene in organic semiconducting materials, for solution-processed BHJ organic solar cells.

2.5 References

1. Choi, Y. S. and Jo, W. H. *Organic Electronics* **2013**, *14*, 1621.
2. Lee, J. W.; Choi, Y. S. and Jo, W. H. *Organic Electronics* **2012**, *13*, 3060.
3. Park, J. K.; Kim, C.; Walker, B.; Nguyen, T.-Q. and Seo, J. H. *RSC Advances* **2012**, *2*, 2232.
4. Shahid, M.; Ashraf, R. S.; Huang, Z.; Kronemeijer, A. J.; McCarthy-Ward, T.; McCulloch, I.; Durrant, J. R.; Siringhaus, H. and Heeney, M. *J. Mater. Chem.* **2012**, *22*, 12817.
5. Li, G.; Zhu, R. and Yang, Y. *Nature Photon.* **2012**, *6*, 153.
6. Woo, C. H.; Beaujuge, P. M.; Holcombe, T. W. Lee, O. P.; and Fréchet, J. M. J. *J. Am. Chem. Soc.* **2010**, *132*, 15547.
7. Walker, B.; Tamayo, A. B.; Dang, X.-D.; Zalar, P.; Seo, J. H.; Garcia, A.; Tantiwiwat, M. and Nguyen, T.-Q. *Adv. Funct. Mater.* **2009**, *19*, 3063.
8. (a) Takimiya, K.; Konda, Y.; Ebata, H.; Niihara, N. and Otsubo, T. *J. Org. Chem.* **2005**, *70*, 10569. (b) Takimiya, K.; Kunugi, Y.; Konda, Y.; Niihara, N. and Otsubo, T. *J. Am. Chem. Soc.* **2004**, *126*, 5084. (c) Nakano, M.; Mori, H.; Shinamura, S. and Takimiya, K. *Chem. Mater.* **2012**, *24*, 190. (4) Nakano, M.; Niimi, K.; Miyazaki, E.; Osaka, I. and Takimiya, K. *J. Org. Chem.* **2012**, *77*, 8099.
9. Fréchet, J. M. J. and Thompson, B. C. *Angew. Chem. Int. Ed.* **2008**, *47*, 58.

Chapter 3. Low Band Gap and Solution- Processable Furan-Containing Diketopyrrolopyrrole-Based Small Molecules as Acceptor Materials in Organic Solar Cells

3.1 Introduction

In recent years, high performing organic semiconducting materials based on the diketopyrrolopyrrole (DPP) unit have been developed rapidly, owing to their superior optoelectronic properties, and great chemical versatility. One of the promising studies might be the effort to design novel electron-accepting small molecules, because the DPP was considered as an excellent electron-withdrawing block, thus allowing energy levels to be lowered sufficiently. The DPP-based acceptor materials designed with well-organized push-pull structures would have superior photophysical properties, surpassing PCBM which is widely used for acceptor material. It means these DPP-based materials would be quite advantageous on light absorption, which indicates they can take more amounts of photons at the same wavelength and absorb light in even longer wavelength region.

Nevertheless, the acceptor materials in organic solar cells have been rarely discussed. Zhan and coworkers¹ quite recently published a novel DPP-based

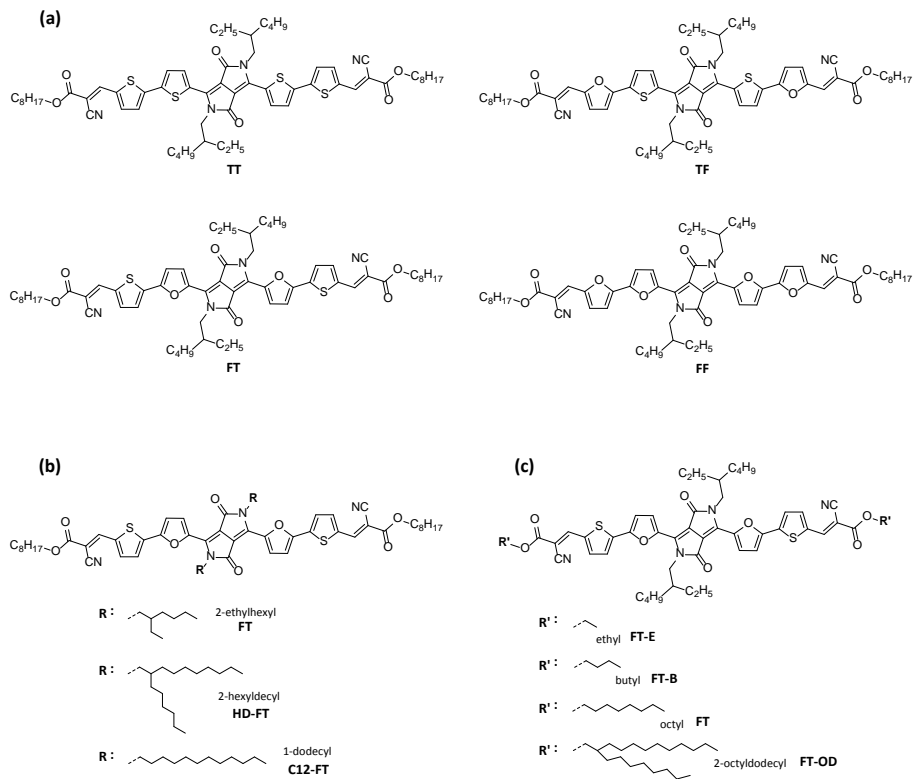
acceptor with a noticeable solar cell efficiency of as high as 2.05%, however, most of the DPP-based acceptor materials have still accomplished low efficiencies of 0.1 to 1%.²

As already discussed in the previous part, it was successfully demonstrated that furan moiety has promising potential of replacing thiophene in the organic semiconductors. And, it also provided great solubility without introducing long and branched alkyl side chains which inevitably reduce intermolecular π - π stacking, thus enabling solution-processing. Herein, I designed several furan-containing DPP-based small molecules as acceptor materials, which are shown in the Scheme 3.1.

Target materials were successfully synthesized and characterized to confirm fascinating design concepts, as follows; 1) well-organized push-pull structures through novel A-D-A-D-A type π -conjugated backbone, leading to efficient intramolecular charge transfer (ICT) and lowering band gap, 2) incorporation of the furan moieties in the backbone, in order to provide electron-donating force and discuss the effects of furan, systematically, 3) adopting electron-withdrawing alkyl cyanoacetate groups, since these end-capped groups were exhibiting enhanced film forming properties as well as solubility according to their alkyl chain length,³ and 4) alkyl chain modification for desirable film morphology, with the optimized length and shape, through both vertical and horizontal directions.

In this chapter, I identified the effects of furan moiety on material properties, depending on the number and its position, systematically. Target materials were fabricated with P3HT as a donor, thus obtaining PCE of 0.43% at the

optimized condition. This study is implying that furan-containing DPP-based small molecules are also available in organic solar cells as acceptor materials, exhibiting superior photophysical properties and ability for solution-processing.

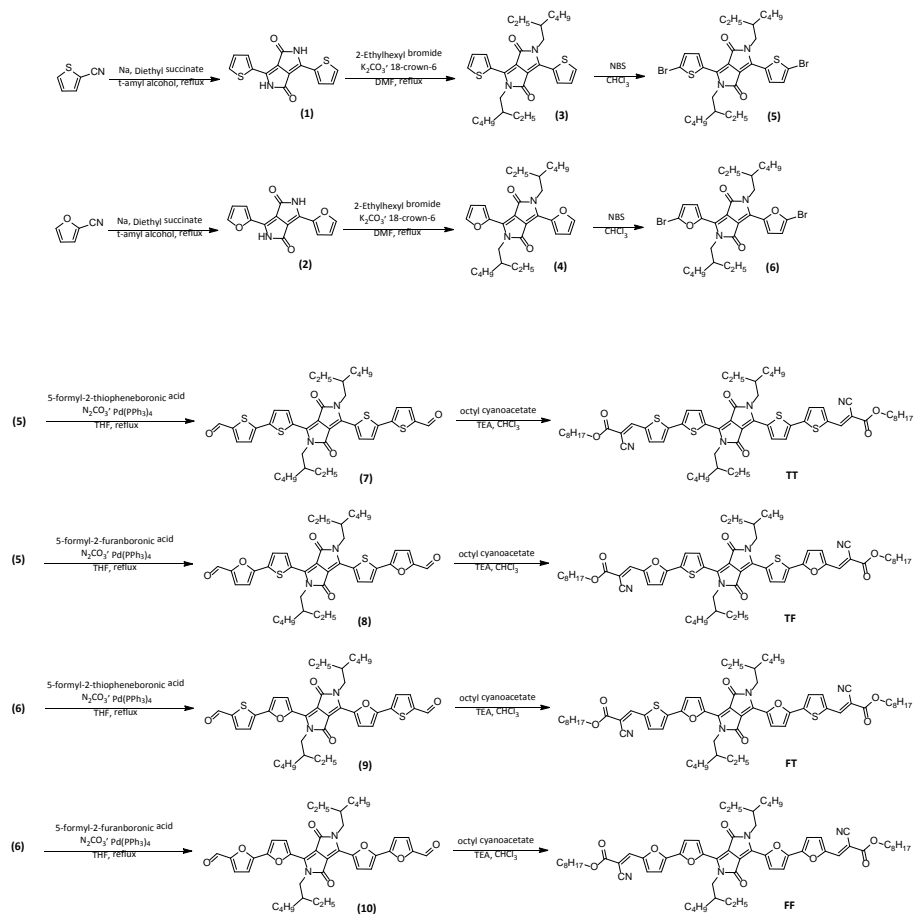


Scheme 3.1 Chemical structures of target materials. **(a): TT, TF, FT** and **FF**. Alkyl chain modifications of **FT** were presented by **(b)** and **(c)**. **(b):** Vertical modifying for **FT**, **HD-FT** and **C12-FT**. **(c):** Horizontal modifying for **FT-E**, **FT-B**, **FT** and **FT-OD**.

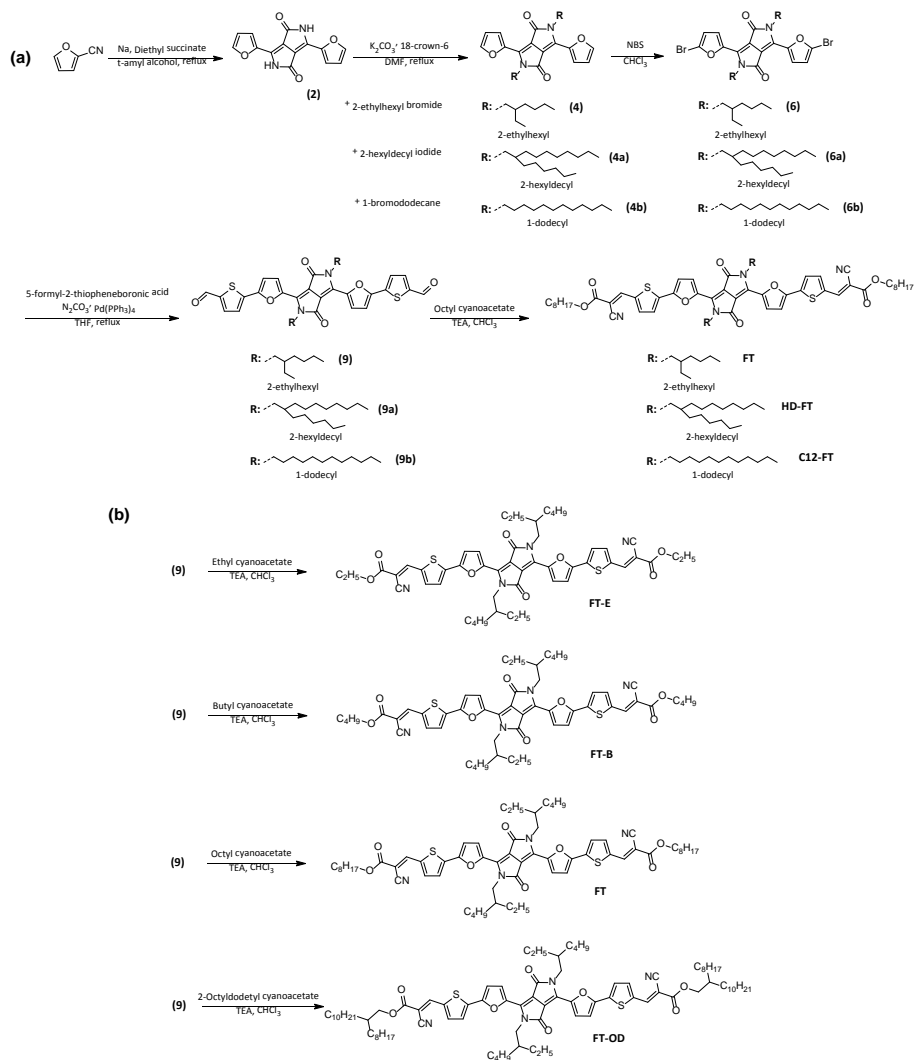
3.2 Experimental section

3.2.1 Synthesis

Scheme 3.2 illustrated a synthetic procedure of target materials, **TT**, **TF**, **FT**, and **FF**, which are containing same alkyl solubilizing chains of 2-ethylhexyl and octyl, and different electron-donating (D) building blocks, such as thiophene-thiophene, thiophene-furan, furan-thiophene, and furan-furan. The synthetic scheme of Scheme 3.3 displayed alkyl chain modifications in both vertical and horizontal direction, at a same π -conjugated backbone with **FT** whose D block is furan-thiophene. All reagents were commercially available from Sigma-Aldrich, TCI chemicals, and Alfa-Aesar. The solvents which were used in each reaction were purchased from above companies or Junsei chemicals without further purification, except tetrahydrofuran (THF), freshly distilled one before use. Other chemicals required during workup or purifying processes in each procedure were affordable from Samchun Chemicals and Daejung Chemicals & Metals. The target materials were synthesized according to the literature as reported before, with some modification in case of need.



Scheme 3.2 Synthesis of target materials: **TT**, **TF**, **FT** and **FF**.



Scheme 3.3 Synthesis of **FT** derivatives with alkyl chain modifications. **(a)**: Vertical modifying for **FT**, **HD-FT** and **C12-FT**. **(b)**: Horizontal modifying for **FT-E**, **FT-B**, **FT** and **FT-OD**.

Synthesis of 3,6-di(thiophene-2-yl)pyrrolo[3,4-*c*]pyrrole-1,4(2H,5H)-dione (1): This compound was prepared by the same procedure as described in previous chapter.

Synthesis of 3,6-di(furan-2-yl)pyrrolo[3,4-*c*]pyrrole-1,4(2H,5H)-dione (2): This compound was prepared by the same procedure as described in previous chapter.

Synthesis of 2,5-di-(2-ethylhexyl)-3,6-di(thiophene-2-yl)pyrrolo[3,4-*c*]pyrrole-1,4(2H,5H)-dione (3): This compound was prepared by the same procedure as described in previous chapter. ¹H NMR (300 MHz, CDCl₃): δ (ppm) 8.89 (dd, 2H), 7.63 (dd, 2H), 7.28 (d, 2H), 4.05 (dd, 4H), 1.8-1.9 (m, 2H), 1.2-1.4 (m, 16H), 0.8-1.0 (m, 12H).

Synthesis of 2,5-di-(2-ethylhexyl)-3,6-di(furan-2-yl)pyrrolo[3,4-*c*]pyrrole-1,4(2H,5H)-dione (4): This compound was prepared by the same procedure as described in previous chapter. ¹H NMR (300 MHz, CDCl₃): δ (ppm) 8.33 (d, 2H), 7.61 (d, 2H), 6.69 (dd, 2H), 4.04 (d, 4H), 1.80-1.68 (m, 2H), 1.39-1.26 (m, 16H), 0.95-0.85 (m, 12H).

Synthesis of 2,5-di-(2-hexyldecyl)-3,6-di(furan-2-yl)pyrrolo[3,4-*c*]pyrrole-1,4(2H,5H)-dione (4a): This compound was prepared by the same procedure as described in compound 4. With compound 2 (2.0 g, 7.46 mmol) and 2-hexyldecyl iodide (10.5 g, 29.8 mmol), through recrystallization by ethyl

acetate, resulting 1.70 g of orange powder was isolated. (Yield = 32%) ^1H NMR (300 MHz, CDCl_3): δ (ppm) 8.32 (d, 2H), 7.60 (d, 2H), 6.68 (dd, 2H), 4.03 (d, 4H), 1.80 (bs, 2H), 1.28-1.22 (m, 48H), 0.88-0.82 (m, 12H).

Synthesis of 2,5-di-(1-dodecyl)-3,6-di(furan-2-yl)pyrrolo[3,4-c]pyrrole-1,4(2H,5H)-dione (4b): This compound was prepared by the same procedure as described in compound 4. With compound 2 (1.5 g, 5.59 mmol) and 1-bromododecane (10.5 g, 29.8 mmol), through recrystallization by ethyl acetate, resulting 1.77 g of dark red powder was isolated. (Yield = 52%) ^1H NMR (300 MHz, CDCl_3): δ (ppm) 8.30 (d, 2H), 7.63 (d, 2H), 6.69 (dd, 2H), 4.11 (t, 4H), 1.69-1.67 (m, 4H), 1.34-1.24 (m, 36H), 0.87 (t, 6H).

Synthesis of 3,6-di(5-bromothiophene-2-yl)-2,5-di(2-ethylhexyl)pyrrolo[3,4-c]pyrrole-1,4(2H,5H)-dione (5): To a 500mL three-neck round bottom flask, Compound 3 (2.5 g, 4.76 mmol) and 300 mL of CHCl_3 was added. At 0 °C, N-bromosuccinimide (1.95 g, 11.0 mmol) was added in small portions, in the dark. The mixture was stirred for overnight at room temperature, and then washed with water. After organic phase extracted with methylene chloride was dried over MgSO_4 and evaporated under vacuum. The crude product was further purified by silica gel packed flash column chromatography using CHCl_3 as an eluent. Finally, through cold MeOH, the precipitates were isolated, affording 2.07 g of purple powder. (Yield = 64%-99%) ^1H NMR (300 MHz, CDCl_3): δ (ppm) 8.64 (d, 2 H), 7.22 (d, 2 H), 3.92 (m, 4 H), 1.88-1.78 (m, 2 H), 1.39-1.19 (m, 16 H), 0.90-0.84 (m, 12 H).

Synthesis of 3,6-di(5-bromofuran-2-yl)-2,5-di(2-ethylhexyl)pyrrolo[3,4-c]pyrrole-1,4(2H,5H)-dione (6): This compound was prepared by the same procedure as described in compound **5**. With compound **4** (1.0 g, 2.03 mmol), red-purple powder of 1.38 g was isolated. (Yield = 98%) ¹H NMR (300 MHz, CDCl₃): δ (ppm) 8.30 (d, 2 H), 6.62 (d, 2 H), 3.99 (m, 4H), 1.78-1.68 (m, 2 H), 1.39-1.24 (m, 16 H), 0.99-0.85 (m, 12 H).

Synthesis of 3,6-di(5-bromofuran-2-yl)-2,5-di(2-hexyldecyl)pyrrolo[3,4-c]pyrrole-1,4(2H,5H)-dione (6a): This compound was prepared by the same procedure as described in compound **6**. With compound **4a** (1.0 g, 1.39 mmol), resulting 1.02 g of purple powder was isolated. (Yield = 84%) ¹H NMR (300 MHz, CDCl₃): δ (ppm) 8.29 (d, 2H), 7.62 (d, 2H), 3.98 (d, 4H), 1.78 (bs, 2H), 1.29-1.23 (m, 48H), 0.88-0.82 (m, 12H).

Synthesis of 3,6-di(5-bromofuran-2-yl)-2,5-di(1-dodecyl)pyrrolo[3,4-c]pyrrole-1,4(2H,5H)-dione (6b): This compound was prepared by the same procedure as described in compound **6**. With compound **4b** (0.5 g, 0.827 mmol), resulting 479 mg of purple powder was isolated. (Yield = 74%) ¹H NMR (300 MHz, CDCl₃): δ (ppm) 8.25 (d, 2H), 7.63 (d, 2H), 4.05 (t, 4H), 1.71-1.64 (m, 4H), 1.39-1.25 (m, 36H), 0.88 (t, 6H).

Synthesis of 5',5'''-(2,5-di(2-ethylhexyl)-3,6-dioxo-2,3,5,6-tetrahydropyrrolo[3,4-c]pyrrole-1,4-diyl)di((2,2'-bithiophene)-5-

carbaldehyde)) (7): Compound **5** (1.0 g 1.47 mmol) was dissolved in 70 mL of fresh distilled THF into a 250 mL two-neck round bottom flask, and anhydrous Na₂CO₃ (4.66 g, 44.0 mmol) was dissolved in 24 mL of DI water into clean vial. These solutions prepared separately were sealed and degased by argon for 10min. After adding Na₂CO₃ aqueous solution and Pd(PPh₃)₄ into the 250 mL flask, connected a condenser and dropping funnel. In the dark, the mixture was stirred for 30 min at 45 °C the in inert argon condition. Upon stirring, prepared 5-formyl-2-thiopheneboronic acid (0.686 g, 4.40 mmol) and 30 mL of distilled THF solution in clean vial, and followed sealing and degasing process. After the reaction temperature rose to 70 °C, put the 5-formyl-2-thiopheneboronic acid solution in the dropping funnel by using a syringe, and open its cock a little. The mixture was stirred for overnight, and washed with water. The extract phase using methylene chloride was dried over MgSO₄, column chromatography on a silica gel was followed to further purification, using blend eluent of methylene chloride, ethyl acetate, and n-Hex (ratio = 5:0.5:4.5). Evaporated product was isolated from precipitation by cold MeOH, affording 425 mg of dark blue powder. (Yield = 39%) ¹H NMR (300 MHz, CDCl₃): δ (ppm) 9.91 (s, 2H), 8.93 (d, 2H), 7.72 (d, 2H), 7.49 (d, 2H), 7.39 (d, 2H), 3.04 (dd, 4H), 1.90 (m, 2H), 1.42-1.25 (m, 16H), 0.95-0.85 (m, 12H).

Synthesis of 5',5'''-(2,5-di(2-ethylhexyl)-3,6-dioxo-2,3,5,6-tetrahydropyrrolo[3,4-c]pyrrole-1,4-diyl)di((2-furan-2'-thiophene)-5-carbaldehyde)) (8): This compound was prepared by the same procedure as

described in compound **7**. With compound **5** (0.5 g 0.733 mmol) and 5-formyl-2-furanboronic acid (0.307 g, 2.20 mmol), resulting 162 mg of dark blue product was isolated. (Yield = 31%) ¹H NMR (300 MHz, CDCl₃): δ (ppm) 9.69 (s, 2H), 8.95 (d, 2H), 7.62 (d, 2H), 7.34 (d, 2H), 6.86 (d, 2H), 4.06 (dd, 4H), 1.90 (m, 2H), 1.41-1.27 (m, 16H), 0.94-0.85 (m, 12H).

Synthesis of 5',5'''-(2,5-di(2-ethylhexyl)-3,6-dioxo-2,3,5,6-tetrahydropyrrolo[3,4-c]pyrrole-1,4-diyl)di((2-thiophene-2'-furan]-5-carbaldehyde)) (9): This compound was prepared by the same procedure as described in compound **7**. With compound **6** (0.33 g 0.507 mmol) and 5-formyl-2-thiopheneboronic acid (0.237 g, 1.52 mmol), resulting 251 mg of dark blue product was isolated. (Yield = 69%) ¹H NMR (300 MHz, CDCl₃): δ (ppm) 9.93 (s, 2H), 8.49 (d, 2H), 7.75 (d, 2H), 7.47 (d, 2H), 7.03 (d, 2H), 4.14 (d, 4H), 1.89 (m, 2H), 1.50-1.24 (m, 16H), 0.91 (t, 6H), 0.84 (t, 6H). elemental analysis: calculated for C₄₀H₄₄N₂O₆S₂: C 67.39, H 6.22, N 3.93, O 13.46, S 8.99; found: C 67.45, H 6.21, N 3.97, O 13.40, S 9.01.

Synthesis of 5',5'''-(2,5-di(2-hexyldecyl)-3,6-dioxo-2,3,5,6-tetrahydropyrrolo[3,4-c]pyrrole-1,4-diyl)di((2-thiophene-2'-furan]-5-carbaldehyde)) (9a): This compound was prepared by the same procedure as described in compound **9**. With compound **6a** (0.5 g, 0.572 mmol), resulting 84 mg of dark blue powder was isolated. (Yield = 16%) ¹H NMR (300 MHz, CDCl₃): δ (ppm) 9.93 (s, 2H), 8.47 (d, 2H), 7.74 (d, 2H), 7.47 (d, 2H), 7.02 (d, 2H), 4.14 (d, 4H), 1.91 (bs, 2H), 1.35-1.19 (m, 48H), 0.86-0.82 (m, 12H).

Synthesis of 5',5'''-(2,5-di(1-dodecyl)-3,6-dioxo-2,3,5,6-tetrahydropyrrolo[3,4-c]pyrrole-1,4-diyl)di((2-thiophene-2'-furan]-5-carbaldehyde)) (9b): This compound was prepared by the same procedure as described in compound **9**. With compound **6b** (0.4 g, 0.524 mmol), resulting 93 mg of dark blue powder was isolated. (Yield = 21%) ¹H NMR (300 MHz, CDCl₃): δ (ppm) 9.93 (s, 2H), 8.45 (d, 2H), 7.75 (d, 2H), 7.46 (d, 2H), 7.03 (d, 2H), 4.19 (t, 4H), 1.84-1.75 (m, 4H), 1.48-1.43 (m, 4H), 1.35-1.23 (m, 32H), 0.86 (t, 6H).

Synthesis of 5',5'''-(2,5-di(2-ethylhexyl)-3,6-dioxo-2,3,5,6-tetrahydropyrrolo[3,4-c]pyrrole-1,4-diyl)di((2,2'-bifuran]-5-carbaldehyde)) (10): This compound was prepared by the same procedure as described in compound **7**. With compound **6** (0.35 g 0.538 mmol) and 5-formyl-2-furanboronic acid (0.226 g, 1.61 mmol), resulting 164 mg of dark blue product was isolated. (Yield = 45%) ¹H NMR (300 MHz, CDCl₃): δ (ppm) 9.70 (s, 2H), 8.47 (d, 2H), 7.35 (d, 2H), 7.17 (d, 2H), 6.89 (d, 2H), 4.13 (d, 4H), 1.88 (m, 2H), 1.45-1.23 (m, 16H), 0.92 (t, 6H), 0.84 (t, 6H).

Synthesis of TT: Compound **7** (100 mg, 0.134 mmol) was dissolved in 40 mL of CHCl₃ to a 100 mL three-neck round bottom flask. After stirring until the mixture was completely soluble at 45 °C, a catalytic amount of triethylamine was added, then excess amount of octyl cyanoacetate (502 mg, 2.54 mmol). The resulting solution was stirred for overnight, and then washed with water.

The organic phase was extracted with methylene chloride and dried over MgSO_4 . A column chromatography on a silica gel was performed with blend eluent of methylene chloride : ethyl acetate : n-Hex = 5:0.5:4.5. The separated solution was passed through alumina packed short column, and evaporation was followed. Through the further purification, recrystallization using ethyl acetate, highly pure green solid was affordable, thus 56 mg. (Yield = 38%) ^1H NMR (300 MHz, CDCl_3): δ (ppm) 8.93 (d, 2H), 8.27 (s, 2H), 7.73 (d, 2H), 7.51 (d, 2H), 7.39 (d, 2H), 4.31 (t, 4H), 4.05 (dd, 4H), 1.92-1.88 (m, 2H), 1.81-1.71 (m, 4H), 1.44-1.23 (m, 36H), 0.95-0.85 (m, 18H).

Synthesis of TF: This compound was prepared by the same procedure as described in compound **TT**. With compound **8** (100 mg 0.140 mmol), resulting 131 mg of green product was isolated. (Yield = 87%) ^1H NMR (300 MHz, CDCl_3): δ (ppm) 8.96 (d, 2H), 7.98 (s, 2H), 7.66 (d, 2H), 7.43 (d, 2H), 6.93 (d, 2H), 4.31 (t, 4H), 4.07 (d, 4H), 1.92-1.90 (m, 2H), 1.81-1.69 (m, 4H), 1.42-1.25 (m, 36H), 0.93-0.84 (m, 18H).

Synthesis of FT: This compound was prepared by the same procedure as described in compound **TT**. With compound **9** (80 mg 0.112 mmol), resulting 108 mg of green product was isolated. (Yield = 90%) ^1H NMR (300 MHz, CDCl_3): δ (ppm) 8.50 (d, 2H), 8.28 (s, 2H), 7.78 (d, 2H), 7.48 (d, 2H), 7.06 (d, 2H), 4.31 (t, 4H), 4.15 (d, 4H), 1.91-1.89 (m, 2H), 1.80-1.71 (m, 4H), 1.47-1.25 (m, 36H), 0.95-0.80 (m, 18H). MS (m/z): $[\text{M}]^+$ calculated for $\text{C}_{62}\text{H}_{78}\text{N}_4\text{O}_8\text{S}_2$, 1071.53; found 1071.53. elemental analysis: calculated for

$C_{62}H_{78}N_4O_8S_2$: C 69.50, H 7.34, N 5.23, O 11.95, S 5.99; found: C 69.22, H 7.36, N 5.23, O 12.02, S 5.93.

Synthesis of HD-FT: This compound was prepared by the same procedure as described in compound **TT**. With compound **9a** (80 mg, 0.085 mmol), resulting 84 mg of green powder was isolated. (Yield = 76%) 1H NMR (300 MHz, $CDCl_3$): δ (ppm) 8.48 (d, 2H), 8.28 (s, 2H), 7.78 (d, 2H), 7.48 (d, 2H), 7.05 (d, 2H), 4.31 (t, 4H), 4.14 (d, 4H), 1.90 (bs, 2H), 1.78-1.71 (m, 4H), 1.45-1.19 (m, 68H), 0.91-0.79 (m, 18H).

Synthesis of C12-FT: This compound was prepared by the same procedure as described in compound **TT**. With compound **9b** (80 mg, 0.097 mmol), resulting 48 mg of green powder was isolated. (Yield = 42%) 1H NMR (300 MHz, $CDCl_3$): δ (ppm) 8.46 (d, 2H), 8.27 (s, 2H), 7.77 (d, 2H), 7.45 (d, 2H), 7.05 (d, 2H), 4.30 (t, 4H), 4.19 (t, 4H), 1.78-1.71 (m, 8H), 1.49-1.22 (m, 56H), 0.89-0.84 (m, 12H).

Synthesis of FT-E: This compound was prepared by the same procedure as described in compound **TT**. With compound **9** (60 mg, 0.084 mmol) and ethyl cyanoacetate (0.18 g, 1.595 mmol), resulting 53 mg of green powder was isolated. (Yield = 70%) 1H NMR (300 MHz, $CDCl_3$): δ (ppm) 8.50 (d, 2H), 8.29 (s, 2H), 7.78 (d, 2H), 7.48 (d, 2H), 7.06 (d, 2H), 4.39 (q, 4H), 4.15 (d, 4H), 1.89 (bs, 2H), 1.47-1.25 (m, 22H), 0.92 (t, 6H), 0.83 (t, 6H).

Synthesis of FT-B: This compound was prepared by the same procedure as described in compound **TT**. With compound **9** (100 mg, 0.14 mmol) and butyl cyanoacetate (0.375 g, 2.66 mmol), resulting 92 mg of green powder was isolated. (Yield = 69%) ^1H NMR (300 MHz, CDCl_3): δ (ppm) 8.50 (d, 2H), 8.28 (s, 2H), 7.78 (d, 2H), 7.48 (d, 2H), 7.06 (d, 2H), 4.32 (t, 4H), 4.15 (d, 4H), 1.89 (bs, 2H), 1.77-1.70 (m, 4H), 1.51-1.26 (m, 20H), 0.98 (t, 6H), 0.92 (t, 6H), 0.83 (t, 6H). MS (m/z): $[\text{M}]^+$ calculated for $\text{C}_{54}\text{H}_{62}\text{N}_4\text{O}_8\text{S}_2$, 959.40; found 959. elemental analysis: calculated for $\text{C}_{54}\text{H}_{62}\text{N}_4\text{O}_8\text{S}_2$: C 67.62, H 6.52, N 5.84, O 13.34, S 6.68; found: C 67.68, H 6.52, N 5.84, O 13.32, S 6.66.

Synthesis of FT-OD: This compound was prepared by the same procedure as described in compound **TT**. With compound **9** (50 mg, 0.07 mmol) and 2-tyldodecyl cyanoacetate (0.615 g, 1.68 mmol), resulting 91 mg of green powder was isolated. (Yield = 93%) ^1H NMR (300 MHz, CDCl_3): δ (ppm) 8.50 (d, 2H), 8.27 (s, 2H), 7.78 (d, 2H), 7.48 (d, 2H), 7.06 (d, 2H), 4.21 (d, 4H), 4.15 (d, 4H), 1.90 (bs, 2H), 1.77 (bs, 2H), 1.47-1.26 (m, 80H), 0.95-0.81 (m, 24H).

Synthesis of FF: This compound was prepared by the same procedure as described in compound **TT**. With compound **10** (120 mg 0.176 mmol), resulting 139 mg of green product was isolated. (Yield = 83%) ^1H NMR (300 MHz, CDCl_3): δ (ppm) 8.47 (d, 2H), 7.99 (s, 2H), 7.46 (d, 2H), 7.20 (d, 2H), 6.95 (d, 2H), 4.31 (t, 4H), 4.13 (d, 4H), 1.85-1.83 (m, 2H), 1.81-1.72 (m, 4H), 1.49-1.25 (m, 36H), 0.94-0.81 (m, 18H).

3.2.2 Characterization methods and instrumental measurements

Chemical structures were identified by ^1H NMR spectra obtained from NMR spectrometer (Bruker, Avance-300) with deuterated chloroform (CDCl_3) solvent. In addition, Mass spectrometry (JEOL, JMS-700) and elemental analysis (EA1110, CE Instrument) were performed. Density functional theory (DFT) calculation was accomplished with Gaussian09 quantum-chemical package at B3LYP/6-31G (d, p) level, and optimized by global minimum, in the gas phase. The program of Gauss View 5.0 was explored, providing information about optimized ground state geometry and electron density at HOMO and LUMO states. The solubility of materials was measured by using a $0.50\ \mu\text{m}$ PTFE syringe filter which was purchased from Toyo Roshi Kaisha. Photophysical properties were performed by an UV-Vis spectrophotometer (SHIMADZU, UV-1650PC) in both solution and film state, and a photoluminescence spectrometer (Photon Technology International, QM40) in only solution state. The molecular orbital was characterized by measuring their HOMO level from ultraviolet photoelectron spectroscopy (UPS) and cyclic voltammetry (CV). Ultraviolet photoelectron spectrometer (Hitachi High Tech, AC-2) provided molecular work function in the film state. Cyclic voltammetry (CV) experiments were performed using standard three electrode potentiostat system (Princeton Applied Research, 273A), and carried out between 0 V and 2.0 V with three-electrode cell which is consisting of Ag/Ag^+ reference electrode, platinum wire counter electrode, and platinum working electrode. The 0.1 M of tetrabutylammonium tetrafluoroborate

(TBATFB) in dichloromethane (DCM) was used in CV testing, for the solution state, or acetonitrile solution containing 0.1 M tetrabutylammonium hexafluorophosphate (TBAHFP) as a supporting electrolyte, for the film state. The LUMO level was calculated by the difference of optical band gap energy and HOMO level. The study on thin film morphology was carried out through atomic force microscopy (AFM), whose operating measurement is a Multimode with a NanoScope V controller, Bruker.

3.2.3 Device fabrication and measurements of solar cells

The materials comprising of solar cell device were purchased and fabricated according to following terms. The ITO glass substrates exhibiting a sheet resistance of less than 10 Ω /square were cleaned with three steps in ultrasonication bath; each step was taking 10min, by using trichloroethylene, acetone, and isopropyl alcohol respectively. After these washed glasses were dried by blowing nitrogen stream, exposed to UV light (360 nm) for 10 min. On the substrate, PEDOT:PSS (Clevios P) was spin-coated at 5000 rpm for 30 sec, achieving 30 nm of thickness, and baked at 150 °C for 20 min. The day before device fabrication, P3HT polymer (Sigma Aldrich) and the synthetic materials were dissolved in anhydrous THF, toluene, or others, followed by stirring for overnight. These prepared solutions were spin-coated on the PEDOT:PSS layer, with 1000 rpm/60 sec, thus providing approximately 160 nm of thickness for active layer(KLA Tencor, AlphaStep IQ). The aluminum at the cathode was deposited on the top by thermal evaporation, thus accomplishing 100 nm thick electrodes. The effective active area of each cell was 0.09 cm², and post annealing procedure was carried out at certain temperature, selectively.

The photovoltaic properties were characterized by the current density-voltage (*J-V*) curves, which were carried out with a Keithley 4200 source measurement unit. The solar simulation conditions provided by an Oriel Sol 3A were under AM 1.5G (100 mW/cm²). The *J-V* characteristics were measured by using a metal mask of 0.09 cm².

3.3 Result and discussion

3.3.1 Synthesis and characterization

In order to design high performing organic semiconducting materials, the optimum combination of the electron-donating (D) and electron-accepting (A) unit is essential, thereby facilitating efficient ICT, upon maintaining planar geometry. I was particularly interested in the diketopyrrolopyrrole as an A block with various electron-donating (D) furan-containing blocks, applying in the BHJ organic solar cells. Well-organized push-pull structures through incorporation of furan moieties into the DPP-based polymers have been investigated by several research groups.⁴⁻¹⁰ I also identified the effects of furan moieties on the small molecular donor material, in the previous part of this chapter.

In this chapter, I noticed acceptor materials, and designed furan-containing DPP-based small molecules modified with strong electron-withdrawing alkyl cyanoacetate group. This end-capped group could be exhibiting enhanced film forming properties and improving solubility, depending on its alkyl chain.³ Herein, I synthesized novel A-D-A-D-A type DPP-based small molecules, **TT**, **TF**, **FT** and **FF**, in order to discuss the effects of furan, systematically. Their fundamental characterizations using some measurements, and photovoltaic properties as acceptor materials were investigated. From the results, I found that **FT** showed potential of accepting material with P3HT as a donor; hence further optimization was carried out through synthesis.

Several **FT** derivatives with various alkyl chains were designed for obtaining

desirable film morphology in the BHJ organic solar cells. Alkyl chain modification was performed with two directions; one is vertical, at the position of N-substitution in DPP core, the other is horizontal, at the cyanoacetate end-capped group. I optimized length (long/short) and shape (linear/branched) of side chains, trying to control phase separation. For example, 2-hexyldecyl and linear dodecyl groups were adopted vertically, resulting in **HD-FT** and **C12-FT** respectively. In addition, through horizontal modifying with ethyl, butyl, and 2-octyldodecyl side chains, **FT-E**, **FT-B**, and **FT-OD** were accomplished.

For all of target materials, their synthetic methods were based on conventional reactions, such as Suzuki coupling and Knoevenagel reactions, or with some modifications. Materials were purified with several repetitive column chromatographies on an alumina and silica gel, and further recrystallization followed. Synthetic molecular structures were identified by ¹H NMR spectroscopy, mass spectroscopy and elemental analysis, and they carefully kept in argon-purged vial with dried and pure condition, because it is important factor of existence of impurities in organic solar cells.

3.3.2 Density functional theory (DFT) calculation

By density functional theory (DFT) calculations, the optimized geometry of **TT**, **TF**, **FT** and **FF** was characterized at energy-minimized ground state, in gas phase. To briefly discuss the effects of furan moieties depending on the number and position, theoretical calculation was performed for the modified structures, which were substituted with methyl group instead of 2-ethylhexyl and octyl groups. As shown in the top and front view in the Figure 3.1, diketopyrrolopyrrole (DPP) and furan/thiophene units could maintain their planarity, along the whole conjugated backbone, without tilting and torsion. High structural planarity of these molecules was kept even by end-capped alkyl cyanoacetate groups, thereby enabling efficient intermolecular π - π interactions and charge carrier transport. It is noticeable that straight-line distance of molecules displayed a growing tendency in order of **FF**<**FT**<**TF**<**TT**, which indicates it was affected by the number and position of furan moieties. The more and the closer to DPP core furan moieties are, the shorter lineal distance of molecules would be. This result showing more compact geometry was attributed to the smaller atomic radius of oxygen in furan.

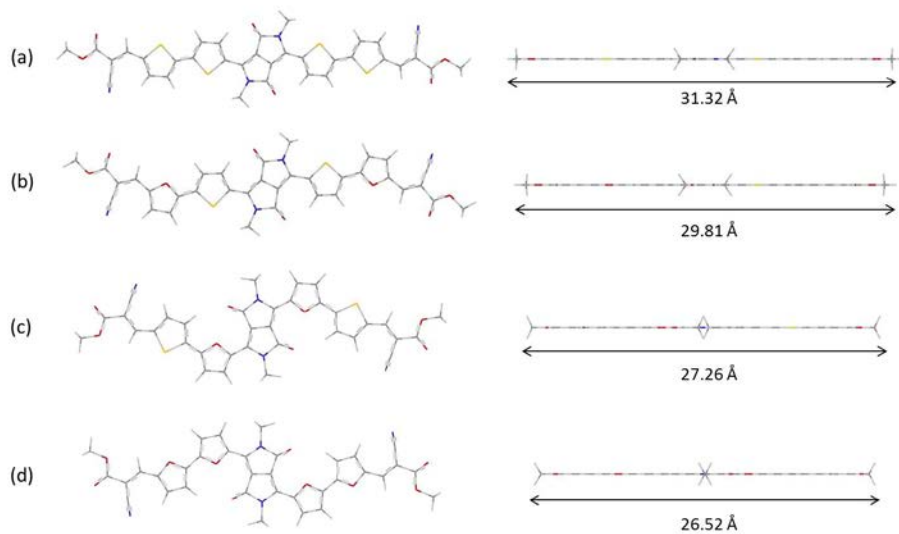


Figure 3.1 Energy-minimized structure (B3LYP/6-31G(d, p)) of a methyl-substituted (a) **TT**, (b) **TF**, (c) **FT** and (d) **FF**, with top (left) and front (right) view and lineal distance along the molecular π -conjugated backbone obtained from Gaussian view 5.0.

3.3.3 Solubility assay

As I have already described, the active layer of BHJ organic solar cells should have optimized thickness to satisfy following contradictory requisites; one is absorbing sufficient photon energy with a thick layer, the other is accomplishing efficient charge transport through a short length between two electrodes. One of the several methods to control film thickness is changing concentration of blend solution, which emphasizes solubility issue. The solubility of materials was measured by using a 0.50 μm PTFE syringe filter which was purchased from Toyo Roshi Kaisha. I prepared 2.0 to 25 mg of **TT**, **TF**, **FT** and **FF** in the 8 mL of vials, separately, and then added chloroform solvent by 0.5 mL at a time. After mild heating, solution was ejected using a syringe with this filter. Next, injecting solution into the vial, the syringe filter was then examined whether there were remained undissolved molecules, or not.

For the **TF**, **FT** and **FF**, more than 15 mg was completely dissolved in the 0.5 mL of chloroform, thus resulting in solubility of ≥ 30 mg/mL. On the other hand, less than 5 mg of **TT** was dissolved in 0.5 mL of chloroform with much effort, such as heating harshly and using an ultra-sonication bath, thus resulting in solubility of < 10 mg/mL.

Furthermore, for **HD-FT**, **C12-FT**, **FT-E**, **FT-B** and **FT-OD**, molecules with modifying alkyl chains, solubility assay was carried out with same procedure. I couldn't find remarkable difference in solubility between **FT** and **HD-FT** (≥ 30 mg/mL), which was vertically modified with 2-hexyldecyl. However,

modifying with linear dodecyl group reduced solubility, significantly, thus examined to ≤ 15 mg/mL of solubility in **C12-FT**. And, it was rarely dissolved in non-halogenated solvent, such as toluene. It means branched alkyl chain has greater effect on solubility rather than long linear alkyl chain.

I also found out that horizontal modifying alkyl chain also changed molecular solubility. At the end-capped alkyl cyanoacetate group, various alkyl chains were substituted such as ethyl (**FT-E**), butyl (**FT-B**), octyl (**FT**) and 2-octyldodecyl group (**FT-OD**). The longer length and the more bulkiness alkyl chains have, the more amounts of materials are dissolved. Therefore, I could obtain molecular solubility of < 15 mg/mL, < 30 mg/mL, > 30 mg/mL, and ~ 50 mg/mL for **FT-E**, **FT-B**, **FT**, and **FT-OD**, respectively.

All of furan-containing target materials displayed adequate solubility for solution processing, except **C12-FT**, hence being available of BHJ organic solar cells.

3.3.4 Photophysical properties

In order to discuss the effects of furan moieties on photophysical properties, the optical characteristics were investigated by UV-Vis absorption and photoluminescence spectroscopy. The UV-Vis absorption spectra of compound **3**, **4** and target materials (**TT**, **TF**, **FT** and **FF**) was recorded in solution state (1×10^{-5} M in chloroform), as shown in the Figure 3.2(a). Compared compound **4** with **3**, furan moiety affected much higher molar absorptivity in solution, and slight blue-shifted profiles. The blue-shift is mainly due to lower aromatic of furan, which has been commonly observed in furan-containing molecules.¹³ This tendency was also founded in **TT**, **TF**, **FT** and **FF**, which was shown in Figure 3.2(b). The **FF** comprised of only furan moieties presented the highest molar absorptivity of $80,800 \text{ M}^{-1}\text{cm}^{-1}$ (Table 3.1) and the most blue-shifted spectra than **TF** and **FT**, from the **TT**. In the Figure 3.2(b), I particularly paid attention to intramolecular charge transfer (ICT) band and its profiles, thereby obtaining the information about molecular conformation in solution state.¹¹ As attached in the magnified box on the right, the **TT** displayed broad and unstructured absorption profiles, indicating rotational freedom between two thiophene rings. Unlike other molecules, the additional band wasn't detected in the **TT** (Table 3.1), which suggested non-planar and twisted conformation in the solution. In contrast, as amounts of furan increased, narrower absorption band with distinct profiles derived from vibrational transitions was identified. That means a high degree of conformational rigidity and planar conformations of furan-containing

materials. Comparing profiles of **TF** and **FT**, I could study about the relation between the position of furan moiety and molecular conformations. From the spectra in solution state, it was verified that more planar conformation could be obtained at the interior of furan moiety. Therefore, **FT** displayed similar profiles with **FF**, and **TF** did similar with **TT**. These features could be explained with a smaller van der Waals radius of furan, avoiding the issue of steric repulsion, and thus stabilizing planar conformation. In conclusion, I understood effects of furan moieties on molar absorptivity and molecular conformations, depending on the number and position, systematically.

Since **TT**, **TF**, **FT** and **FF** have extended conjugation length and strong electron-withdrawing groups of octyl cyanoacetate, they achieved around 60,000 to 80,000 of high molar absorption coefficient at long wavelength region, which would be favorable for photon absorption in organic solar cells. They also have excellent photophysical properties in film state, exhibiting largely red-shifted spectra with approximately 30nm than in the solution state (Figure 3.2(b)). The distinct aggregation band indicating efficient intermolecular interaction was detected in all of them, thereby accomplishing quite low optical band gaps of 1.49 to 1.60 eV. As you see in solution spectra, furan-containing materials have blue-shifted absorption profiles in the film state, which results in larger band gap rather than thiophene-containing materials. It is because low aromatic stability of furan moiety affects inefficient π -electrons along the backbone, thereby reducing effective π -conjugation length.¹³

Furthermore, the photoluminescence (PL) properties of solution state were

characterized, in the Figure 3.3. From the Figure 3.3(a), it was found that improved PL and blue-shifted emission spectra of compound **4**, comparing with compound **3**. I confirmed this growing tendency of PL intensity and decreasing of λ_{em} in order of **TT**, **TF**, and **FF**, in the Figure 3.3(b). Generally, furan-containing molecules show superior emissive characteristic and slightly blue-shifted emission spectrum than thiophene- or selenophene-containing ones,¹² which agreed well with my investigations.

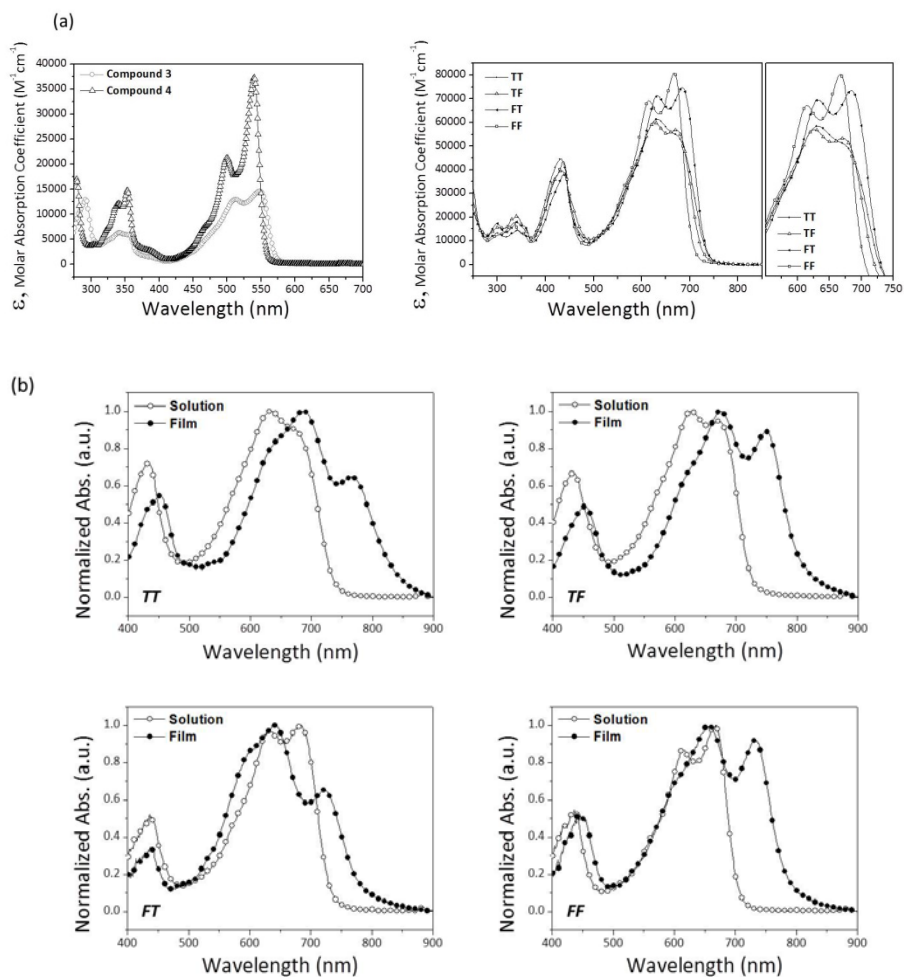


Figure 3.2 UV-Vis absorption spectra of **TT**, **TF**, **FT** and **FF**. (a) Molar absorption coefficient (molar absorptivity) profiles of compound **3** and **4** (left) and **TT**, **TF**, **FT** and **FF** (right) in $CHCl_3$ (1×10^{-5} M). (b) Normalized UV-Vis absorption spectra of **TT**, **TF**, **FT** and **FF** in both solution and film state.

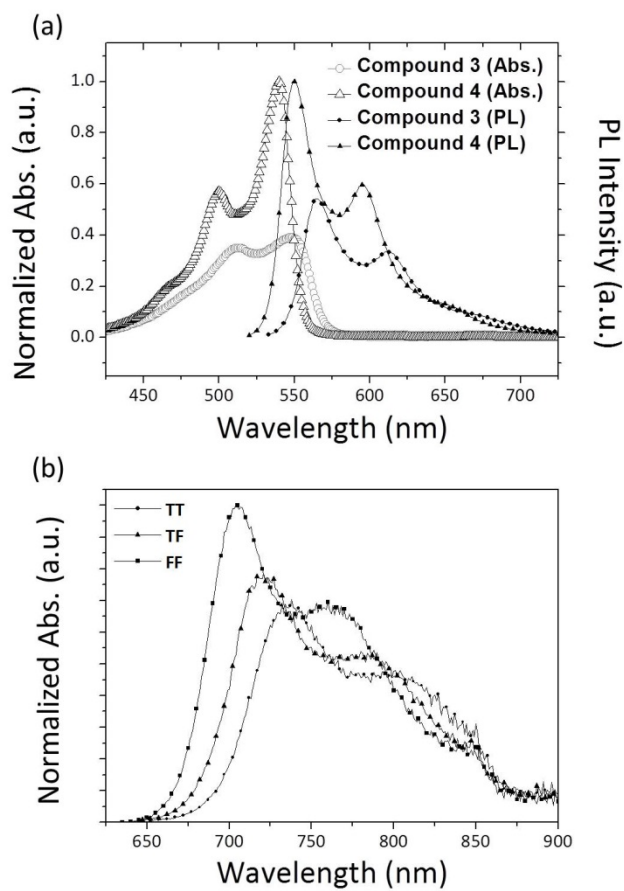


Figure 3.3 Photoluminescence spectra of compound **3** and **4** in (a), and **TT**, **TF** and **FF** in (b), obtained from concentration of 1×10^{-5} M in CHCl_3 solution.

Table 3.1 Optical properties of **TT**, **TF**, **FT** and **FF**.

	$\lambda_{\text{abs.sol}}$ (nm) ^{a)}	$\lambda_{\text{em.sol}}$ (nm) ^{a)}	ϵ_{max} (M ⁻¹ cm ⁻¹) ^{a)}	$\lambda_{\text{abs.film}}$ (nm) ^{b)}	$\lambda_{\text{onset.film}}$ (nm)	$E_{\text{g}}^{\text{opt}}$ (eV) ^{c)}
TT	633	738	61,300	766, 686	831	1.49
TF	671, 627	721	60,000	749, 675	805	1.54
FT	682, 632	730	74,600	721, 637	775	1.60
FF	668, 617	704	80,800	732, 654	780	1.59

^{a)} These values were measured in solution state which was 1×10^{-5} M concentration in CHCl_3 . ^{b)} Measured in film state which was fabricated with spin-coating (1000 rpm/60 sec) from 10 mg/mL CHCl_3 solution on the cleaned glass. ^{c)} Optical band gap was calculated from the $\lambda_{\text{onset.film}}$, according to the equation of: $E_{\text{g}}^{\text{opt}}$ (eV) = $[1240/\lambda_{\text{onset.film}}(\text{nm})]$.

3.3.5 Photoelectrical properties

When I designed the donor or acceptor materials for the BHJ organic solar cells, suitable molecular orbital should be required considering energy levels of the acceptor or donor materials. The energy level is related to the device functions, such as 1) open circuit voltage, which is determined by the difference between HOMO level of donor and LUMO level of acceptor,¹⁴ and 2) charge separation, which is requiring driving force to photo-induced electron transfer, and determined by the difference between LUMO levels.¹⁵

Herein, the HOMO levels of the designed acceptor materials, **TT**, **TF**, **FT** and **FF** were characterized in the solid state by UPS measurement. Work functions were obtainable from the cutoff of UPS profiles in the Figure 3.4, thereby accomplishing HOMO levels. The LUMO level was calculated based on HOMO level and optical band gap, by using the equation of $E_{\text{LUMO}} = - [E_{\text{HOMO}} + E_{\text{g}}^{\text{opt}}]$, hence materials energy levels were summarized in the Table 3.2. The furan-containing **TF**, **FT** and **FF** displayed slight higher HOMO levels than **TT**, which is correlated with my prediction and cyclic voltammetry data. The difference of LUMO levels between P3HT (donor) and these materials (acceptor) were around 0.8-1.0 eV which is sufficient for charge separation, due to being larger than 0.3 eV.¹⁵

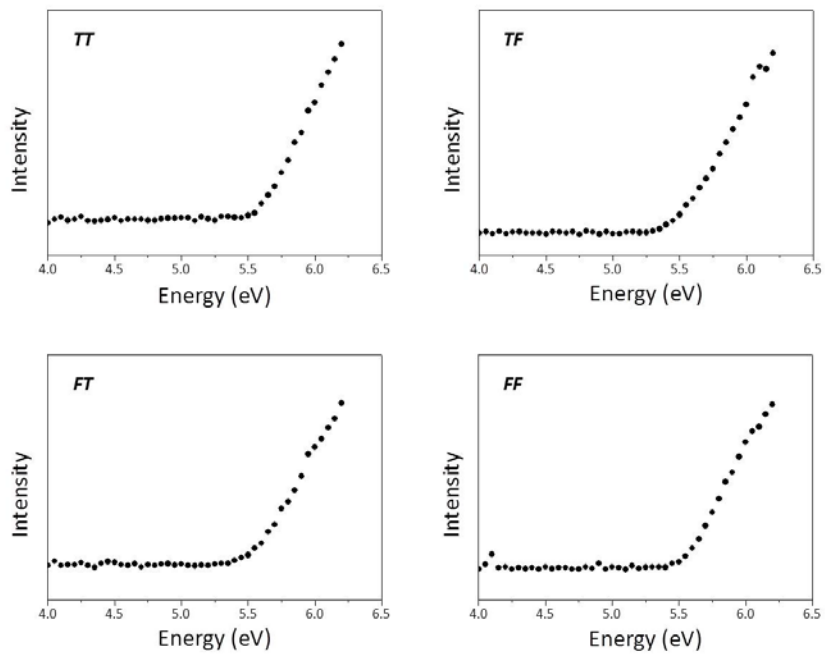


Figure 3.4 Ultraviolet photoelectron spectroscopy (UPS) profiles of the **TT**, **TF**, **FT** and **FF**, for the spin-coated (1000 rpm/60 sec) films on the glasses.

3.3.6 Electrochemical properties

The electrochemical properties were investigated using cyclic voltammetric (CV) measurement, in both solution and film states. From the CV, I could measure molecular oxidation potential, thus obtaining HOMO level by using the difference with reference material. All of materials were dissolved in dichloromethane containing 0.1 M of tetrabutylammonium tetrafluoroborate (TBATFB) as the supporting electrolyte, and then the testing was performed with in only oxidation region at scan rate of 50 mV/s, in solution state. (Figure 3.5(a)) The ferrocene was used as a reference, to calculate the frontier energy of molecular orbital, through following equation: $E_{\text{HOMO}} = [-(E_{\text{Onset}} - E_{\text{Ferrocene}}) - 4.8]$.

Furthermore, the testing was also carried out in the film state. (Figure 3.5(b)) I prepared films on ITO coated glasses by drop-casting from 15mg/mL of chloroform solution (except **TT**, I used 10 mg/mL solution due to low solubility). I measured only oxidation region, at scan rate of 50 mV/s, with 0.1 M of tetrabutylammonium hexafluorophosphate (TBAHFP) in acetonitrile solution, and ferrocene was used as a reference, too. The HOMO levels in the film state were calculated using same equation, thus summarized in the Table 3.2.

The obtained values of $E_{\text{HOMO,sol}}$ was quite different from those of $E_{\text{HOMO,film}}$ and $E_{\text{HOMO,UPS}}$, because of without considering molecular packing effect. I found that the $E_{\text{HOMO,film}}$ of **TT**, **FT** and **FF** correlated well with $E_{\text{HOMO,UPS}}$, in contrast, for the **TF**, the pretty lower-lying HOMO was achieved in CV. I

regarded that $E_{\text{HOMO, film}}$ of **TF** was calculated from second oxidation potential, not from first oxidation potential which was hard to be detected.

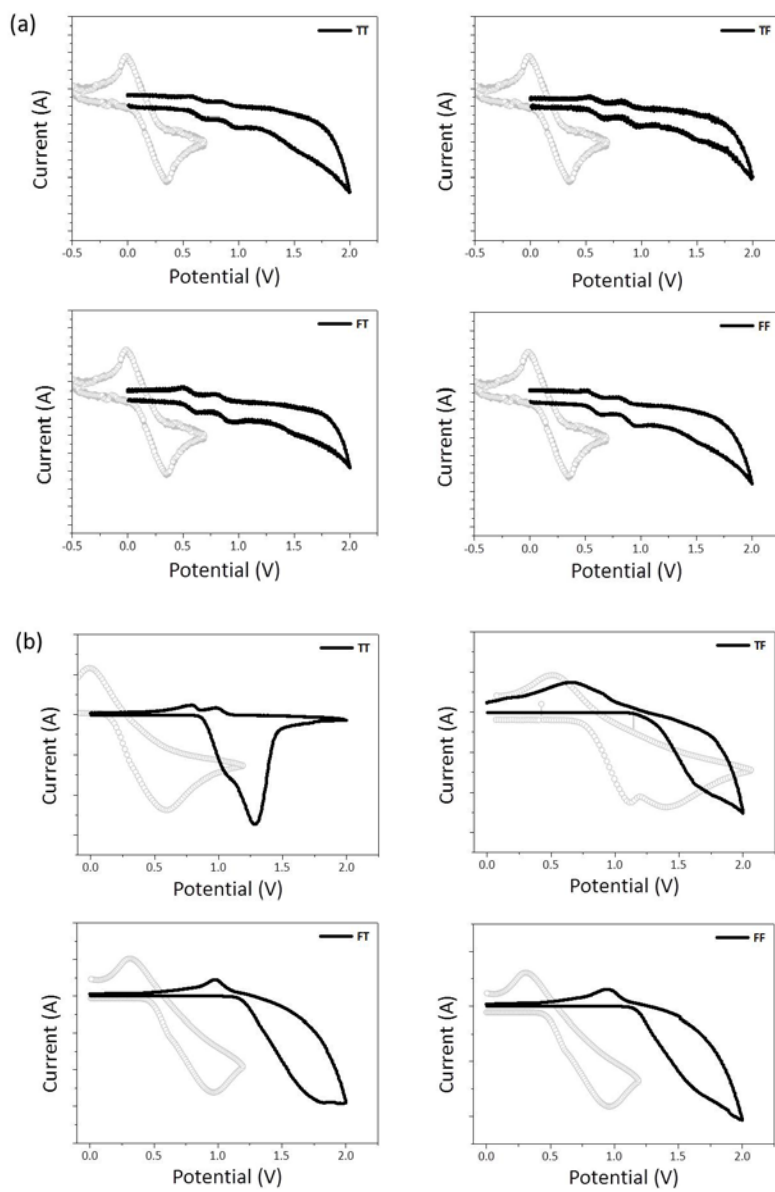


Figure 3.5 The cyclic voltammograms of **TT**, **TF**, **FT** and **FF**, in solution **(a)** and film **(b)** state. The gray lines were obtained from ferrocene.

Table 3.2 Molecular energy levels obtained from UPS and cyclic voltammetric measurements, for **TT**, **TF**, **FT** and **FF**.

	E_g^{opt} (eV)	$E_{\text{HOMO,UPS}}$ (eV) ^{a)}	$E_{\text{HOMO,film}}$ (eV) ^{b)}	$E_{\text{HOMO,sol.}}$ (eV) ^{c)}	E_{LUMO} (eV) ^{d)}
TT	1.49	-5.59	-5.52	-5.27	-4.10
TF	1.54	-5.42	-5.71	-5.24	-3.87
FT	1.60	-5.54	-5.53	-5.21	-3.94
FF	1.59	-5.55	-5.49	-5.23	-3.96

^{a)} Obtained from work functions by UPS measurement. ^{b)} Calculated by the equation of: $E_{\text{HOMO}} = [-(E_{\text{Onset}} - E_{\text{Ferrocene}}) - 4.8]$. Cyclic voltammetric measurement was carried out for the film state (drop-casting on the ITO glass from 15 mg/mL CHCl_3 solution, except **TT** (10 mg/mL), with 0.1 M acetonitrile solution containing tetrabutylammonium hexafluorophosphate (TBAHFP) as a supporting electrolyte. ^{c)} Calculated by the equation of: $E_{\text{HOMO}} = [-(E_{\text{Onset}} - E_{\text{Ferrocene}}) - 4.8]$. Cyclic voltammetric measurement was carried out for the solution state (1 wt% concentration in dichloromethane (DCM) with 0.1 M of tetrabutylammonium tetrafluoroborate (TBATFB)). ^{d)} Calculated from the equation of: $E_{\text{LUMO}} = -[E_{\text{HOMO,UPS}} + E_g^{\text{opt}}]$.

3.3.7 Photovoltaic properties

The photovoltaic properties of **TT**, **TF**, **FT**, and **FF** as acceptor materials were characterized by fabricating BHJ organic solar cell devices with P3HT as a donor. The device structure was comprised of [ITO/PEDOT:PSS/P3HT:DPP derivatives (DPPs)/Al]. In the toluene solvent, **TT**, **TF**, **FT** and **FF** displayed *J-V* characteristics shown in the Figure 3.6(a), under AM 1.5G (100 mW/cm²) condition. Because **TT** was hard to dissolve in toluene at high concentration, all of devices were fabricated with 15 mg/mL concentration, at first. In spite of such low concentration restricting sufficient light absorption due to thin active layer, the device comprising of P3HT and **FT** showed promising efficiency of 0.28%. (Table 3.3(a))

Based on the results from above screening test, I modified alkyl chains in both vertical and horizontal directions, thus trying to control film morphologies through fine-tuned molecular structures. I additionally synthesized 2-hexyldecyl and linear dodecyl substituted molecules in **FT** backbone; however, the solubility of dodecyl substitution, **C12-FT**, was too low to process for device fabrication, as commented previous in solubility assay. The Figure 3.6(b) and Table 3.3(b) presented photovoltaic properties of **FT** and **HD-FT** that were fabricated in higher concentration of 20mg/mL than before; thereby yielding enhanced PCE of 0.37% for **FT**. The bulky 2-hexyldecyl substitution, **HD-FT**, exhibited quite lower efficiency, which is because 2-hexyldecyl side chain hindered molecules from accomplishing effective π - π interactions, thus disturbing charge carrier transport.

I also investigated the effect of alkyl chains with structural modification toward horizontal direction, thus designing **FT-E**, **FT-B** and **FT-OD**, additionally. Each material was ethyl, butyl and 2-otylododecyl substitution at end-capped alkyl cyanoacetate group. Device fabrication condition was optimized about each material, with blend ratio, concentration of blend solution, solvent, spin-rate, post-annealed temperature and time, and so on. (Figure 3.6(c)) After much trial, organic solar cells comprising **FT-B** with P3HT donor exhibited power conversion efficiency of as high as 0.43% (Table 3.3(c)), which was higher than **FT** and comparable with other DPP-based acceptor materials². This result indicated that 2-ethylhexyl at N-position and butyl at end-capped group are favorable to device functions, in other words, optimum length of side chain does exist. In order to further understand effects of alkyl chains on phase separation in active layer, I carried out morphological investigation using AFM, in the following part.

As you see in the Table 3.3(c), after post-annealed at 130 °C for 5 min, **FT-B** as an electron acceptor exhibited 0.43% of PCE, 0.45 V of V_{OC} , 2.51 mA/cm² of J_{SC} , and 37.7% of FF , in using THF solvent. I have already confirmed that this furan-containing material showed following characteristics; 1) extremely planar optimized geometry, which is favorable of intermolecular interaction and charge transport, 2) relative high solubility of close to 30mg/mL in common organic solvent, 3) outstanding photophysical properties, such as high molar absorptivity, superb light absorption, and low band gap energy (~1.60 eV of E_g^{opt} obtained from **FT**), and 4) adequate energy levels that HOMO and LUMO levels are -5.54 and -3.94 eV (obtained from **FT**). In spite

of these favorable characteristics, device properties of **FT-B** were lower than my expectations. Its low V_{oc} was especially regarded as a parameter to be improved, because it was quite smaller than the difference between HOMO level of P3HT and LUMO level of **FT-B** (approximately 1 eV).

Further work: Hence I decided to align energy levels of acceptor materials, by 1) replacing thiophene with phenyl ring, or 2) incorporating additional thiophene rings into the π -conjugation system. These design strategies were described in Scheme 3.4, with several experimental data, briefly. The first approach (Scheme 3.4(a)) resulted in significant high-lying LUMO level (-3.66 eV) due to the higher HOMO level (-5.34 eV) and larger band gap energy (1.68 eV) of **FB-B**, thus obtaining enhanced V_{oc} of 0.72 V. However, its solar cell efficiency was much lower, because **FB-B** has limited light absorption (Figure 3.7(a)) and low J_{sc} being disadvantageous for charge transport. With the second approach (Scheme 3.4(b)), which is introducing additional thiophene rings to raise energy levels, I couldn't achieve initial goal. The LUMO level (-3.88 eV) of **FTT** was not changed a lot, and hence its V_{oc} (0.50 V) and PCE (0.01%) were still low, despite enhanced photophysical properties (Figure 3.7(b)). Therefore, I concluded that furan-thiophene building block of **FT-B** would be more favorable for acceptor material in BHJ organic solar cells, rather than that of **FB-B** or **FTT**.

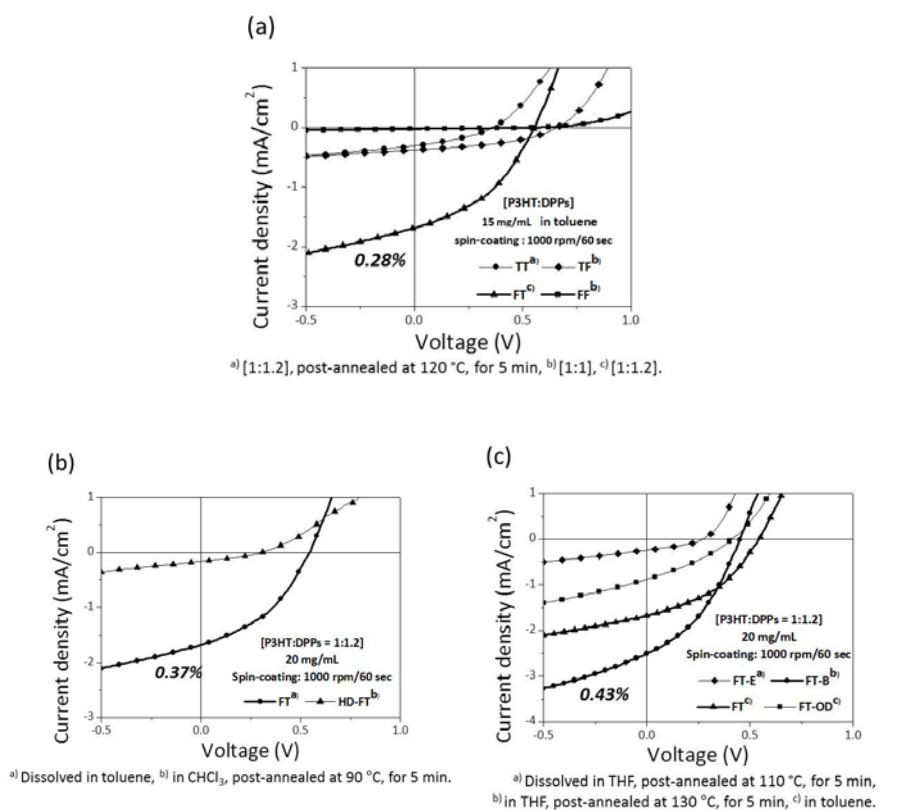


Figure 3.6 *J-V* curves of BHJ organic solar cells fabricated with P3HT and DPP small molecules with various backbone and alkyl chin modified derivatives. (a) Screening test of **TT**, **TF**, **FT** and **FF** in toluene solvent. (b) Vertical modifying for **FT** and **HD-FT** with high concentration. (c) Horizontal modifying for **FT-E**, **FT-B**, **FT** and **FT-OD**. Specific fabricating conditions were noted at the below each curve.

Table 3.3 Photovoltaic properties in (a)-(c). Specific fabricating conditions were noted at the below of each table.

(a) Screening test of **TT**, **TF**, **FT** and **FF** in toluene solvent.*

	<i>PCE</i> (%)	V_{OC} (V)	J_{SC} (mA/cm ²)	<i>FF</i> (%)
TT ^(a)	0.04	0.36	0.31	34.6
TF ^(b)	0.10	0.66	0.38	41.8
FT ^(c)	0.28	0.57	1.07	45.1
FF ^(b)	0.004	0.57	0.02	28.6

*Active layer was fabricated by spin-coating (1000 rpm/60 sec) from toluene solution with 15 mg/mL. ^(a) Blend ratio of P3HT:**TT** was 1:1.2, and device was post-annealed at 120 °C for 5 min. ^(b) Blend ratio was 1:1. ^(c) Blend ratio was 1:1.2.

(b) Vertically alkyl chain modifying for **FT** and **HD-FT** with high concentration.*

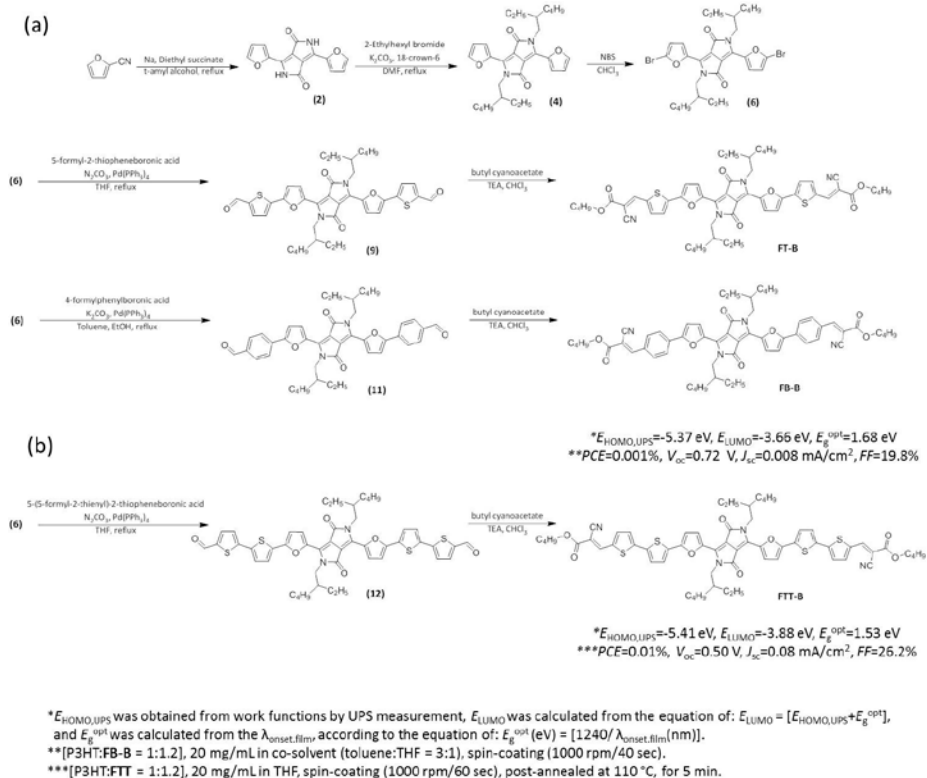
	<i>PCE</i> (%)	V_{OC} (V)	J_{SC} (mA/cm ²)	<i>FF</i> (%)
FT ^(a)	0.37	0.54	1.67	40.6
HD-FT ^(b)	0.02	0.30	0.16	32.0

*Active layer was fabricated by spin-coating (1000 rpm/60 sec) from 20 mg/mL solution with blend ratio of 1:1.2. ^(a) P3HT and **FT** were dissolved in toluene. ^(b) P3HT and **HD-FT** were dissolved in CHCl₃, and device was post-annealed at 90 °C for 5 min.

(c) Horizontally alkyl chain modifying for **FT-E**, **FT-B**, **FT** and **FT-OD** with optimized solvent.*

	<i>PCE</i> (%)	V_{OC} (V)	J_{SC} (mA/cm ²)	<i>FF</i> (%)
FT-E ^{a)}	0.02	0.27	0.24	35.4
FT-B ^{b)}	0.04	0.53	0.31	26.3
FT-B ^{c)}	0.43	0.45	2.51	37.7
FT ^{d)}	0.37	0.54	1.67	40.6
FT-OD ^{d)}	0.11	0.41	0.88	32.0

*Active layer was fabricated by spin-coating (1000 rpm/60 sec) from 20 mg/mL solution with blend ratio of 1:1.2. ^{a)} P3HT and **FT-E** were dissolved in THF, and device was post-annealed at 110 °C for 5 min. ^{b)} Pristine film from THF solution. ^{c)} Device was post-annealed at 130 °C for 5 min. ^{d)} P3HT and **FT/FT-OD** were dissolved in toluene.



Scheme 3.4 Synthesis and solar cell applications of **FB-B** and **FTT**. Synthesis of **FB-B** (a) and synthesis of **FTT** (b) with summarized experimental data and photovoltaic properties.

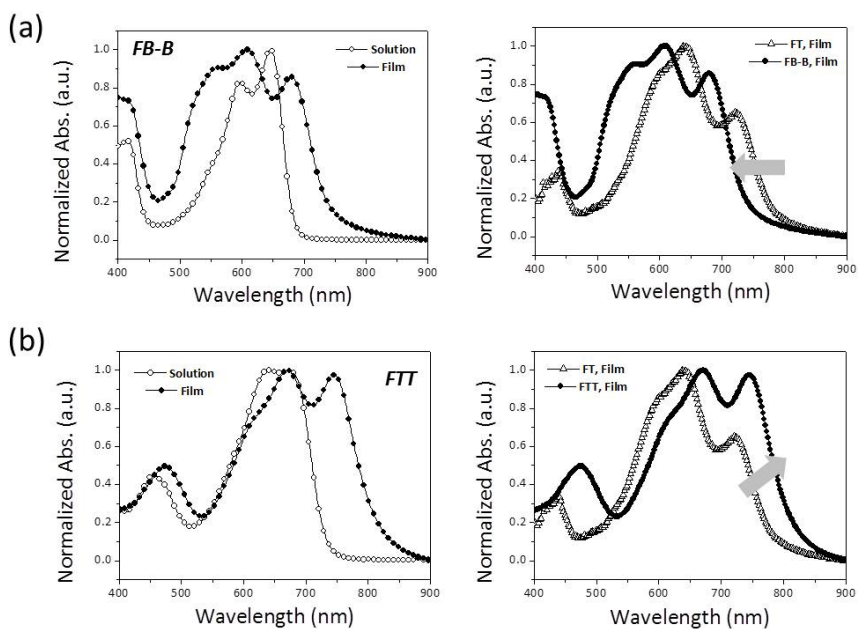


Figure 3.7 UV-Vis absorption profiles of **FT-B** (a, left) and **FTT** (b, left) in the solution (1×10^{-5} M in CHCl_3) and film by spin-coating (1000 rpm/60 sec) from 10 mg/mL CHCl_3 solution. And absorption spectra of **FT-B** and **FTT** in the film state compared with that of **FT** on the right of (a) and (b).

3.3.8 Morphology investigations

For the high performing BHJ organic solar cells, the morphology control of active layer has been considered as significant issue, in these days. Since exciton diffusion and charge carrier transport are determined by phase separation, I should understand molecular ordering and supramolecular structures to obtain favorable nano morphologies.

Herein, the surface morphology of the pristine films fabricated from **TT**, **TF**, **FT** and **FF** with P3HT was investigated by using tapping mode AFM measurement. The **TT** in the Figure 3.8A(a) displayed highly crystalline structures and segregated domains with large roughness of 6.23nm, rather than **TF** (b), **FT** (c) and **FF** (d). In contrast, among the furan-containing materials, **FT** and **FF** showed smooth surfaces with pretty low roughness, that is 0.97 and 1.66 nm respectively. From the morphological studies, I found that thiophene moieties of **TT** and **TF** contributed to forming well-ordered crystalline domains with large segregation, which was disadvantageous to accomplish desirable phase separation and charge transport in solar cells.

Generally the thin film morphology can be affected by processing conditions, such as blend ratio, concentration of blend solution, solvent, spin-rate, annealing temperature and time, additive, etc. In addition, molecular structures can control nano-structural morphologies, effectively. In order to verify the latter relationships in detail, morphological study was carried out about fine-tuned materials with various alkyl chains. Depending on the length (short/long) and shape (linear/branched) of alkyl chains, I designed **FT**

derivatives, and obtained surface images in nano-scale from AFM measurement.

Along the horizontal direction, butyl, octyl, and 2-octyldodecyl side chains were introduced into end-capped cyanoacetate groups, thus generating **FT-B**, **FT**, and **FT-OD**. As shown in the Figure 3.8B, structural modification of side chains induced morphological change in active layer. I observed a decreasing tendency to roughness, in increasing order of alkyl chain length and bulkiness, like this: 4.28 nm (**a**, **FT-B**) > 0.97 nm (**b**, **FT**) > 0.71 nm (**c**, **FT-OD**) of roughness. The **FT-B** containing butyl cyanoacetate displayed appropriate phase separated surface morphology and adequate roughness, thus leading to enhanced solar cell efficiency (PCE of 0.43%). The surface morphology of **FT-OD** bearing much longer and bulkier 2-octyldodecyl chain was too amorphous without any structural domains, which might be related to low device properties.

In this study, I paid attention to the solvent effects, based on morphological investigations. The THF is commonly considered as good solvent, over toluene. Pristine film fabricated from the THF solvent would be amorphous without large segregation or aggregation. In contrast, when the film was spin-coated using mild or poor solvent, such as toluene, its surface morphology would be quite different, showing highly segregated domains with large roughness. An excessively amorphous or crystalline morphology is unfavorable in organic solar cells, hence I have to find an adequate solvent condition, to obtain desirable phase separation. One of approaches is using co-solvent system, which means adjusting blend ratio between good solvent and

poor solvent, thus controlling nano-structural structures.

I tried to use mixed solvents of THF and toluene, with different ratios, such as 1:3, 1:1, and 3:1, and found that desirable surface morphology could be accomplished in 1:3 condition, thus obtaining 0.32% of PCE comparable efficiency with only toluene solvent system. For example, as shown in the Figure 3.8C, the surface morphology and roughness of **FT** and P3HT were dependent to the ratio of co-solvents. Compared with Figure 3.8B(b), the Figure 3.8C exhibited much different surface images, in spite of same material. In addition, solar cell efficiencies were different in between them.

Interestingly, the optimum device fabricating condition of **FT-B** was using THF solvent and post-annealing at 130 °C for 5min, unlike **FT**, whose fabricating condition was using toluene and without annealing process. Here, I noticed the relationships between annealing and solvent effects. For the amorphous film which can be derived from good solvent, post-annealing has been widely carried out to induce some degree of aggregation, thus achieving desirable phase separation in solar cells.

Based on this annealing effect, pristine **FT-B** film fabricated with THF solvent could accomplish suitable nano-structural morphology through post-annealing process. As summarized in Table 3.3(c), the efficiency was significantly improved from 0.04% to 0.43%, through annealing at 130 °C. It was attributed to the J_{SC} , which is more than eight times largely increased. This result demonstrated that ideal percolating networks from suitable phase separation can improve the current, thereby enhancing device properties.

As you see in the Figure 3.8D, highly segregated surface with large roughness

was examined in toluene condition of **FT-B (a)**. On the other hand, amorphous structure in THF condition would be transformed toward slight crystalline structure, by using annealing process or co-solvent system, which means annealing effect or solvent effect, respectively. Through these two approaches, appropriate phase separation could be obtained, as shown in the Figure 3.8**D(b)** and **(c)**. I concluded that there are same effects on film morphology between annealing process and solvent condition.

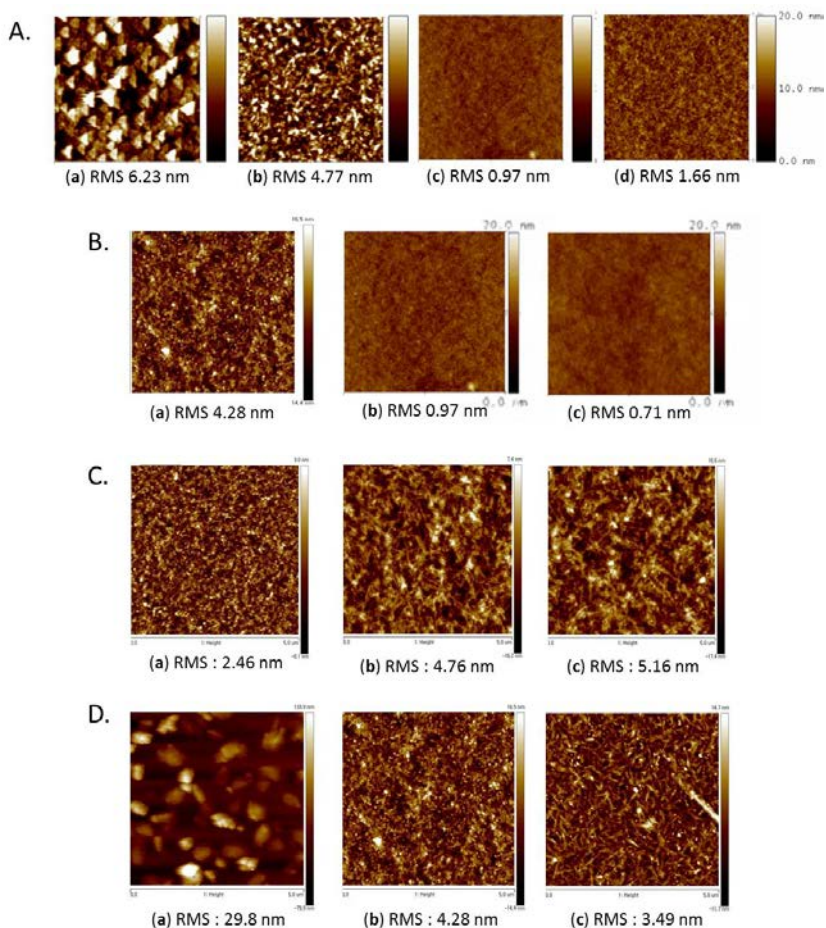


Figure 3.8 Morphological images with roughness obtained by AFM of BHJ organic solar cells. **A:** (a) **TT** (toluene), (b) **TF** (toluene), (c) **FT** (toluene), (d) **FF** (toluene). **B:** (a) **FT-B** (THF, annealed at 150 °C), (b) **FT** (toluene), (c) **FT-OD** (toluene). **C:** (a) **FT** (co-solvent of 1:3, 150 °C), (b) **FT** (co-solvent of 1:1, 150 °C), (c) **FT** (co-solvent of 3:1, 150 °C). **D:** (a) **FT-B** (toluene, annealed at 150 °C), (b) **FT-B** (THF, annealed at 150 °C), (c) **FT-B** (co-solvent of 1:3, annealed at 150 °C).

3.4 Conclusions

According to the several related papers⁴⁻¹⁰, it was found that substitution of furan in diketopyrrolopyrrole (DPP)-based copolymers shows great solubility with comparable device properties for electron donating p-type materials in solar cells and transistors. I have also confirmed the favorable effects of furan moiety in DPP-based small molecule as a donor. In this study, I successfully synthesized several furan-containing acceptor materials, which were modified with optimized alkyl side chains and strong electron accepting part of cyanoacetate groups into DPP unit. The effects of the number and position of furan moiety on optimized geometry, optical, electrochemical, and morphological properties were discussed, systematically. In addition, thin film morphologies were investigated to identify correlation between fine-tuning of alkyl chain and phase separation. I noticed that these novel molecules show excellent photophysical properties, including broad absorption, high extinction coefficient and low optical band gap, as well as enhanced solubility for solution-processing. Organic solar cells comprising of these acceptors with P3HT as a donor were fabricated to show power conversion efficiencies (PCEs) as high as 0.43%, in optimized condition. From this work, I demonstrated the effects of furan thoroughly, and concluded that furan moiety would be also promising as acceptor materials.

3.5 References

1. Lin, Y.; Li, Y. and Zhan, X. *Adv. Energy Mater.* **2013**, *3*, 724.
2. (a) Lin, Y.; Cheng, P.; Li, Y. and Zhan, X. *Chem. Commun.* **2012**, *48*, 4773. (b) Chen, T. L.; Zhang, Y.; Smith, P.; Tamayo, A.; Liu, Y. and Ma, B. *ACS Appl. Mater. Interfaces* **2011**, *3*, 2275. (c) Sonar, P.; Ng, G.-M.; Lin, T. T.; Dodabalapur, A. and Chen, Z.-K. *J. Mater. Chem.* **2010**, *20*, 3626. (d) Karsten, B. P.; Bijleveld, J. C. and Janssen, R. A. *Macromol. Rapid Commun.* **2010**, *31*, 1554.
3. (a) Liu, Y.; Wan, X.; Wang, F.; Zhou, J.; Long, G.; Tian, J.; You, J.; Yang, Y. and Chen, Y. *Adv. Energy Mater.* **2011**, *1*, 771. (b) Mun, J.-W.; Cho, I.; Lee, D.; Yoon, W. S.; Kwon, O. K.; Lee, C. and Park, S. Y. *Organic Electronics*, **2013**, *14*, 2341.
4. Woo, C. H.; Beaujuge, P. M.; Holcombe, T. W. Lee, O. P.; and Fréchet, J. M. J. *J. Am. Chem. Soc.* **2010**, *132*, 15547.
5. Yiu, A. T.; Beaujuge, P. M.; Lee, O. P.; Woo, C. H.; Toney, M. F.; and Fréchet, J. M. J. *J. Am. Chem. Soc.* **2012**, *134*, 2180.
6. Biljlevled, B. P.; Karsten, S. G. J.; Wienk, M. M.; de Leeuw D. M. and Janssen, R. A. J. *J. Mater. Chem.* **2011**, *21*, 1600.
7. Li, Y.; Sonar, P.; Singh, S. P.; Zeng, W. and Soh, M. S. J. *Chem. Mater.* **2011**, *21*, 10829.
8. Li, Y.; Sonar, P.; Singh, S. P.; Ooi, Z. E.; Lek, E. S. and Loh, M. Q. *Phys. Chem. Chem. Phys.* **2012**, *14*, 7162.

9. (a) Sonar, P.; Foong, T. R. B.; Singh, S. P.; Li, Y. and Dodabalapur, A. *Chem. Commun.* **2012**, *48*, 8383. (b) Sonar, P.; Singh, S. P.; Williams, E. L.; Li, Y.; Soh, M. S.; and Dodabalapur, A. *J. Mater. Chem.* **2012**, *22*, 4425.
10. (a) Dou, L.; Chang, W.-H.; Gao, J.; Chen, C.-C.; You, J. and Yang, Y. *Adv. Mater.* **2013**, *25*, 825. (b) Chen, C.-C.; Dou, L.; Gao, J.; Chang, W.-H.; Lia, G. and Yang, Y. *Energy Environ. Sci.* **2013**, *6*, 2714.
11. Henssler, J. T. and Matzger, A. J. *J. Org. Chem.* **2012**, *77*, 9298.
12. (a) Bunz, Uwe H. F. *Angew. Chem. Int. Ed.* **2010**, *49*, 5037. (b) Gidron, O.; Dadvand, A.; Sheynin, Y.; Bendikov, M. and Perepichka, D. F. *Chem. Commun.* **2011**, *47*, 1976.
13. (a) Takimiya, K.; Konda, Y.; Ebata, H.; Niihara, N. and Otsubo, T. *J. Org. Chem.* **2005**, *70*, 10569. (b) Takimiya, K.; Kunugi, Y.; Konda, Y.; Niihara, N. and Otsubo, T. *J. Am. Chem. Soc.* **2004**, *126*, 5084. (c) Nakano, M.; Mori, H.; Shinamura, S. and Takimiya, K. *Chem. Mater.* **2012**, *24*, 190. (4) Nakano, M.; Niimi, K.; Miyazaki, E.; Osaka, I. and Takimiya, K. *J. Org. Chem.* **2012**, *77*, 8099.
14. Li, G.; Zhu, R. and Yang, Y. *Nature Photon.* **2012**, *6*, 153.
15. Fréchet, J. M. J. and Thompson, B. C. *Angew. Chem. Int. Ed.* **2008**, *47*, 58.

초 록

용액공정용 유기태양전지를 위한 퓨란을 포함하는 디케토피롤로피롤 유도체의 분자 설계 및 합성에 관한 연구

오늘날, 용액공정용 Bulk heterojunction (BHJ)의 유기태양전지는 미래의 대체 가능한 에너지 시스템 개발을 위한 목적으로 많은 주목을 받고 있다. 특히, 본 논문에서는 유기 반도체 재료에서 전자 끌개 체로 널리 사용되는 우수한 광학적, 전기적 특성을 갖는 디케토피롤로피롤 (DPP) 구조에 관심을 가지고 연구하였다. 최근 A-D-A 또는 D-A-D의 공액구조를 갖는 DPP 기반의 단분자는 우수한 태양전지 효율을 나타내며 빠르게 발전하고 있다. 하지만 이들은 DPP의 강한 수소결합에서 기인한 낮은 용해도 문제에 직면할 수 있다. 본 연구에서는 매우 길거나 분기 사슬을 도입하는 대신, 퓨란을 도입함으로써 용액 공정이 가능한 유기태양전지 재료를 설계하는 전략을 채택하였다.

퓨란을 포함하는 DPP 기반의 단분자들의 합성, 특성 평가, 그리고 BHJ의 유기태양전지로의 응용이 진행되었다. 2단원에서는 DPP와 Dithienothiophene (DTT)로 구성된 새로운 A-D-A 구조의 전자 공여체를 디자인하였다. 보다 간단한 합성 과정을 통해 합성된 **F2**는

태양전지 특성은 그대로 유지하면서, 동시에 용해도와 개방 전압이 개선되었다. 이를 통해 퓨란이 싸이오펜을 대체할 수 있음을 증명하였다. 결과적으로 **F2**와 **PC₆₁BM**은 1 vol%의 **DIO** 조건에서 2.1%의 전력 변환 효율과 0.75 V의 향상된 개방 전압을 나타내었다. 더불어 퓨란이 분자의 특성에 미치는 영향을 체계적으로 논의하였다. 3단원에서는 퓨란의 개수와 위치에 따라 4가지의 서로 다른 **A-D-A-D-A** 구조의 단분자를 디자인하였다. 퓨란을 포함하는 **DPP** 기반의 단분자는 우수한 광 물리적 특성을 보이며, 용액공정이 가능한 **BHJ**의 유기태양전지에서 전자 수용체 분자로써의 가능성을 나타내었다.

주요어: 디케토피롤로피롤, 유기태양전지, 퓨란
학 번: 2012-22539

List of Presentation

1. **Jeong-A Oh**, Won Sik Yoon, Jung-hwa Park, Soo Young Park, “Low Band Gap and Solution-Processable Furan-Containing Diketopyrrolopyrrole-Based Small Molecules as Acceptor Materials in Organic Solar Cells”, **2nd Korea-UK Student Exchange Program**, March 25, 2013, Seoul National University, Korea.
2. **Jeong-A Oh**, Won Sik Yoon, Jung-hwa Park, Soo Young Park, “Novel Acceptor Materials of Furan-Containing Diketopyrrolopyrrole Derivatives for Solution-Processed Organic Solar Cells”, **The International Symposium On Carbon Electronics 2013 (ISCE)**, May 6, 2013, Seoul National University, Korea.
3. **Jeong-A Oh**, Won Sik Yoon, Jung-hwa Park, Soo Young Park, “Low Band Gap and Solution-Processable Furan-Containing Diketopyrrolopyrrole-Based Small Molecules as Acceptor Materials in Organic Solar Cells”, **The 15th Asian Chemical Congress**, August 20-22, 2013, Singapore, Singapore.

감사의 글

2012 년 1 월을 시작으로 2013 년 12 월 본 논문이 나오기까지 대학원 생활을 하는 내내 언제나 묵묵히 뒤에서 지켜봐 준 우리 가족 모두 감사 드립니다. 항상 같은 자리에서 저를 응원해 주시고, 이 세상 누구보다 자랑스러운 아빠, 엄마. 두 분의 아낌없는 희생과 정성 가득한 사랑에 다시 한번 감사 드립니다.

제가 2 년 동안 몸 담았던 초분자광전자재료 연구실(CSOM)을 이끌어 나가고 계시는 박수영 교수님께 이 글을 통해 감사 인사를 전합니다. 바쁜 일정 속에서도 저의 연구 활동에 관심을 가져주시고, 무엇보다 제 자신을 믿고 2 년 동안 지도해 주신 점에 진심으로 감사 드립니다.

그리고 CSOM 구성원 여러분께도 감사 드립니다. 그 누구보다 원식 오빠. 귀중한 시간을 들여 제 연구에 물심양면 도움을 주셨던 것뿐만 아니라 작은 것 하나까지 신경 써 주셨던 것들 모두 잊지 못할 것입니다. 모든 면에서 원하는 바 이루시리라 믿으며 항상 건강하시길 바라겠습니다.

뿐만 아니라 자상하게 저의 연구활동을 봐주신 서장원 박사님, 졸업을 앞두고 많은 시간 도움 주신 동원 오빠와 석사 과정 동안 큰 도움이 되어 주신 정화 오빠께 감사 드립니다. 그리고 다정하신 동렬 오빠와 성실한 지언 오빠, 한결 같이 젠틀한 오규 오빠, 바쁘셨던 일훈 오빠, 똑똑하신 중한 오빠, 그리고 바쁘던 와중에도

신경 써 주시던 상규 오빠께 감사 드립니다. 또한 친절하신 준모 오빠, 앞으로도 잘 하시리라 기대하는 진홍 오빠와 꼼꼼하고 성실한 준걸 오빠에게 감사합니다. 몸과 마음이 지칠 때 서로에게 힘이 되던 민아 언니와 서로에게 위로가 되던 헤어짐이 아쉬운 유진씨, 그리고 항상 열심히 하던 혜연이와 같은 팀으로써 앞으로 좋은 결과 잇길 바라는 영주, 유쾌하고 열정적인 상윤이, 어리지만 누구보다 잘 해나갈 형주, 재미있고 착한 도진이, 그리고 짧은 시간이지만 다정했던 영광이와 부지런한 정훈이, 이제 곧 입학할 동하와 민우까지 이 글을 통해 응원과 감사 인사를 전합니다. 마지막으로 지치던 순간마다 옆에서 격려해주던 친구들에게도 감사하며 앞으로도 고마운 마음 늘 간직하도록 하겠습니다.